Experiments on scattering lasers from Mie to random

Karen Liana van der Molen

Promotiecommissie

Promotor	Prof. Dr. A. Lagendijk
Assistent Promotor	Dr. A. P. Mosk
Overige leden	Prof. Dr. J. Knoester
	Prof. Dr. L. Kuipers
	Prof. Dr. M. Pollnau
	Prof. Dr. W. L. Vos
	Prof. Dr. D. S. Wiersma
Paranimfen	A. A. M. Kok
	E. A. Reinshagen

EXPERIMENTS ON SCATTERING LASERS

FROM MIE TO RANDOM

PROEFSCHRIFT

ter verkrijging van
de graad van doctor aan de Universiteit Twente,
op gezag van de rector magnificus,
prof. dr. W.H.M. Zijm,
volgens besluit van het College voor Promoties
in het openbaar te verdedigen
op woensdag 25 april 2007 om 13.15 uur

door

Karen Liana van der Molen

geboren op 9 April 1980

te Rotterdam.

Dit proefschrift is goedgekeurd door:

Prof. Dr. A. Lagendijk en Dr. A. P. Mosk

Aan mijn ouders

"There are no short cuts to any place worth going."

Beverly Sills

Dankwoord

"Een proefschrift schrijf je nooit alleen", een veelvoorkomende uitspraak, wellicht een cliché, maar ik heb de afgelopen vier jaar ervaren dat deze uitspraak, zoals de meeste clichés, heel erg waar is. Daarom wil ik bij deze alle mensen bedanken die mij hebben geholpen en bijgestaan. Dit zijn er zoveel, dat het onmogelijk is om een ieder bij naam te noemen. Ik wil echter een paar mensen apart noemen.

Allereerst mijn promotor Ad. Ad, bedankt voor je sturende rol gedurende de afgelopen vier jaar. Hoe ik ook je kamer binnen kwam, ik kwam er altijd weer vol motivatie uit. Dankzij je inzicht in de wetenschap en de wetenschappelijke wereld is mijn promotie geworden zoals zij is.

En dan natuurlijk Allard, mijn dagelijkse begeleider die altijd de tijd nam om te praten over metingen, modellen en opstellingen. Dank je wel voor al die tijd, kennis en oneindige hoeveelheid ideeën die je me gegeven hebt.

Tijdens mijn promotie is het mij een waar genoegen geweest om Peter Zijlstra te begeleiden bij zijn afstuderen. De hoofdstukken 2 tot en met 4 in dit proefschrift waren niet tot stand gekomen zonder hem. Peter, bedankt voor je enorme inzet.

Voordat we onze opstelling gebouwd hebben, zijn we bij twee soortgelijke opstellingen gaan kijken. Allard en ik zijn samen op bezoek geweest bij het Amolf instituut. Daar hebben we van Astrid van der Horst een uitgebreide uitleg gekregen over de optische val die daar in de groep van Marileen Dogterom werd gebruikt. Daarnaast heb ik het geluk gehad dat ik een aantal dagdelen met Martin Bennink van het Mesa$^+$ Instituut en de leerstoel Biophysical Engineering metingen heb gedaan aan een werkende optische val. Ook later hebben we nog veel overleg

gehad met de leerstoel Biophysical Engineering: dankzij Kees van der Werf hebben we onze karakterisatie werkend gekregen.

Cock, hoe vaak heb je me niet geholpen met diverse apparatuur, bestellingen en technische details. En niet te vergeten de tijd en energie die je besteed hebt aan de Infinity laser. Dankzij jouw inspanningen is het toch gelukt om die laatste mooie resultaten binnen te slepen!

Voor een aantal metingen aan random lasers heb ik gebruik mogen maken van een picoseconde lichtbron. Tijmen en Willem Vos, bedankt hiervoor. Willem, ook bedankt voor de (wetenschappelijke) discussies die we hebben gevoerd.

Verder zou ik ook graag Carlo Beenakker bedanken, voor de discussies die hij met Ad heeft gevoerd over random matrix theorie en random lasers.

Het Techno Centrum voor Onderwijs en Onderzoek (TCO) heeft me ook enorm veel geholpen. Klaas, André, Theo en Rindert, bedankt!

Samen met Boris Bret heb ik de eerste metingen gedaan aan een gallium fosfide random laser, merci! Daarnaast wil ik je ook graag bedanken voor je hulp bij het karakteriseren van mijn samples. Ook Paolo en Sanli hebben me bijgestaan bij het karakteriseren van de samples, bedankt. Willem Tjerkstra, dank je wel voor je steun zowel binnen als buiten het chemisch lab.

Léon, dank voor de chemische ondersteuning. Daarnaast was je ook altijd aanwezig om met je nuchterheid orde op zaken te stellen. En mijn andere kamergenoot voor lange tijd: Ivo. Ik vond het heel plezierig om, naast de vele wetenschappelijke discussies, ook over andere zaken te kunnen praten.

Bauke, Joanna, Lisette en Renske, dank voor jullie vriendschap en de wetenschap dat een telefoontje alles is wat nodig is om een luisterend oor te vinden.

Anne-Mei en Els, ook bij jullie vond ik altijd een luisterend oor. En jullie hebben ingestemd om mijn paranimfen te zijn. Ik kan me geen betere paranimfen indenken, vooral als ik bedenk hoe (absurd) rustig ik me voel als ik denk aan de (organisatie van de) grote dag.

Kathrine en Fernand, het zal voor jullie wel een grote overgang zijn geweest, opeens zo'n "Nederlandse" over de vloer. Dank voor jullie gastvrijheid en steun.

Pap en mam, ik hou van jullie. Ik prijs mezelf enorm gelukkig dat jullie mijn ouders zijn. En hoe kan ik dat beter tot uiting brengen, dan dit proefschrift aan jullie op te dragen? En broertje, wat kan ik zeggen? Het is fijn een grote broer te hebben.

De laatste paar regels van dit dankwoord zijn voor een heel speciaal persoon in mijn leven. Ik wil hem natuurlijk bedanken voor alle (theoretische) steun op het werk, maar dat is slechts het topje van de diamant. Mijn liefste Tom, merci voor je geduld, je luisterend oor, je advies en je vriendschap. Maar bovenal: bedankt dat je er bent. Het voelt elke dag opnieuw als een wonder. Met z'n tweetjes stappen we de volgende fase van ons leven binnen.

Karen

Contents

General Introduction

Mie Lasers

Random Lasers

Appendices

General Introduction

Introduction to scattering lasers

These days the laser is an essential tool in our society. In many households the laser is used on a daily basis, for example in compact-disc (cd) and digital-versatile-disc (dvd) players, or in hospitals where the laser is used for high-precision surgery. The ongoing developments in nanotechnology (for example the decrease of the length scales of integrated optical components) have led to the quest for nanolasers. In general, the behavior of such small lasers is rather hard to describe theoretically. In this thesis we will describe experiments on two different small lasers which share two key components: their feedback is implemented through scattering of light, and as such they allow for a (partially) microscopic theoretical description. Due to the nature of their feedback these lasers are referred to as scattering lasers. In section 1.1 we start by giving a qualitative and quantitative description of a conventional laser. In section 1.2 we give a brief introduction to scattering lasers in general. In section 1.3 an overview of this thesis is presented.

1.1   Lasers

Besides the many applications that have been discovered since the first experimental demonstration in 1960 by Theodore Maiman [63], the laser itself has also been subject of intense scientific study. The main part of conventional-laser theory uses the amplification-plus-cavity mechanism.[92] In Fig. 1.1 a scheme of a conventional laser is presented. The amplification of light in the cavity takes place in the gain medium (G), which is pumped by an external pump source (PS). The cavity is
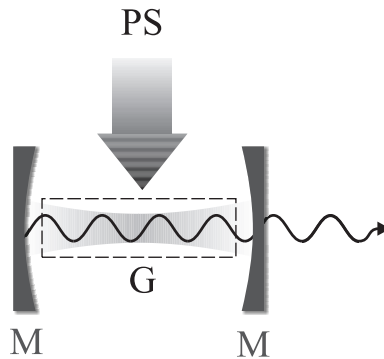
Figure 1.1: Schematical impression of a laser: two mirrors (M) with a gain medium (G) in between. The two mirrors form a cavity, which confines the light and provide the optical feedback. The right mirror is partly transmitting. One of the cavity modes is shown. The gain medium is pumped with an external pump source (PS). The resulting laser light is directional, with a small spectral bandwidth. (Figure taken from [83])

formed by two mirrors (M), which confine the light and provide optical feedback. One of the two mirrors, the right one in Fig. 1.1, is partly transmitting. In the cavity light intensity can build up in one or several laser modes, of which one is shown. The resulting electromagnetic radiation (light) that exits a single-mode cavity has a narrow spectral bandwidth that is orders of magnitude narrower than that of spontaneous emission.

1.1.1 Population inversion

The essential elements of a laser system, i.e. a gain medium and a feedback mechanism, come in a great variety of forms and fashions. For simplicity we will assume from now on that the gain medium consists of molecules. The pumping process excites these molecules into a higher quantum-mechanical energy level. For laser action to occur, the pumping process must produce not only excited molecules, but must in addition induce population inversion. Population inversion means that there are more molecules in the excited state than in the ground state. If population inversion is present in the cavity, light in the system can be amplified.

1.1.2 Threshold

A laser will lase when the loss inside the cavity (for example caused by light leaking out of the cavity) equals the gain. The point at which the gain exactly compensates the loss is referred to as the threshold of the laser. At threshold, the net round-trip gain factor (taking into account both losses and gain the light experiences in a
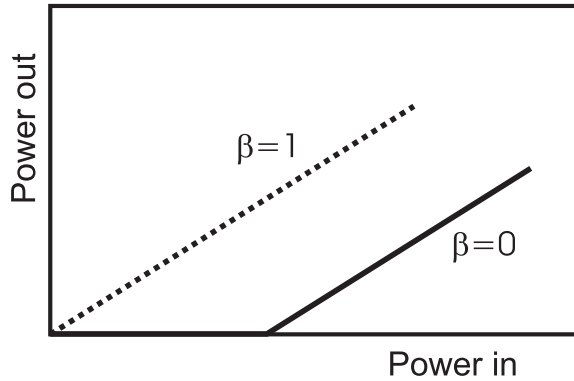
Figure 1.2: *The influence of β on the shape of the power out versus power in curve. This curve is plotted for two extreme cases: $\beta = 1$, and $\beta = 0$. When all the emitted photons end up in the lasing mode $\beta = 1$ (dotted line), the laser has no threshold. If $\beta = 0$ (solid line) the laser has a well-defined threshold. The value of the power in where the slope of the $\beta = 0$ curve changes, is referred to as the threshold power.*

round trip) is unity. In experiments this threshold can be observed for instance in the power out versus power in graph, as we will show below.

1.1.3 Beta factor

A quantitative description of a laser system is given in terms of rate equations.[92] These equations describe the time evolution of the number of excited molecules N_1 and the number of photons q inside the cavity. It is clear that the fraction of the pumping power P absorbed by the molecules inside the cavity is of great importance, since this pumping has to establish population inversion. Furthermore the loss, that is photons that leak from the cavity mode, should be taken into account; this is done by introducing the cavity decay time τ_c. The spontaneous-emission life time of excited molecules, τ, is an important parameter. Using these parameters we can formulate the rate equations

$$\frac{dN_1(t)}{dt} = P(t) - \frac{\beta q(t) N_1(t)}{\tau} - \frac{N_1(t)}{\tau}, \tag{1.1a}$$

$$\frac{dq(t)}{dt} = -\frac{q(t)}{\tau_c} + \frac{\beta N_1(t)}{\tau} \left[q(t) + 1 \right]. \tag{1.1b}$$

The first equation describes the temporal evolution of the excited molecules N_1. The first term is the pumping term, followed by the stimulated-emission term. The last term describes the spontaneous emission of the excited molecules. The second equation describes the temporal evolution of the number of photons q in the cavity.

The first term describes the photons that leak from the cavity mode, followed by the stimulated emission term. The last term describes the spontaneous emission. In these equations one more parameter has been introduced: the β factor of a laser. The definition of β is the amount of spontaneous emission that contributes to the lasing mode. The rest of the spontaneous emission does not contribute to the lasing mode is lost and does not contribute to q. As β represents a fraction, its value is always between 0 and 1.

The behavior of a laser for the two limits of β is given in Fig. 1.2. When β is equal to 1 all the spontaneously emitted photons end up in the laser mode. When we plot the power out versus the power in of the laser, we will retrieve a straight line through the origin. When β is 0 the laser has a well-defined threshold. The pump power at which the net round-trip gain is unity is the threshold pump power, corresponding to the point in Fig. 1.2 where the slope changes abruptly. For $0 < \beta < 1$ there is a threshold, which becomes less sharp as β gets larger.

1.2 Scattering lasers

A scattering laser is a laser in which the feedback is provided through scattering of light, instead of being provided by a cavity.[83] In this thesis we will discuss two scattering lasers. In section 1.2.1 we describe a special class of scattering laser: the Mie laser. The Mie laser consists of only one sphere, and can therefore be fully analytically described. In this sphere, the light is multiply scattered at the boundary of the sphere. In terms of scattering particles, the Mie laser is a one-body system. A Mie laser can also be described as a cavity laser. Conversely, in section 1.2.2 we proceed by exploring the many-body limit and introduce random lasers, in which the feedback is provided by multiple scattering of light at many scattering particles.

1.2.1 Mie lasers

In a Mie laser, the mirrors of a conventional laser are replaced by the boundary of a microsphere. Light is multiply scattered at the boundary, and along the boundary whispering gallery modes at a certain wavelength exist for specific sizes of the sphere. The name of these modes refer to the observation of Lord Rayleigh in the dome in St. Paul's Cathedral in London: He observed sound ("whispers") propagating along the walls and circling around the dome several times. A whispering gallery mode is depicted in Fig. 1.3. Whispering gallery modes occur at particular resonant wavelengths of light. At such resonant wavelengths, the light undergoes total internal reflection at the particle surface, and, after one roundtrip, interferes constructively. Experimentally Ashkin and Dziedzic were the first to observe optical whispering gallery mode resonances in microspheres.[8] In the Mie laser described
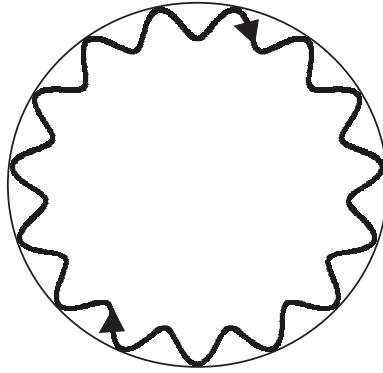
Figure 1.3: Schematical impression of a whispering gallery mode inside a microsphere. Light propagates along the boundary of the sphere, and interferes constructively after one round trip. If the whispering gallery mode is above its threshold, the intensity in that mode increases after each round trip.

in this thesis, the gain medium is inside the microsphere, and light is amplified in a whispering gallery mode along the border of a microsphere.

1.2.2 Random lasers

In 1968 Letokhov predicted that light amplification is possible in a random medium with "negative absorption", i.e. gain.[58] A clear experimental demonstration of such a random laser was done by Lawandy and coworkers in 1994.[56] In a random laser, the mirrors of a conventional laser are replaced by many small scatterers (typical radius of a scatterer is 100 nm). In the random laser systems described in this thesis, the scatterers are dispersed in a medium that has gain. A visualization of a random laser system is depicted in Fig. 1.4. Through spontaneous emission events, excited molecules emit photons inside the random laser. These photons propagate along a random path through the sample. Along this path the light is amplified and may reach a lasing threshold. In contrast to the conventional laser, the resulting laser light is omnidirectional.

1.3 Overview of this thesis

In this thesis we will describe experiments on scattering lasers. The next part of this thesis will describe experiments on and theory of Mie lasers, a one-body scattering laser. In chapter 2 a detailed introduction is given to Mie lasers, followed in chapter 3 by a description of our experimental apparatus used for our experiments on
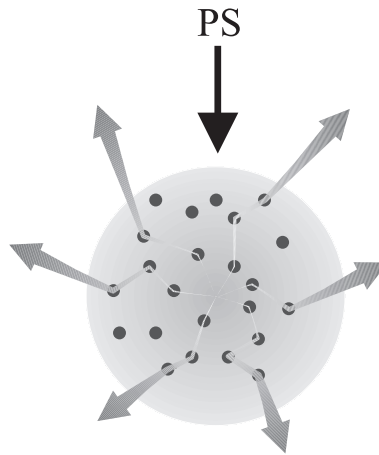
Figure 1.4: Schematical impression of a random laser: a gain medium (gray area) with randomly placed scattereres. The gain medium is pumped with an external pump source (PS). The resulting laser light is omnidirectional. (Figure taken from [83].)

Mie lasers. In chapter 4 experimental results, combined with extended Mie theory will be discussed.

After the one-body system (Mie laser) is fully explored, we will continue in the last part of of this thesis with the many-body limit: the random laser. We start in chapter 5 with a detailed description of the random laser, and the current models for this type of scattering laser. In chapter 6 we give a description of the used random laser samples and setups. In chapters 7, 8, 9, and 10 we describe experimental and theoretical work on random lasers.

Mie Lasers

2

Introduction to Mie lasers

The first class of scattering lasers we discuss in this thesis are Mie lasers. Mie lasers are a special class of microcavity lasers, consisting of a single small dielectric sphere with gain in which light can be amplified. Their attractiveness lies in their ability to be described analytically. In section 2.1 we will give a short overview of measurements on microcavities in general, followed in section 2.2 by an introduction to Mie theory. In section 2.3 we will introduce an extension and an extrapolation of Mie theory.

2.1 Microcavities

Optical microcavities have been studied extensively in recent years and can have different geometries, like posts, toroids and spheres.[101] The theoretical advantage of microspheres compared to the other geometries is that light scattering off a single sphere can be analytically described. Mie [66], Debye and Lorentz [17] all worked on a theory, generally referred to as Mie theory, that describes the scattering and absorption of electromagnetic waves by spherical particles, and cylinders of infinitely length. Chew applied this Mie theory to light sources (dipoles) inside the sphere.[28, 29] Full treatments of the scattering of light waves off spherical particles can be found in various textbooks.[17, 103] Mie theory predicts the existence of morphology-dependent resonances (MDRs).

Experimentally, Ashkin and Dziedzic were the first to observe optical MDRs in the scattered field intensity of a microsphere.[8] They attributed these resonances to dielectric surface waves, and compared the results to Mie theory. Optical reso-

11
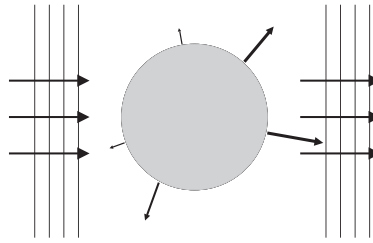
Figure 2.1: *Visualization of an incident continuous plane wave (left of the figure) that is scattered. The resulting field, computed with Mie theory, is a superposition of the incoming and the scattered wave.*

nances were observed in other materials as well, for instance Benner *et al.* measured MDRs in polystyrene spheres [15], and Holler and coauthors observed the MDRs in the spontaneous emission spectra of fluorescent microdroplets [47]. Holler *et al.* compared the spectra to the applied Mie theory by Chew. Mie theory will be discussed below shortly.

In the presence of gain, the MDR of a Mie sphere can become a laser mode. The microspheres with gain in terms of lasing oscillations have resonances with a high quality factor for such a small geometry.[101] The first experimental observation of laser oscillation in millimeter-sized spheres was done by Garrett and coauthors.[37] Laser oscillations are also observed in droplets,[59, 77, 100] cylindrical silicon nitroide microcavities,[10] polystyrene microspheres,[53] and silica spheres.[20, 82]

2.2   Mie Theory

Mie theory describes the scattering of an incoming continuous plane wave off a sphere.[17] In this theory metallic, magnetic, and dielectric spheres can be considered; we will focus on dielectric spheres. A visualization of this incoming wave and the scattering of this wave by a microsphere is depicted in Fig. 2.1. A plane wave propagates through free space and is scattered by the sphere. Mie theory describes the resulting field, which is a superposition of the incoming and the scattered wave.

2.2.1   General introduction

We will not give a complete derivation of Mie theory, as full treatments can be found in several textbooks.[17, 103] We will only give relevant formulas that are used in chapter 4. We use with respect to the time harmonic factor the convention of Van de Hulst ($e^{i\omega t}$).[103] The magnetic permeability is set to 1.

We consider an incident wave of unit amplitude

$$\mathbf{E} = \mathbf{a_x}e^{-ikz+i\omega t},\tag{2.1}$$

$$\mathbf{H} = \frac{n_0}{c}\mathbf{a_y}e^{-ikz+i\omega t},\tag{2.2}$$

with $\mathbf{E}$ the electric field, $\mathbf{H}$ the magnetic field, $\mathbf{a_x}$ and $\mathbf{a_y}$ unit vectors along the x-axis and y-axis, k the wave number (given by $2\pi n_O/\lambda$, with λ the wavelength of light in vacuum, c the speed of light in vacuum, and n_O the refractive index of the surrounding medium), z the propagation direction, and ω the circular frequency of the light. This incident wave is scattered off a spherical particle with radius a and refractive index n_I. The sphere is surrounded by a medium with a refractive index n_O. The resulting scattered field far away from the sphere is given in spherical coordinates by

$$E_\theta^{sca} = \frac{c}{n_O}H_\phi^{sca} = -\frac{i}{kr}e^{-in_O kr+i\omega t}\cos\phi S_2(\theta),\tag{2.3a}$$

$$E_\phi^{sca} = \frac{c}{n_O}H_\theta^{sca} = \frac{i}{kr}e^{-in_O kr+i\omega t}\sin\phi S_2(\theta),\tag{2.3b}$$

$$E_r^{sca} = H_r^{sca} = 0,\tag{2.3c}$$

with $S_1(\theta)$ and $S_2(\theta)$ the scattering amplitude functions

$$S_1(\theta) = \sum_{n=1}^{\infty}\frac{2n+1}{n(n+1)}\left[a_n\pi_n(\cos\theta) + b_n\tau_n(\cos\theta)\right],\tag{2.4a}$$

$$S_2(\theta) = \sum_{n=1}^{\infty}\frac{2n+1}{n(n+1)}\left[b_n\pi_n(\cos\theta) + a_n\tau_n(\cos\theta)\right],\tag{2.4b}$$

where in this formula n represents the mode number, indicating the number of light wavelengths around the circumference of the sphere. The angle dependent functions π_n and τ_n are functions of the P_n^1 Legendre polynomials.[103] The parameters a_n and b_n are the scattering coefficients of the sphere.

2.2.2 Scattering coefficients a_n and b_n

The scattering coefficients a_n and b_n are given by

$$a_n = \frac{n_O\psi_n'(y)\psi_n(x) - n_I\psi_n(y)\psi_n'(x)}{n_O\psi_n'(y)\zeta_n(x) - n_I\psi_n(y)\zeta_n'(x)},\tag{2.5a}$$

$$b_n = \frac{n_I\psi_n'(y)\psi_n(x) - n_O\psi_n(y)\psi_n'(x)}{n_I\psi_n'(y)\zeta_n(x) - n_O\psi_n(y)\zeta_n'(x)},\tag{2.5b}$$

where the variable $x = n_O ka$ is the size parameter of the system, and $y = n_I ka$. The prime denotes differentiation with respect to the argument. The functions ψ_n en ζ_n are the Ricatti Bessel functions.[103]
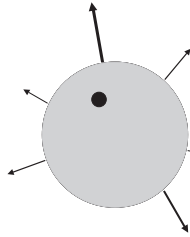
Figure 2.2: A schematic impression of a sphere with dipole sources inside. The resulting field, computed with the applied Mie theory by Chew, originates from the oscillating dipoles in the sphere.

2.2.3 Width of the resonances

It can be shown that a pole in the scattering coefficient a_n gives rise to a transverse-magnetic (TM) mode, while a pole in b_n defines the transverse-electric (TE) modes. The presence of a pole in a_n or b_n reflects the existence of a resonance; if this resonance is narrow, we speak of a morphology-dependent resonance (MDR). The real part of the pole is the spectral position of the resonance, and the imaginary part is, for narrow resonances, the width Γ of the resonance.[55] Both TE and TM modes are MDRs.

2.3 Applications and extrapolations of Mie theory

2.3.1 Application of Mie theory: dipole sources

Chew has applied Mie theory to a dipole source at any position, both outside and inside the sphere.[28, 29] In Fig. 2.2 a schematic impression of the scattering of light described by this applied Mie theory is shown. Instead of considering scattering off an incident wave, we now consider scattering of light emitted by point sources (dipoles) inside the sphere. This applied Mie theory describes the field of the scattered wave.

As a side remark, we note that the poles of the scattering coefficients are the same for both Mie theory and the applied Mie theory by Chew. Therefore, the width of the resonance from both theories are the same.[17, 28]

2.3.2 Extrapolated Mie theory to the gain regime

In Mie theory the refractive index of the sphere n_I can be any complex-valued number. The imaginary part of the refractive index represents the loss (negative) or gain

(positive) of the medium under consideration. Various authors have extrapolated Mie theory to the gain regime (this extrapolation is referred to as EMTG) to calculate time-independent scattering coefficients of spheres with gain.[3, 30, 48, 50, 51, 79] We will show in chapter 4 that this extrapolation is only valid up to the laser threshold.

Experimental details of Mie laser measurements

In section 3.1 we will give a description of the Mie laser samples, followed in section 3.2 by a description of the experimental setup used to measure these samples.

3.1 Samples

The samples used in the Mie-laser experiments consist of a suspension of dye-doped polystyrene microspheres in water from Duke Scientific Corporation (catalogue number G1000), with a specified mean diameter of 10.1 μm, and a specified size dispersion of 5% (standard deviation). The spheres are composed of polystyrene and doped with a dye. The molecular structure of this dye is considered a trade secret. This dye has a specified quantum efficiency of 60%. The specified amount of dye inside the microspheres is 2% by weight of the polystyrene. Since the dye is incorporated in the polymer matrix (the dye is mixed with the polymer during the production process of the spheres), leakage of the dye into the solution is excluded and the dye concentration according to Duke Scientific is homogeneous throughout the microsphere. A typical emission spectrum of an ensemble of dye-doped polystyrene microspheres is plotted in Fig. 3.1. This spectrum is measured with a concentration of 10^{12} microspheres cm^{-3}, and a CW Argon laser with a wavelength of 447 nm. The peak of the emission spectrum is at 19500 cm^{-1}.

For a determination of the absorption index (negative imaginary part of the
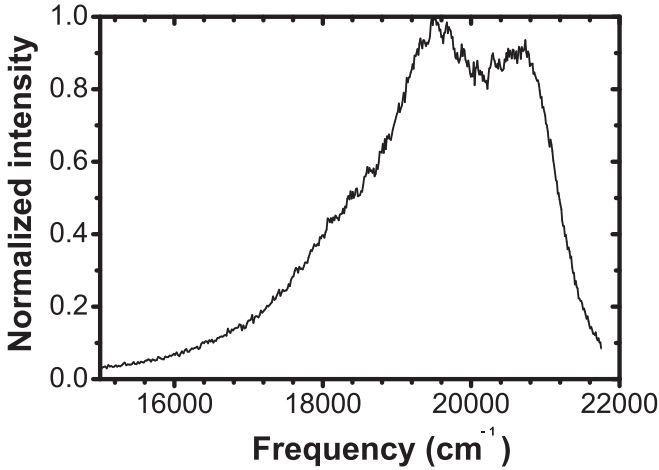
Figure 3.1: Measured emission spectrum of an ensemble of dye-doped polystyrene microspheres. The intensity is normalized to its maximum. The emission maximum is at 19500 cm^{-1}.

refractive index) of the spheres, we have measured the emission linewidths with low-power continuous-wave excitation at as wavelength of 488 nm (the experimental setup used for this measurement is described in the next section). From this linewidth we obtain a value for the absorption index of $(1.5 \pm 1.5) \times 10^{-5}$ at an emission frequency of 19500 cm^{-1} using the formula for the width as described in section 2.2.3.

3.2 Experimental apparatus

The suspension of the dye doped polystyrene microspheres with a sphere concentration of 6000 cm^{-3} is put in a borosilicate glass capillary from VitroCom Inc., with internal dimensions $0.1 \times 2 \times 40$ mm^3 (glass thickness, 0.1 mm). The ends of the capillary were closed by melting. With this concentration we have a reasonable amount of spheres in the glass capillary (30-50 microspheres), without clustering of the spheres.

The setup used for the Mie-laser measurements is schematically depicted in Fig. 3.2. We will first describe the approach to measure the emitted light by a dye-doped microsphere, followed by a description of the trapping of this microsphere.
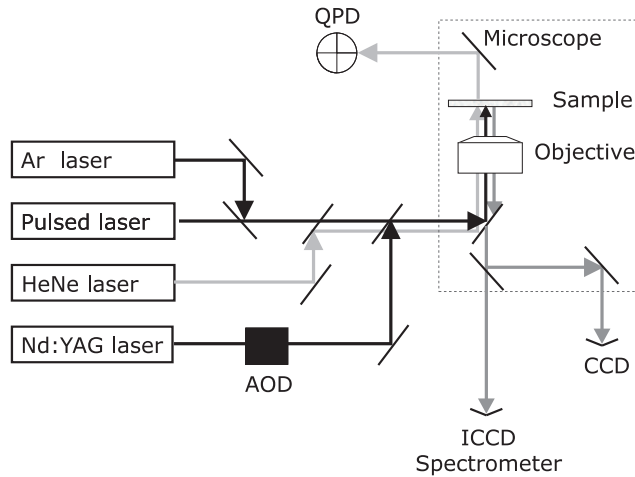
Figure 3.2: Setup used to measure light emitted by dye-doped polystyrene microspheres. Light from a pump laser (either the pulsed laser or the continuous-wave (CW) argon laser) was focused in a microscope on the sample. The emitted light of the sample was collected with the same microscope objective, dispersed by a spectrometer and collected with an intensified charge-coupled device camera (ICCD). At a second output port of the microscope a charge-coupled device camera (CCD) was attached to obtain information about the sample. This sample consists of a polystyrene microsphere, trapped with optical tweezers. The trap laser of the optical tweezers is the Nd:YAG laser. Light from this laser is guided through a set of acousto- optic deflectors (AOD), with which the angle of the light is controlled. The helium neon (HeNe) laser is used to characterize the optical trap in terms of the trap stiffness. This trap stiffness is measured with a quadrant photodiode (QPD).

3.2.1 Measurement of the emission of a dye-doped microsphere

To measure the emission of a dye-doped microsphere, we used two different pump sources: a continuous-wave (CW) and a pulsed source. The CW source is an argon laser (Spectra Physics, Satellite 2016) and is used for low-power CW excitation. The maximum output power of this CW laser is 30 mW at a wavelength of 488 nm. As a pulsed pump source we used the output of an optical parametric oscillator (OPO), pumped by a Q-switched Nd:YAG laser (Coherent, Infinity 40-100/XPO). The pump pulse had a duration of 3 ns and a repetition rate of 50 Hz. The pulse energy is 15 mJ at 470 nm. The pulse energy incident on the sample is controlled with two Glan laser prisms, the light was attenuated to approximately 100 nJ per pulse at the sample.

To measure the pulse energy at the sample, we placed an anti-reflection coated round-wedge prism (Thorlabs) in the pump beam, after the Glan laser prisms. The reflection of the light on this prism was collected with a photodiode (PDA55, Thorlabs), which was readout by an oscilloscope (Tektronix TDS 2024). The signal of this oscilloscope was calibrated with the light intensity coming through the microscope objective with an Ophir power meter (PD300-3W).

The pump light was guided into a microscope (Nikon, TE2000-U), and slightly defocused on the sample with a microscope objective (water-immersed, numerical aperture NA = 1.2, Nikon CFI Plan Apochromat 60x WI). Since we slightly defocused the light on our sample, the whole microsphere is illuminated. Our microscope has several output ports. In this setup we used three ports.

The first port guided the light to the intensified charge-coupled device camera (ICCD) and spectrometer (Oriel Intstruments, type MS257): The light emitted by the sample was collected by the same water-immersed microscope objective, dispersed by the spectrometer and recorded by the ICCD. The ICCD-spectrometer combination has a Gaussian response function with a width of 4 cm^{-1}. One count on the ICCD corresponds roughly to one emitted photon. Below threshold we averaged over 10.000 pulses and above threshold over 500 pulses to obtain a good signal-to-noise ratio. The emission spectra are corrected for background due to stray light.

The second port guided the light to a charge-coupled device camera (CCD, Sony SSC-M388CE). This CCD was attached to the microscope to obtain information about the trapped microsphere, for example how many microspheres are trapped, is there damage of the microsphere.

The third output port at the condensor is used to characterize the optical tweezers and guides the light to an quadrant photodiode (QPD). This port will be discussed below.

3.2.2 Trapping of a dye-doped optical microsphere

Introduction to optical tweezers

A single microsphere was trapped with optical tweezers and lifted by several times its diameter from the surface of the glass capillary. Optical tweezers use radiation pressure, a term that refers generally to forces exerted on matter by the absorption, scattering, emission or reradiation of energy (i.e. by photons). Radiation pressure may manifest itself in several ways.

Perhaps the most familiar form is the *scattering force*, which is defined as the force due to light scattering that is proportional to the light intensity and acts in the direction of propagation of light. Optical tweezers, however, owe their trapping ability to the *gradient force*, which is proportional to the spatial gradient in light intensity: a strong gradient near the focus creates a potential well, in which a particle with a refractive index higher than its surrounding medium is trapped in three dimensions.

The use of optical tweezers was first demonstrated by Ashkin.[7] He demonstrated that optical forces could displace and levitate micron-sized particles in different environments. Together with Dziedzic he showed the use of the levitation trap: a single vertical beam confines a macroscopic particle at a point where gravity and the upward scattering force are in balance.[8]

Optical tweezers - experiment

The laser used to trap single microspheres was an infra-red laser (Laser Quantum Ventus, cw Nd:YAG) emitting at 1064 nm. The maximum output power of this laser is 3.5 W in a single transversal mode. As polystyrene is transparent at 1064 nm, this laser does not heat or deform the microspheres. The beam path of the trapping laser was fully shielded to prevent additional noise in the laser trap due to airflow.

The laser beam passed through a two-axis acousto-optic deflector system (AOD system, IntraAction Corporation, DTD-274HD6). This system consists of two AOD's and can control the angle of light in two directions: An AOD is a dynamic grating created by passing a sound wave through a tellurium dioxide crystal. The total transmission of light through this AOD system was 40%. The position of the beam in the focal plane could be controlled by changing the frequency of the sound wave in the crystal.[38, 57] After the AOD system, the beam waist was expanded four times to a diameter of 20 mm to ensure complete filling of the water-immersed microscope objective.

Optical tweezers - characterization

The position of the microsphere, and the trap stiffness of the optical tweezers was determined with a helium neon (HeNe) laser and a quadrant photodiode (QPD,

type Spot 9DMI, UDT). This laser emits light with a wavelength of 632.8 nm, and a power of 5 mW (Melles Griot, 25LHP151-230).

The port at the condensor lead to the QPD, which was placed in the back focal plane of the condensor. The QPD consists of a square grid of four Silicon photodiodes. By adding and subtracting the signals of these four quadrants the three-dimensional position and movement of the microsphere can be determined.[75, 80] In our experiments the position detection was only done in two dimensions by imaging the trapped microsphere on the QPD. We used for this imaging the HeNe laser, and not the trapping laser, since silicon photodiodes are more sensitive and faster at a wavelength of 632.8 nm. The attained detection bandwidth was 100 kHz, with an accuracy of $1 \, nm/\sqrt{Hz}$. The accuracy was limited by the background noise level of the electrical circuits in the QPD.

An experimental method to characterize the trap is to determine the trap stiffness. This determination is done by looking at the power spectrum of the Brownian motion of a trapped microsphere.[97] Brownian motion is in our system caused by thermal fluctuations in the water. As a result of these fluctuations, the particle moves in a random way due to collisions with water molecules. When the particle is trapped, the Brownian motion of this particle is smaller than the motion of an untrapped particle. By Fourier transforming the time-resolved signal on the QPD the power spectrum of the Brownian motion of the trapped particle is obtained and the trap stiffness (in units of force) can be calculated.[40] The trap stiffness depends on the power of the trap laser: a higher power leads to a stiffer trap. For a power of 1 W of the trap laser, the trap stiffness in the lateral directions was 190 pN/µm. The experimental uncertainty in the trap stiffness is 25%.

Generally, the trap stiffness in both lateral directions (x and y) is comparable as the intensity gradient of the trapping laser is cylindrically symmetrical around the axial direction. In the axial direction (z) the intensity gradient of the trapping laser is lower, resulting in a lower trap stiffness compared to the lateral direction. We have not measured the axial trap stiffness, but in our system the axial trap stiffness was still good enough to lift 10.1 µm diameter polystyrene microspheres from the surface.

Laser threshold of Mie resonances

In this chapter we describe an experimental and theoretical study of the laser properties of a Mie laser.[108] An impressive body of experiments on microspheres has been successfully described with Mie theory (see, e.g., the selection of Ref. [52] and the recent papers of Refs. [20, 21, 53, 59, 82]). As we described in section 2.3, various authors have extrapolated Mie theory to the gain regime (referred to as the EMTG) to calculate time-independent scattering coefficients of spheres with gain, an approach widely used.[3, 30, 48, 50, 51, 79]

In this chapter we will show that time-independent scattering coefficients calculated from EMTG have physical meaning only if the gain is below a critical value. This critical value is identified by us as the laser threshold. On basis of this newly developed insight, we performed experiments on dielectric microspheres with gain trapped with optical tweezers. We start in section 4.1 by elaborating on Mie theory in spheres with gain. In section 4.2 we describe our experimental apparatus. In section 4.3 we discuss our experimental observations, followed in section 4.4 by a comparison between our experimental results and the EMTG.

4.1   Violation of Kramers-Kronig relations

In chapter 2 we described that microspheres can exhibit laser oscillations in the presence of gain. This lasing process occurs predominantly in the morphology-dependent resonances (MDRs).[101] In the extrapolated Mie theory to the gain regime (EMTG), gain is introduced as a positive imaginary part in the refractive

index of the sphere.[3, 30, 48, 50, 51, 79] This imaginary part of the refractive index is referred to as the gain index. (We follow the standard convention that absorption corresponds to a negative sign of the gain index.[14, 45])

Using the method presented in section 2.2.3, we calculate the width of the MDRs for a sphere with gain, as a function of the gain index. This calculation shows that at a critical value of the gain index the spectral width becomes zero, and the corresponding emission intensity diverges. Exactly at this point, the round trip amplification is equal to one [70], and the laser is at threshold. Above threshold EMTG predicts Mie resonances to have negative widths, i.e. the poles of the scattering coefficients have shifted from the lower half to the upper half of the complex plane. This shift has drastic consequences: if the poles are above the real frequency axis, the scattering coefficients (evaluated at real frequencies) no longer have any physical meaning.[93] Specifically, a causal time-independent response function cannot be obtained by the usual Fourier-Laplace transform along the real frequency axis. Various phenomena have been erroneously predicted from EMTG in this regime, such as broadening of resonance lines and decrease of scattered intensity with increasing gain,[3, 30, 48, 50, 51, 79] all based on the physically meaningless scattering coefficients at real frequency. In appendix A we elaborate more on the origin of the break-down of causality above the laser threshold. We stress that for small gain, i.e. up to threshold, the predictions from EMTG are correct. To model the laser at and above threshold one should introduce pump and gain dynamics, thus avoiding any divergence.

4.2 Experimental apparatus

The measurements are performed on polystyrene spheres in water. These microspheres are doped with a fluorescent dye with a broad emission band $\lambda_0 = 480 - 540$ nm, see for more details section 3.1. A single polystyrene is trapped with optical tweezers and lifted by several times its diameter from the surface of the glass capillary the spheres were put in. More details can be found in section 3.2.

4.3 Experimental observations

We have measured the emitted light of a dye-doped polystyrene microsphere. In Fig. 4.1(a) we present the measured emission spectrum for low pumping power (1 nJ/pulse on the sample). The morphology-dependent resonances (MDRs) are clearly observed and are characterized by their mode numbers and additonally labeled TE (transverse electric) or TM (transverse magnetic).[17] The theoretical curve in Fig. 4.1(a) that is fitted to the experimental data was convolved with the Gaussian response function of the spectrograph and has been normalized to
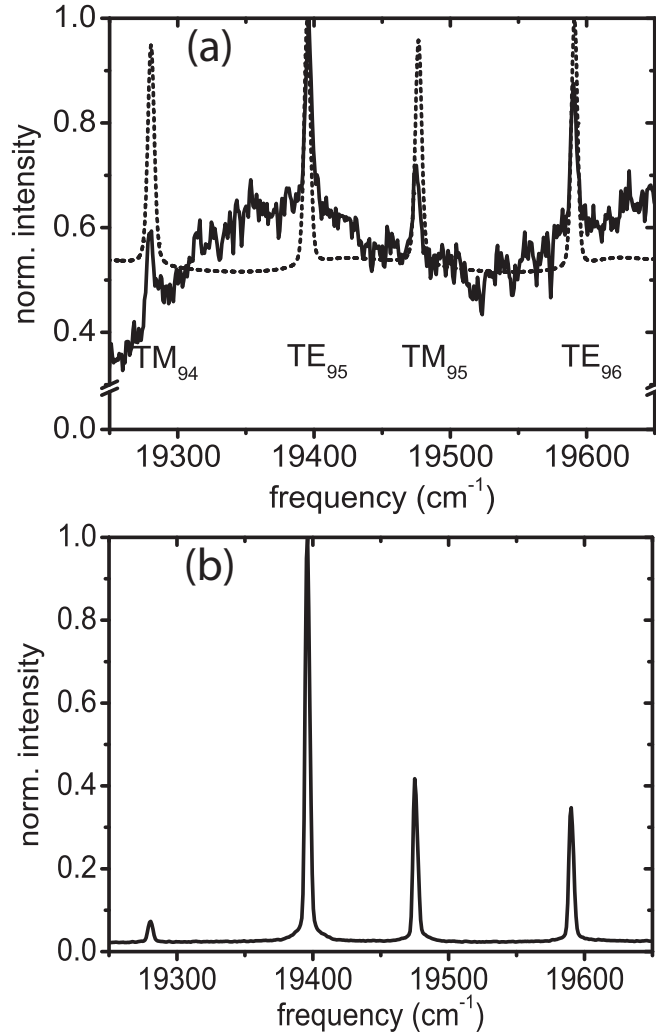
Figure 4.1: (a) Experimental emission spectrum of a microsphere excited with a low pumping power of 1 nJ/pulse (normalized to the peak intensity of the TE_{95} mode). The dashed curve shows a theoretical fit of Mie theory. (b) Experimental spectrum of the same sphere measured at 100 nJ/pulse, above threshold.
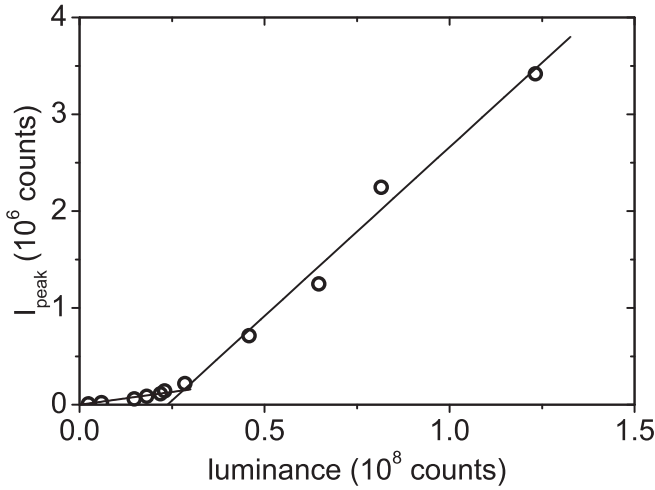
Figure 4.2: Measured integrated intensity in the TE_{95} mode versus luminance of a sphere with gain (the lines are a guide to the eye). The laser threshold is clearly visible.

the peak intensity of the TE_{95} mode. Fit parameters were n'_I, the real refractive index of the sphere, and a, the radius of the sphere. We found the best fit for $n'_I = 1.583 \pm 0.001$ and $a = 5.29 \pm 0.01$ µm. The value for n'_I corresponds within 1% to reported measurements on pure polystyrene micospheres.[62] As can be seen in Fig. 4.1(a), our measured and calculated emission spectra are in good agreement.

In Fig. 4.1(b) we show the experimental emission spectrum of the same microsphere ate a pulse energy of 100 nJ/pulse, which is above threshold. Three intense modes are visible in the spectrum with an intensity of up to 30 times the intensity of the fluorescent background and a width smaller than the width of the peaks below threshold. We have verified that all three modes (TE_{95}, TM_{95}, and TE_{96}) are above threshold, show similar behavior, and that their widths remain constant if the pump intensity is further increased. In the next section, we discuss only the results for the TE_{95} mode, which has the lowest threshold. We explore the data only up to this threshold. In this regime no other modes are lasing, and the intensities of the different modes below threshold are low enough that mode competition may be ignored.

4.4   Laser threshold and EMTG

We verify the lasing behavior of TE_{95} by considering the integrated intensity in the laser mode at 19400 cm^{-1} versus the luminance. The luminance is defined as the integrated intensity in the complete emission spectrum and is proportional
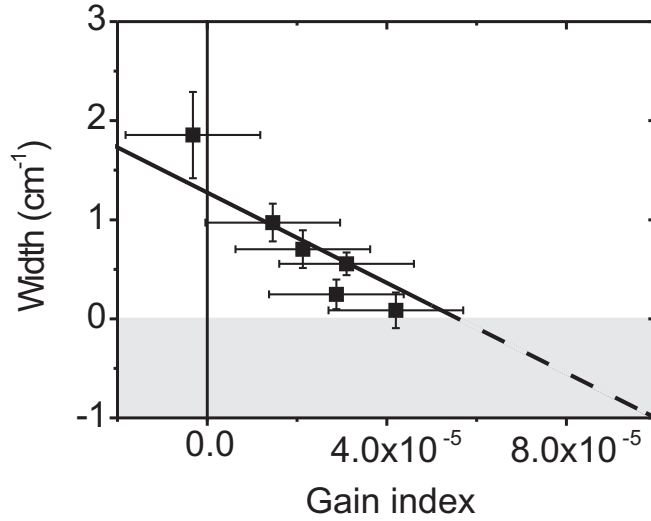
Figure 4.3: Width of the TE$_{95}$ mode versus the gain index. The line represents the calculated width from EMTG. The squares are data points from fits to the measured spectra. The error bar for the width are taken from the fits; the error bars for the gain index are taken from cw experiments. The gray area indicates the nonphysical area. Above the laser threshold the measured data points are not presented, as the gain saturates in the experiment.

to the pump power absorbed by the microsphere. Figure 4.2 shows the resulting integrated intensity versus the luminance. We see the expected threshold behavior for a laser (see also section 1.2) and obtain from this graph the laser threshold in terms of luminance.

We now compare the prediction of our model, i.e. the point at which the width becomes zero is the laser threshold, with our experiments. For the measured emission spectra (below and above threshold), we determined the Lorentzian width of the TE$_{95}$ by fitting it with a Voigt profile. A Voigt profile is a convolution of a Lorentzian and a Gaussian profile. The Gaussian linewidth is equal to the response of the intensified charge-coupled device camera. We know the theoretical width from EMTG as a function of the gain index, and the experimental widths as a function of the luminance. A linear relation is assumed between the luminance and the gain index. Two points fix their relation: at threshold we know both the gain index (from the fit to our data) and the luminance (see Fig. 4.2); at zero luminance the gain is zero and the (negative) gain index is given by the absorption of the sphere.

In Fig. 4.3 we present the theoretical as well as the experimentally observed width of the TE$_{95}$ mode as a function of the gain index. Below threshold the data are in good agreement with EMTG. Above threshold we measured a very small linewidth as expected from laser theory with gain dynamics.[92]

As a side remark, we note that one could question the assumption of a homogenous gain, as the pump light will also undergo Mie scattering. However, given the large absorption index due to the dye molecules inside the sphere, Mie resonances are washed out at the pump wavelength.

To conclude this discussion, we now compare our model with a phenomenological formula for the determination of the laser threshold in microspheres reported by Campillo *et al.* [21] We compare our rigorous criterion with this phenomenological approach for a relevant mode, the transverse electric (TE) mode with mode number 95. Campillo *et al.* [21] used essentially as criterion for lasing that the gain per unit length be larger than the loss per unit length. The amplitude gain per unit length is $2/\ell_g$, with ℓ_g given by $\lambda_0/(2\pi n_I'')$. The gain index threshold calculated using the model of Campillo *et al.* lies 7.1% below the value we obtained using the linear relation discussed above. This discrepancy is a direct consequence of the fact that Campillo *et al.* do not take into account that a substantial fraction of the electromagnetic energy of the resonance (7.1% in our case) is stored in the evanescent field just outside the sphere.[18]

4.5   Summary

We observed that in the case of spheres with time-independent gain index EMTG gives physical results up to a certain threshold. We identify this threshold as the laser threshold. Above this threshold, an extended, time-dependent Mie theory (e.g., with pump and gain dynamics) is needed to describe the laser behavior correctly. In our experiments we have measured narrowing of the TE_{95} mode as a function of the gain index up to the lasing threshold, confirming both the validity of EMTG below threshold, and our interpretation of the point of the divergence of the scattering coefficients as the laser threshold.

Random Lasers

5

Introduction to random lasers

In a random laser gain is combined with multiple scattering of light. Typical phenomena of a random laser include a clear threshold behavior, gain narrowing, and in some cases additional narrow spectral emission peaks. In section 5.1 we will give a detailed introduction to random lasers. In section 5.2 we will describe two different models that explain the origin of the narrow spectral emission peaks: the "local-mode" model, and the "open-mode" model.

5.1 Random lasers

In the description of a conventional laser, scattering of light is regarded as loss and detrimental to the laser process. In contrast, in a disordered medium with gain light scattering turns out to have a positive effect on the laser process. Multiple scattering of light increases the time that light spends inside the sample and thus increases the time that the light will be amplified. The combination of multiple scattering of light and gain are the essential ingredients of a random laser. Due to their low threshold and their ease of manufacturing random lasers are expected to be applicable in many utilizations, such as coding of clothes [78] and the detection of dangerous materials [81]. There are two main classes of random lasers: one in which the scatterers themselves have gain, and one in which passive scatterers are embedded in a gain medium. Examples of the first class are zinc-oxide nanorod arrays [119] or zinc-oxide polycrystalline films [27]. Examples of the second class are titanium-dioxide (titania) particles in a solution of rhodamine 640 Perchlorate [56], or aluminium-oxide (alumina) particles in a solution of rhodamine 6G. In
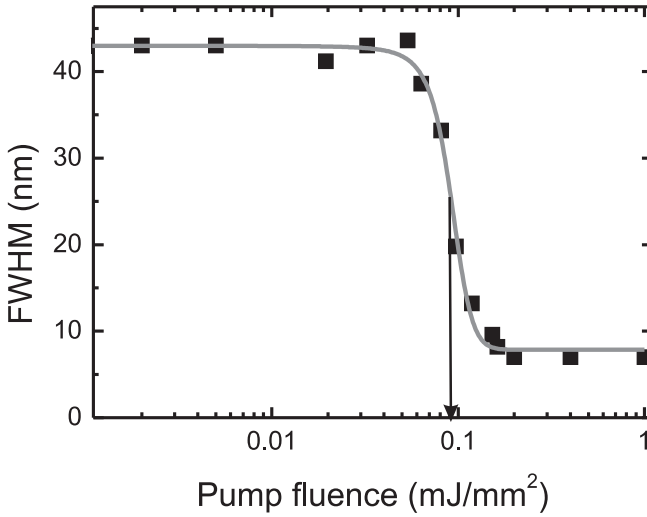
Figure 5.1: Measured width (FWHM) of the emission spectrum versus pump fluence for a titania random laser. The width collapses at the threshold pump fluence, indicated by the arrow.

this thesis we focus on systems with passive scatterers in a gain medium. We will describe some of the known characteristics of random lasers.

5.1.1   Gain narrowing

Gain narrowing denotes a decrease of the width of the spectrum of the emitted light triggered by an increase in the pump fluence. The width will be characterized by the full width at half maximum (FWHM). Gain narrowing is observed in all laser systems.[83] In a random laser the FWHM of the spectrum of the emitted light below the threshold of the laser is approximately the width of the emission spectrum of the gain medium (typical 40 nm). However, far above threshold, this FWHM can be as narrow as 4 nm. A measure for the gain narrowing is the narrowing factor NF, defined as the FWHM of the emitted light below threshold ($\text{FWHM}_{\text{below}}$) divided by the FWHM of the emission spectrum of a random laser far above threshold ($\text{FWHM}_{\text{above}}$)

$$NF \equiv \frac{\text{FWHM}_{\text{below}}}{\text{FWHM}_{\text{above}}}. \tag{5.1}$$

In the case of Fig. 5.1, the narrowing factor (NF) is 5.4 (43/8). The change in the width is sudden: around a certain pump fluence the width decreases rapidly with increasing pump fluence. The pump fluence where the width collapses is also

referred to as the threshold pump fluence, and corresponds in many cases to the same pump fluence at which the slope of the fluence in versus fluence out graph changes, as was depicted in Fig. 1.2. Gain narrowing has been observed in all types of random lasers. [12, 22, 49, 69, 76, 90]

5.1.2 Intrinsic intensity fluctuations

Another interesting random laser phenomenon, first reported by Anglos and coworkers, is the observation of shot-to-shot intensity fluctuations in the emitted light of a random laser, not caused by fluctuations of the pump source.[5] Recently, more and more groups have become interested in these random laser fluctuations, and the underlying principles.[4, 32, 91, 118] We also observed these intensity fluctuations, and will discuss in chapter 7 our experiments, together with a model that clarifies the existence of these fluctuations.

5.1.3 Relaxation oscillations

Relaxation oscillations are well-understood in conventional lasers.[92] Recently, relaxation oscillations were also observed in random lasers pumped with picosecond pump pulses.[94] In chapter 8 we will describe our experimental observation of relaxation oscillations in a random laser system pumped with nanosecond pump pulses.

5.1.4 Narrow spectral features

In 1998 Cao and coworkers discovered narrow spectral features ("spikes") in the emission spectrum of a random laser.[27] An example of an emission spectrum with spikes is shown in Fig. 5.2. The discovery of spikes led to an enormous boost to the field of random lasers: Although spectral narrowing can be explained with a simple amplified spontaneous emission model [69], the occurrence of spikes cannot. Many papers have been published on the observation of spikes in random lasers [23, 36, 67, 68, 74, 119], but there is no general consensus on which parameters influence the occurrence of these spikes. In chapter 9 we present a quantitative analysis that provides a list of parameters that all future publications on random laser experiments should provide. With this prescription, comparison between different experiments, as well as comparison between models and experiments can be performed, and more insight in the physical origin of spikes can probably be obtained.

Besides the many experimental papers, also many theoretical papers appeared that tried to disentangle the physics behind the random lasers.[4, 6, 25, 32, 64, 68, 72, 89, 96] On one hand Cao *et al.* [25], as well as Sebbah and Vanneste [89] and Apalkov *et al.* [6], attribute the spikes to local cavities for light, that are formed
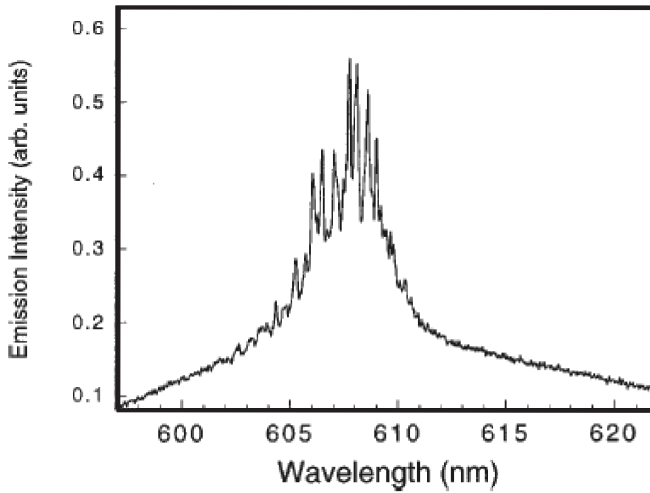
Figure 5.2: Measured emission spectrum of a random laser. Clearly visible are the narrow spectral features on top of the narrowed spectrum, referred to as spikes. (Figure taken from [26].)

by multiple scattering. We will refer to this explanation as the "local-mode" model. On the other hand Mujumdar *et al.* [68], as well as Pinheiro and Sampaio [72], attribute the spikes to single spontaneous-emission events that, by chance, follow very long light paths in the sample and hence pick up a very large gain. We refer to this model as the "open-mode" model. These two approaches are at the moment the two main philosophies trying to explain the origin of these narrow features. In the section 5.2 we will elaborate on both type of models, but first we will discuss the characteristic length scales of a random laser. These length scales are necessary for a clear understanding of the (differences between the) models.

5.2 Models describing random lasers

5.2.1 Local-mode model

In 1997, Wiersma and Lagendijk asked the question: "Can we build a coherent random laser in which feedback is caused by interference in multiple scattering?"[113] In the same line of reasoning Cao and coworkers state that there are two types of random lasers: coherent and incoherent random lasers.[26] According to Cao and coworkers, interference takes place in a coherent or resonant random laser, while in an incoherent or non-resonant random laser no interference effects occur. In their view, the behavior of incoherent random lasers can be described by a model

of light diffusion with gain, where interference effects are neglected.[9] In these incoherent random lasers no sharp spectral features occur.[26] Conversely, according to Cao and coworkers spikes do appear in the emission spectrum of coherent random lasers. In their local-mode model, these spikes are attributed to the existence of local cavities (local modes) for light. Also Sebbah and Vanneste [89] and Apalkov *et al.* [6] attribute the observed spikes to these local modes. The transition between coherent and incoherent random lasers is the transition between coherent feedback and amplified spontaneous emission; According to Cao and coworkers, the scattering strength of the sample, expressed by the transport mean free path of the sample, is the key parameter to distinguish between the different random lasers.[26] According to their model, in a random laser with quenched disorder (the position of the scatterers is rigidly fixed), the spectral position of these spikes is fixed.

We can generalize the line of reasoning of Cao and coauthors. A long path inside the sample ensures enough gain for a spike to occur. In addition, to obtain a spike interference of light is necessary. Therefore, the long path should meet itself again at some point: the long path is folded inside the random laser. The volume that this long path occupies inside the random laser is referred to as the mode volume. This could be the physical origin of spikes that are observed in the emission spectra of some random lasers. In chapter 10 we will elaborate more on this generalization.

5.2.2 Open-mode model

In contrast to to the above local-mode model of Cao and coworkers, Mujumdar *et al.* [68], as well as Pinheiro and Sampaio [72], attribute the spikes to single spontaneous emission events that, by chance, follow very long light paths (open modes) in the sample and hence pick up a very large gain. The influence of these paths on the emission of the random laser is negligible if the gain inside the medium is low, as was computed by Mujumdar and coauthors. In the top of Fig. 5.3 the path length distribution of spontaneously emitted photons in a random laser calculated by Mujumdar *et al.* is depicted. Their calculation is performed with a Monte Carlo simulation. In Fig. 5.3 (b)-(d) the intensity contribution to the emission spectrum as a function of the number of scattering events for various values of pump energy is plotted. The noise in the tail of the path length distribution is not caused by numerical artifacts, but is due to the finite number of excited atoms after a single laser shot. Mujumdar and coworkers show that when the pump energy increases, the contribution of the rare long paths to the emitted light of the random laser increases, until this contribution to the total emission is no longer negligible (Fig. 5.3 (d)); Every long path then corresponds to a spike in the emitted spectrum. In their view, a stronger scattering sample will have a larger chance of producing a spike, but the scattering strength of the sample has no influence if a spike can occur or not. The
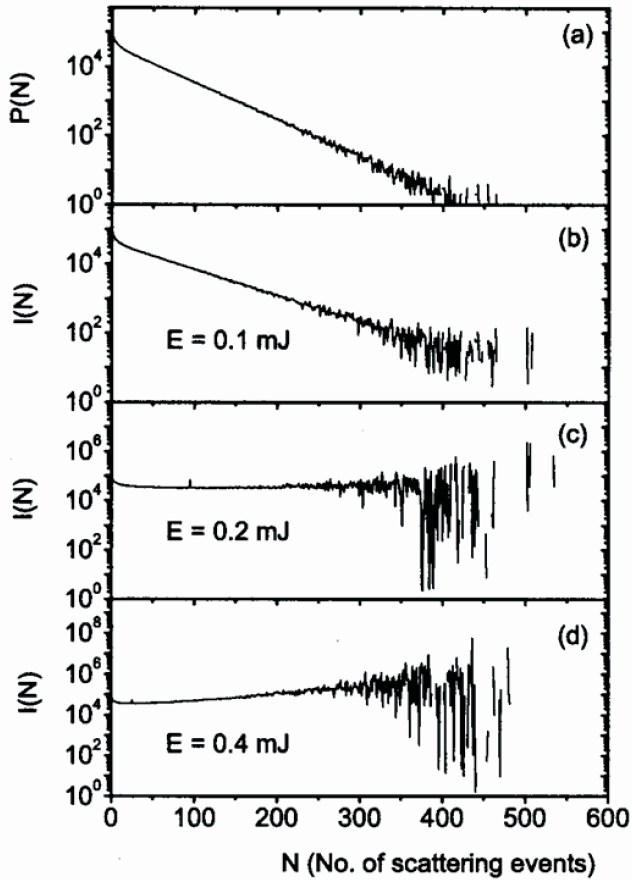
Figure 5.3: (a) Calculated path length distribution of the spontaneous emitted photons. (b)-(d) Intensity contribution to the emission spectrum as a function of number of scattering events for different values of the excitation energy. The noise in the path length distribution is amplified to such an extent that it contributes in a dominating way to the total emission. (Figure taken from [68])

spectral position of each spike differs in every measurement: The "lucky photon" that starts a rare long path (and the corresponding spectral position of the resulting spike) is determined by quantum fluctuations.

5.2.3 Local- versus open-mode model

Differences between the two discussed models taken from literature are:[26, 68]

- In the local-mode model the spectral position of the modes is constant for a random laser with quenched disorder, whereas in the open-mode model the spectral positions can change for every observation (regardless if the position of the scatterers in the sample is rigidly fixed or not).
- The photons are modeled as particles in the open-mode model, and no phase information is included, while in the local-mode model the wave-nature of light is essential.
- According to the local-mode model, a high scattering strength is necessary to observe local cavities, and thus spikes, while in view of the open-mode model the rare long paths can also occur in samples with a lower scattering strength.
- In the local-mode model the spatial extent of a local mode is very small, especially compared to the spatial extent of an open mode in the open-mode model.

In chapter 10 we will compare our experimental observations of a random laser with quenched disorder with the above models. Our results indicate that the local-mode model describes the physics of our random laser better than the open-mode model, but the local-mode model needs more sophistication. In addition, we would welcome the development of new theories.

Experimental details of random laser measurements

For our random laser experiments we have used different random laser samples and apparatus. In section 6.1 we will give a description of the preparation and characterization of the random laser samples, followed in section 6.2 by a detailed description of the experimental setups used to measure these random laser samples. In section 6.3 some general considerations regarding random laser measurements will be discussed.

6.1 Samples

We have used two different random-laser samples: titania (titanium dioxide) samples and porous gallium-phosphide samples. There are two main differences between the samples: the ease of manufacturing, and the rigidity of the samples. The titania samples are very easy to prepare, whereas the gallium-phosphide samples are not. We will discuss the preparation and the characterization of these samples, starting with the titania random laser samples.

6.1.1 Titania random laser

Sample preparation

An amount of 16.8 mg sulforhodamine B from Lambdachrome was added to 30 ml methanol p.a. from Merck (1 mmol/l). To 2.5 ml of this solution 400 mg TiO_2 powder from Sachtleben Chemie GmbH [2] was added. The mean diameter of this powder is 180 nm. The suspension was stirred, and put in an ultrasonic bath for at least 60 minutes. Prior to measurements, the samples were once more put in an ultrasonic bath for at least 60 minutes.

Sample characterization

The transport mean free path of the sample was measured with an escape-function experiment in combination with an enhanced-backscatter-cone experiment.[41, 102, 116] We found a transport mean free path of 0.5 ± 0.1 μm at $\lambda = 633$ nm.

6.1.2 Porous gallium phosphide random laser

This sample consisted of porous gallium phosphide obtained by anodic etching [98] (porosity, 40-50% air; thickness, 48-60 μm). The pores were filled with a 10 mmol/l solution of rhodamine 640 perchlorate from Lambdachrome in methanol p.a. from Merck (pump absorption length, 22 μm; minimal gain length, 12 μm [11]). To ensure the filling of the pores, the sample was placed in the rhodamine 640 perchlorate solution for at least 1 hour before the experiment is performed. In these samples we used a different dye than for the titania samples, since gallium phosphide absorbs light of wavelengths below 560 nm. With rhodamine 640 perchlorate a larger gain can be achieved in the random laser system with a pump wavelength well above 560 nm than with the dye used in the titania samples.

Sample preparation

Gallium phosphide wafers from Marketech (doping 2-8 $\times 10^{17}$ cm^{-3}, n-type) were electrochemically etched in a 0.5 mol/l aqueous solution of H_2SO_4.[33, 42, 98] In contrast to the methods described in these references, we used three steps in our etching process. This new method was applied to remove the top layer of the sample during the electrochemical etch-procedure, instead of removing the top layer with photochemical etching afterwards.[19] The top layer has a higher reflection than the porous gallium phosphide itself, preventing light to enter the strongly scattering material. In Fig. 6.1 a schematic representation of the results of these three steps is depicted. The first step was electrochemical etching at 22.5 V, until an electric charge density of 5 C/cm^2 was reached. The voltage applied has been determined with a current density-potential plot. The voltage of 22.5 V resulted in a high
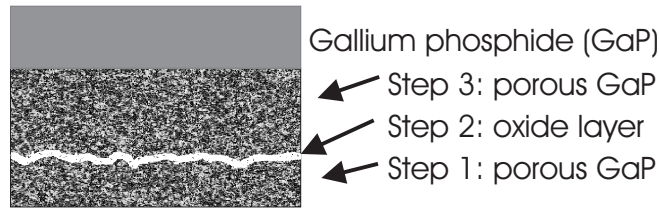
Figure 6.1: *Schematic representation of the etching procedure. The first and third step were identical, only the duration of the etching was different. In these steps, pores were created in the gallium phosphide. The second step was etched at a higher voltage, which resulted in isotropic etching of gallium phosphide. Due to this isotropic etching, the layer created in step 1 was cut off from the layer created in step 3.*

current density in the regime where pores are created. A porous layer was formed. The second step was electrochemical etching at 30 V during 600 s. This voltage was in the regime of passivation due to the formation of an oxide layer. This oxide layer dissolved in the electrolyte, resulting in isotropic etching. The porous layer obtained in the first step was not affected, since etching only occured at the end of the pores. The third step was electrochemical etching at 22.5 V, until an electric charge density of 60 C/cm^2 was reached. The surface of the gallium phosphide after the second step was atomically rough and a new top layer did not form. For more details, see Refs. [42, 98]. Since the oxide layer created with the second step dissolved in the electrolyte, the layer created with the first step in the etching procedure was cut off from the layer created with the third step of the etching procedure. As a result of this cut-off, the top layer was electrochemically removed.

Sample Characterization

The transport mean free path of the samples was measured with an enhanced-backscatter-cone experiment [102, 116]. The effective refractive index of the samples was calculated with three different methods (the Lorentz-Lorenz expression, the Maxwell Garnett theory and the Bruggeman's approach, see for more details Ref. [86]), using the porosity of the sample. The porosity of gallium phosphide can be deduced from the thickness of the porous layer and the electric charge density reached during etching. For a single gallium phosphide atom to be etched 6 electrons are needed, and 1 electric charge density equals 6.25×10^{18} electrons, thus an etching of 1.04×10^{18} gallium phosphide atoms. The density and the molecular mass of gallium phosphide are used to calculate the number of atoms per volume, and thus the total volume of etched gallium phosphide. The total porous volume, combined with the volume of etched gallium phosphide, leads to the porosity of the sample. We found a porosity of 40-50% air, a transport mean free path of
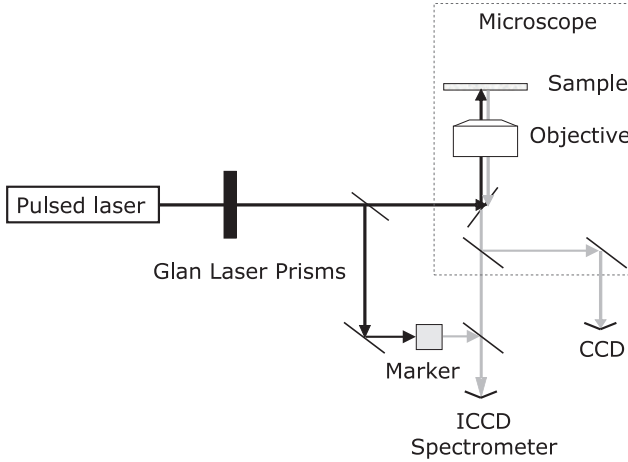
Figure 6.2: Schematic of the emission-spectrum setup. Light from a pulsed laser was at-tenuated with Glan laser prisms and focused in a microscope on the sample. Part of the incident light was guided via a different path through the marker (Cresyl Violet). Both light paths were reunited at the spectrometer slit and collected with an intensified charge-coupled device camera (ICCD). At a second output port of the microscope a charge-coupled device camera (CCD) was detached, to obtain information about the focus area of the incident pump source and about the surface of the random laser sample.

0.6 ± 0.3 µm at λ = 633 nm, with a refractive index n_{eff} of 2.1 ± 0.4.

6.2 Experimental setup

For our measurements we have used three different experimental setups: one to measure the emission spectrum of a titania sample, another one to measure the time evolution of the output signal of a random laser, and a third setup with which we measured the gallium phosphide samples. We will give a description of these setups below.

6.2.1 Emission-spectrum measurement

The titania suspension was put in a fused-silica capillary from VitroCom Inc., with internal dimensions $100 \times 2 \times 0.2$ mm^3. The ends of the capillary were closed by melting. The random laser sample was excited by a pump pulse at 532 nm, provided by an optical parametric oscillator (OPO) pumped by a Q-switched Nd:YAG laser (Coherent Infinity 40-100/XPO). The pump pulse had a duration of 3 ns and a

repetition rate of 50 Hz. The setup is schematically depicted in Fig. 6.2. The pump light was guided into a microscope (Nikon TE2000-U) and focused on the sample with a microscope objective (water-immersed, numerical aperture NA = 1.2, Nikon CFI Plan Apochromat 60x WI).

Our microscope had several output ports. In this setup we used two ports: one port to the intensified charge-coupled device camera (ICCD) and spectrometer (Oriel Instruments, type MS257), and one port to another charge-coupled device camera (CCD, Sony SSC-M388CE). This second CCD was attached to the microscope to obtain information about the focus area of the incident pump light (focus area, 12 ± 6 µm^2) and also to obtain information about the (change of the) surface of the random laser sample during measurements.

The light emitted by the sample was collected by the same water-immersed objective as the one that was used to focus the pump light. A small part of the pump light was split off from the input beam before entering the microscope. This light was used to excite a dye solution (Cresyl Violet, 1.7 mmol/l) which we used as a marker for the pump fluence. This dye solution worked as a wavelength converter for the pump light. The light emitted by Cresyl Violet and by the random laser sample were recorded at the same time with a spectrometer and an intensified charge coupled device camera (resolution of approximately 7.5 cm^{-1} spectral width): in one frame both the emission of the random laser and the pump marker was recorded. To avoid light scattering in the spectrometer the pump light was filtered out of the detection path by use of a colored glass filter with a transmission of less than 1% at the wavelength of the pump laser.

The intensity of the incident pump light on the sample was tuned with two Glan laser prisms in the light path. By positioning 2 prims in a row, we assure that the polarization of the pump light is maintained. The maximum intensity reached on the sample was in the order of 1 mJ/mm^2. To measure this intensity, we placed an anti-reflection coated round wedge prism (Thorlabs) in the pump beam, after the Glan laser prisms. The reflection of the light on this round wedge prism was collected with a photodiode (PDA55, Thorlabs), which was readout by an oscilloscope (Tektronix TDS 2024). The signal of this oscilloscope was calibrated with the light intensity coming through the microscope objective with an Ophir power meter (PD300-3W).

As a picosecond light source we used a stretched pulse of a femtosecond optical parametric amplifier (OPA), pumped by a femtosecond Ti:Sapphire laser. The maximum intensity reached on the sample was in the order of 50 mJ/mm^2, measured with the aforementioned method. The pump wavelength was 532 nm, the repetition rate 50 Hz. The focus area for the picosecond light source was approximately the same as the focus area of the nanosecond pump source. We could not measure the pump pulse width directly, but calculated a width of 15 ± 0.5 ps from the measured bandwidth of the OPA and the configuration of the pulse stretcher.
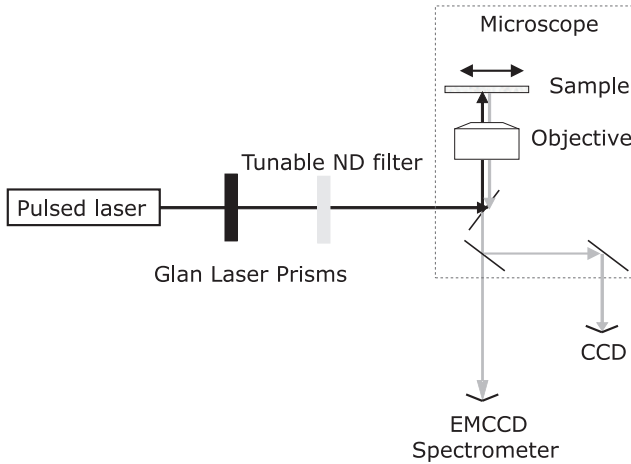
*Figure 6.3: Schematic of the gallium phosphide setup. Light from a pulsed laser was attenuated with Glan laser prisms and focused on the sample. This sample could be translated by means of a stepper motor. The emitted light of the random laser sample was collected by a spectrometer and an electron-multiplier charge-coupled device camera (EMCCD). At a second output channel of the microscope a charge-coupled device camera (CCD) was detached, to obtain information about the focus area of the incident pump source and about the surface of the random laser sample.*

Since we expected almost zero pulse-to-pulse fluctuations in the picosecond pump source, we did not monitor the pulse-to-pulse fluctuations of the picosecond pump source.

6.2.2 Time-resolved setup

For the time-resolved experiment, we used almost the same setup as for the emission-spectrum experiments pumped with nanosecond pumped pulses apart from 2 slight alterations. The marker Cresyl Violet was removed from the setup, and the detection of the emitted light of the random laser was changed: The detector (combination of spectrometer and ICCD) was replaced by a 25 GHz photodiode (New Focus 1404). The signal of this detector was read out by an oscilloscope (Tektronix TDS 7404, analog bandwidth 4 GHz). The resulting temporal resolution was 100 ps. To obtain a good signal-to-noise ratio, every time trace was averaged over 100 sampled time traces.

6.2.3 Measuring gallium phosphide

The setup for measuring the emission spectra of gallium phosphide samples was slightly different than the emission-spectrum setup described above. The main reason for this difference, is the fact that the damage threshold of porous gallium phosphide is much lower than the damage threshold of titania. Furthermore, we have changed the sample holder, since we noticed that we could measure narrow spectral emission peaks (like spikes) in the emitted light of a plain dye solution in glass capillaries (see for more details section 6.3.1). The main differences are the implementation of a spatial filter, the different sample holder, and a new camera behind the spectrometer: an electron-multiplier charge-coupled device camera (EMCCD).

The gallium phosphide sample was put in an airtight sample holder, of which the bottom and top were formed by 3 mm thick sapphire windows. The sample was lightly pushed with a spring onto the sapphire window at the bottom of the sample holder, to avoid large spaces filled with plain dye solution between the sample surface and the sapphire window, and to hold the sample at a fixed position in the holder. This sample holder was mounted on a stage, that could be controlled in one direction with a stepper motor (Z600, Thorlabs).

The random laser was excited by a pump pulse at 567 nm, provided by an optical parametric oscillator (OPO) pumped by a Q-switched Nd:YAG laser (Coherent Infinity 40-100/XPO). The wavelength of the pump source was chosen to obtain high enough gain of the dye, and to avoid damage through absorption of the incident light by the gallium phosphide. The pump pulse had a duration of 3 ns and a repetition rate of 50 Hz. The pump pulse was spatially filtered by 2 positive lenses (focal length, 100 mm), with a pinhole in between (diameter, 150 μm). Due to this filter, the spatial profile of the beam incident on the sample was Gaussian, avoiding hot spots in the focus that could lead to damage of the gallium phosphide.

The pump light was guided into a microscope (Nikon TE2000-U) and focused on the sample with a long-distance microscope objective (NA = 0.55, CFI LU Plan Epi ELWD 50x, Nikon). The setup is schematically depicted in Fig. 6.3. The microscope has different ports. In the setup we used, just as in the case of the emission-spectrum setup, two ports: the port to the electron-multiplier charge-coupled device camera (EMCCD) and spectrometer (Oriel Instruments, type MS257), and the port to a charge-coupled device camera (CCD, Sony SSC-M388CE). This CCD was attached to the microscope to obtain information about the sample itself and the focus area of the incident pump light (focus area, $3 \pm 1 \mu m^2$).

The intensity of the incident pump light on the sample was tuned with 2 Glan laser prisms. The pump energy on the sample was at maximum 0.32 μJ/pulse. To measure this energy, we placed a anti-reflection coated round wedge prism (Thorlabs) in the pump beam, after the Glan laser prisms. The reflection of the light on this round wedge prism was collected with a photodiode (PDA55, Thorlabs),

which was readout by an oscilloscope (Tektronix TDS 2024). The signal of this oscilloscope was calibrated with the light intensity coming through the microscope objective with an Ophir power meter (PD300-3W).

We placed a tunable neutral density (ND) filter in the light path. With this filter we could increase the incident energy on the sample slowly to avoid damage. In between measurements, this check could also be performed, without changing the Glan laser prisms (and thus the incident energy on the sample).

The light emitted by the random laser was collected by the microscope objective, dispersed by a spectrometer and detected by an EMCCD. This EMCCD is more sensitive than the ICCD used in the emission-spectrum setup. The sensitivity of the combined EMCCD and spectrometer was calibrated with a HeNe-laser (5 mW, 25LHP151, Melles Griot) and the aforementioned Ophir power meter.

6.3 General considerations

6.3.1 Spikes from the glass surface

We observed very narrow spectral features in the emitted light of the random laser. These very narrow features were also observed, when we measured the emission of a plain dye solution in a glass capillary. These spikes were due to scattering of light inside a crack in the glass surface. We have investigated different glasses: borosilicate glass, fused silica glass, and quartz. For all these glasses we saw cracks appear above a certain incident pump energy; this incident pump energy was of the same order as the random laser threshold pump energy. However, we did not observe this cracking of the sapphire windows described in section 6.2.3, even for a incident pump energy four times higher than the threshold pump energy of the random laser. Therefore, we used this sapphire window in all our gallium phosphide measurements: we were sure that all spectral narrowing was due to the random laser sample, and not to damage of the window.

6.3.2 Tuning the excitation wavelength

In our gallium phosphide random laser, we used a solution of rhodamine 640 perchlorate in methanol as gain medium. The gain in the sample depends on the number of excited dye molecules, which depends on the pump wavelength, as the absorption cross-section is wavelength dependent. The pump wavelength should not be higher than 580 nm to achieve high enough gain inside the sample. The damage threshold of gallium phosphide depends on the wavelength as well: below a wavelength of 560 nm the absorption of the incident energy is high, leading to an enormous decrease of the damage threshold. There is an optimum, at which the

gain in the system is high, and the damage done to the gallium phosphide random laser is negligible. This optimum is somewhere around 567 nm.

6.3.3 Dye concentration versus spikes

The search for spikes is a tricky one. We have observed in our measurements that in order for spikes to appear the gain in the system, i.e. the concentration of the dye solution, is a crucial factor. In our gallium phosphide random laser, we have tried different dye concentrations of rhodamine 640 perchlorate: 5 mmol/l, 10 mmol/l, and 20 mmol/l. At the low dye concentration of 5 mmol/l no spikes were observed. The dye concentration that leads to high and narrow spikes in our gallium phosphide random laser is 10 mmol/l. At higher dye concentrations, for example 20 mmol/l, spectral features were observed, but these features were much broader ($\sim 3\times$) and had a much smaller relative height ($\sim 10\times$) than spikes measured with a dye concentration of 10 mmol/l.

<div style="text-align:center">

7

Intrinsic intensity fluctuations in random lasers

</div>

Typical well-known phenomena of the random laser are a (low) threshold in the power conversion, spectral narrowing, and sharp features ("spikes") in the emitted spectrum for both picosecond [27, 67, 68, 73] and nanosecond [36] pump pulses. Recently, a new phenomenon of the random laser has been published by Anglos and coauthors [5]: shot-to-shot fluctuations in the emitted light by the random laser, while the system is pumped by a pulsed pump source with constant energy output. These fluctuations occurred only with a random laser system pumped with nanosecond pulses, and not for the same system pumped with picosecond pulses.

In this chapter we will present our elaborated experimental and theoretical study of the statistics of the shot-to-shot fluctuations and introduce a model that clarifies their existence.[104] We performed measurements on a random laser pumped with both picosecond and nanosecond pulses. The experiments are described first in section 7.2, followed by the experimental observations. In section 7.3 a model based on the number of laser modes in the random laser is presented, which includes an effective β factor. Finally, we will compare our experimental observations with the results of our model in section 7.4.

7.1 Experimental apparatus

The intrinsic fluctuations measurements are performed on titania random lasers. These samples consist of a suspension of TiO_2 powder in a 1 mmol/l solution of
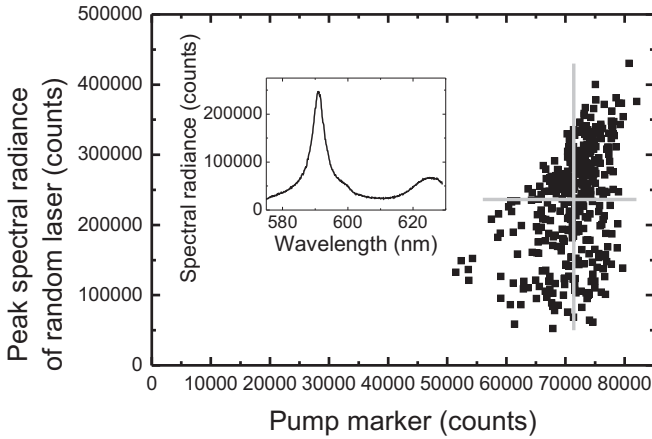
Figure 7.1: Peak of the spectral radiance of the random laser versus the peak height of the pump marker. The two gray lines indicate the mean value of the two peak heights and are used to visualize the correlation. The inset shows a typical single shot spectrum, from which the counts of the peaks are determined.

sulforhodamine B in methanol, and has a transport mean free path of 0.5 µm. A complete description is given in section 6.1.1. The emission-spectrum setup was used, with both the nanosecond, and the picosecond pump source, as described in section 6.2.1.

7.2   Measurement of the intrinsic fluctuations

We are interested in the intrinsic intensity fluctuations of the random laser, i.e., the fluctuations of the random laser which are not the result of fluctuations of the pump laser. A typical single shot emission spectrum shows two peaks, see the inset of Fig. 7.1: the peak of the random laser spectrum is around 594 nm, and the peak of the marker is around 625 nm. The intrinsic fluctuations of the random laser are investigated by comparing the peak height of the light emitted by the random laser with that of the marker. We have taken many single shot measurements (> 400), and from each of these spectra we determine the two peak heights. The peak height of the spectral radiance of the random laser is plotted versus the peak height of the pump marker in Fig. 7.1. The observed correlation between the two peak heights is weak. We expect stronger correlation between the spontaneous emission regime of the random laser and the pump pulse. To check this expectation Fig. 7.1 shows the spectral radiance at 573 nm (relative far away from the random laser emission peak) versus the peak of the pump marker, Fig. 7.2. When we qualitatively compare Figs. 7.1 and 7.2 qualitatively, it is clear that Fig. 7.2 has a stronger correlation than
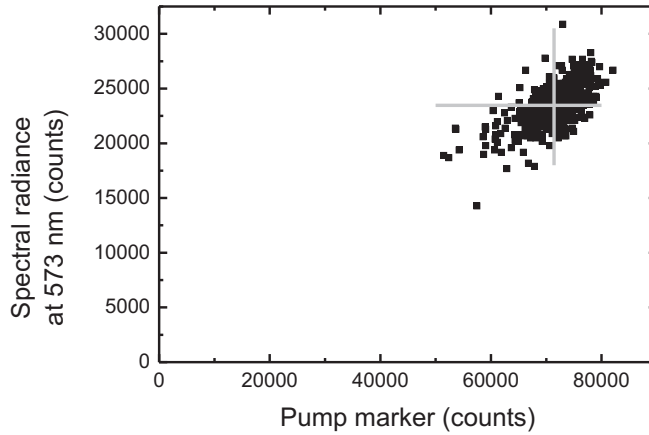
Figure 7.2: Spectral radiance at 573 nm, far outside the random laser emission spectral bandwidth, versus the pump marker. The two gray lines indicate the mean values of the two peak heights and are used to visualize the correlation.

Fig. 7.1.

A better method to compare the two graphs 7.2 and 7.1 is a quantitative method. A quantitative measure for the correlation in the case of linear regression is the correlation coefficient. The correlation coefficient indicates to what extent data points lie on a straight line. A correlation coefficient of 1 means that the points form a straight line with a positive slope, while a correlation coefficient of -1 indicates a straight line with a negative slope. A correlation coefficient of 0 indicates that no linear regression is present. In the case of the peak of the spectral radiance of the random laser versus the pump fluence, we find a correlation coefficient of 0.4, indicating that part of the fluctuations is intrinsic. In the case of the fluorescence versus pump marker we find a stronger correlation coefficient of 0.62, indicating that these fluctuations depend more on pump fluctuations than the fluctuations at the peak of the spectral radiance of the random laser. Although the spectral radiance at 573 nm is still partially influenced by stimulated emission, the effect of the spontaneous emission can be seen from the increase of the correlation coefficient. Apparently, the observed shot-to-shot fluctuations are not due to the fluctuations of the pump laser. We will continue to present a quantitative measure for the intrinsic intensity fluctuations of a random laser.

The intrinsic fluctuation coefficient f is defined as the ratio between the standard deviation of the shot-to-shot intensity of the light emitted by the random laser, ΔI, and the mean value of the intensity of the emitted light $\bar{I}$,

$$f \equiv \frac{\Delta I}{\bar{I}}. \tag{7.1}$$
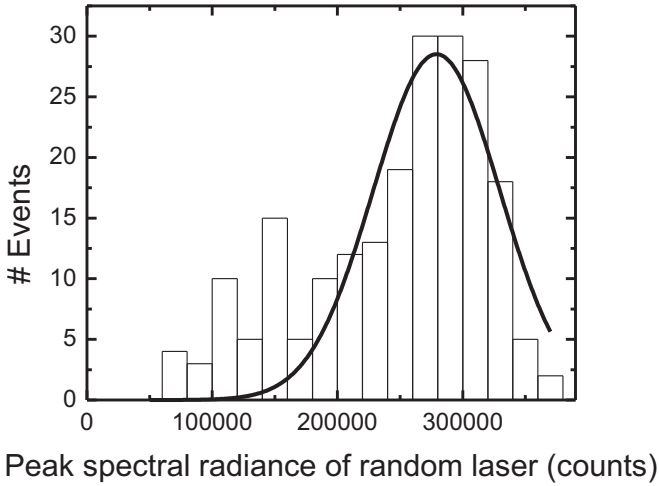
Figure 7.3: Distribution of the peaks of the spectral radiance of the random laser with a pump marker between 70000 and 75000 counts. The Gaussian fit provides the mean value (279047 counts) and the standard deviation (50476 counts). The measured intrinsic fluctuations is 18%.

To determine the intrinsic fluctuations from the data points in Fig. 7.1 we take a small band of pump fluences so that the fluctuations of the pump laser do not influence the outcome. We make a histogram of the accompanying peaks of the spectral radiance of the random laser for a pump marker between 70000 and 75000 counts and fit this histogram with a Gaussian, see Fig. 7.3. From this fit we obtain the standard deviation and the mean value of the peak heights, leading us to the experimental intrinsic fluctuations

$$f_{\mathrm{ns,exp}} = (18 \pm 3)\%, \tag{7.2}$$

where the error margin corresponds to one standard deviation. We have changed the range of the counts of the pump marker. The resulting intrinsic fluctuations were identical.

Due to large technical fluctuations of the pump laser, no reliable estimate of the intrinsic fluctuations follows from the picosecond pumped random laser experiments.

7.3 Our model

In this section we present a model for the origin of the intrinsic fluctuations of random lasers. The approach we take here is based on the concept of pseudomodes.[60]

Pseudomodes are single-frequency eigenmodes, solutions of the Maxwell equations. These modes have an eigenfrequency and decay by leaking to the outside world. This leakage is characterized by a decay time τ_c. Each mode can be a laser mode, depending on the decay time (also referred to as dwell time) of that mode and the gain time of the sample. The decay time is the time that light is inside the sample due to diffusion, and the (amplitude) gain time is defined as the time after which the amplitude is increased with a factor e. If the decay time of a certain pseudomode is longer than the gain time of the system, that pseudomode is a laser mode. We assume the mode volume is equal for each (random) mode, and that the gain in the sample is homogeneous. The number of lasing modes, N_l, is given by

$$N_l = \pi_l N, \tag{7.3}$$

with N the number of pseudomodes and π_l is a random variable ranging between 0 and 1. We define

$$p_l \equiv \overline{\pi_l}, \tag{7.4}$$

with p_l the probability for lasing in a pseudomode, and $\overline{\pi_l}$ is π_l averaged over realizations of the disorder. The emission power of the different lasing modes is assumed equal. The detected emission intensity is entirely due to the lasing modes in the system and is assumed to be proportional to the number of lasing modes. The intrinsic fluctuations f can be determined

$$f = \frac{\Delta I}{\overline{I}} = \frac{\sqrt{\overline{N_l}}}{\overline{N_l}}. \tag{7.5}$$

In the last step of Eq. (7.5), we have assumed a binomial distribution of N_l, which results for the limit of N to infinity to a Gaussian or normal distribution. The standard deviation is given by $\sqrt{\overline{N_l}}$. We combine Eqs. (7.3) and (7.4), and insert the result in Eq. (7.5) to obtain

$$f = \frac{1}{\sqrt{p_l N}}. \tag{7.6}$$

In section 7.3.1 we will show how to calculate p_l from a fit to experimental data. An elaboration on the calculation of N is presented in section 7.3.2.

7.3.1 Determination of the probability of lasing

When we combine Eqs. (7.3) and (7.4) the probability of lasing is given by

$$p_l = \frac{\overline{N_l}}{N}. \tag{7.7}$$

The probability of lasing can be calculated via the distribution of the decay times. The integral of the distribution of the decay times P from the gain time to infinity

will give the probability p_l for a certain mode to be a laser mode,

$$p_l = \int_{\tau_g}^{\infty} P(\tau_c) d\tau_c. \tag{7.8}$$

The distribution of the decay times for a three dimensional (3D) diffusive medium is not known. We therefore use the distribution of the phase-delay times [111], which is expected to be close to the distribution of the decay times.

The gain time is given by

$$\tau_g \equiv \frac{\ell_g n'}{c_0}, \tag{7.9}$$

where n' is the real part of the refractive index. The amplitude gain length ℓ_g is given by

$$\ell_g = \frac{2}{\sigma_e \rho_{\mathrm{exc}}}, \tag{7.10}$$

where σ_e is the stimulated emission cross section of a molecule, and ρ_{exc} is the density of molecules in the excited state in the sample.

If the pump power is large enough, the gain in the system can be saturated. In the case of saturation the gain length will not be decreased any more when the pump power is increased. From Eq. (7.10) we can find a lower bound for the gain length $\ell_{\mathrm{g,b}}$, and thus an indication of gain saturation, when one assumes that all the dye molecules in the medium are in the excited state

$$\ell_{\mathrm{g,b}} \geq \frac{2}{\sigma_e \rho}, \tag{7.11}$$

where ρ is the density of dye molecules in the sample.

The above approach has some disadvantages. First, the distribution of the phase-delay times is expected to be close to the distribution of the decay times, but how close is not known. Secondly, we do not know the exact value of the gain length, and thus the gain time. Therefore, we will determine the probability of lasing directly from our experiments.

Spontaneous emission factor in a multi-mode laser

When we examine Eq. (7.7), we see a similarity between the definition of p_l and the spontaneous emission factor of a laser, the β factor [115]. The single-mode β factor, defined as the fraction of spontaneous emission that contributes to lasing is given by [92]

$$\beta_{\mathrm{sm}} = \frac{1}{N}. \tag{7.12}$$

This β_{sm} factor appears in the four-level rate equations for a single-mode laser [92]

$$\frac{dN_1(t)}{dt} = P(t) - \frac{\beta_{\mathrm{sm}}q(t)N_1(t)}{\tau} - \frac{N_1(t)}{\tau}, \tag{7.13a}$$

$$\frac{dq(t)}{dt} = -\frac{q(t)}{\tau_c} + \frac{\beta_{\mathrm{sm}}N_1(t)}{\tau}\left[q(t) + 1\right], \tag{7.13b}$$

with N_1 the number of excited molecules in the medium, q the number of photons in the lasing mode, P the pump rate (in photons per second), τ the spontaneous emission lifetime of the dye, and τ_c the cavity decay time.

In a random laser many random modes contribute to the laser oscillation. However, for our consideration only the average behavior is relevant. In general, to describe a multi-mode laser one has to write an equation for every mode and couple the different mode equations to the equation for the population. We will now show that for the description of the average behavior of a multi-mode laser only two small changes to the rate equations are necessary: We simply replace β_{sm} and τ_c in the rate equations (7.13) by the effective parameters β_{mm} and $\tau_{\mathrm{c,mm}}$. Since we are interested in the average behavior, we will use this simplified approach. We will prove that this approach is valid in many situations.

For the effective parameter $\tau_{\mathrm{c,mm}}$ we take the mean value of the distribution of the cavity decay times. To determine this distribution we calculate the solution of the diffusion equation for a slab with thickness L, with a source positioned in the middle of the slab. From this solution of the diffusion equation the electric field correlation is derived and the mean value of the phase-delay times follows from the Taylor expansion of this correlation, see for more details appendices B, C, and D. The resulting mean value of the phase-delay time, and thus the mean value of the cavity decay time is given by

$$\tau_{\mathrm{c,mm}} = \frac{1}{8}\frac{L^2}{D}, \tag{7.14}$$

with D the diffusion constant, given by

$$D = \frac{1}{3}\frac{c_0\ell}{n'}, \tag{7.15}$$

with ℓ the transport mean free path. For the effective parameter β_{mm} we take

$$\beta_{\mathrm{mm}} = \frac{\overline{N_l}}{N}, \tag{7.16}$$

where we assumed that all modes contribute equally. When comparing Eqs. (7.7) and (7.16), we see that β_{mm} is equal to p_l.

Spontaneous emission factor in a pulsed laser

Conventionally, the β factor is calculated from the geometry of the experiment.[115] In the continuous wave limit for a single-mode laser in steady state a formula can be analytically derived from the rate equations (7.13) that describes the relation between the output and the input power of a laser,

$$q = -\frac{1 - P\beta_{\mathrm{sm}}\tau_c}{2\beta_{\mathrm{sm}}} + \frac{1}{2}\sqrt{\left(\frac{1 - P\tau_c\beta_{\mathrm{sm}}}{\beta_{\mathrm{sm}}}\right)^2 + 4P\tau_c}. \tag{7.17}$$

If one uses a pulsed pump this should be generalized to include time-dependence, and an analytic solution is no longer available. However, as we will show, for a wide range of parameters Eq. (7.17) still describes the threshold behavior very well for a detector that integrates the output power. We will use Eq. (7.17) for the integrated power while replacing the parameter β_{sm} by an effective parameter β_{eff}.

To examine the applicability of Eq. (7.17) to experiments with a pulsed laser, we calculate with the rate equations (7.13) several output versus input power graphs. We use input parameters relevant to our experiment and vary the pump pulse duration t_p, and β_{sm}. The pump pulse is modeled by a Gaussian function. To the output versus input power graphs we fit Eq. (7.17) and use as fit parameter β_{eff}. In Fig. 7.4 we present the calculated β_{eff} as function of β_{sm}. The different symbols correspond to different pump pulse durations. For a pulse duration of 3000 ps, the calculated values of β_{eff} are identical to the input value of β_{sm}. This correspondence implies that for our system nanosecond pump pulses can be treated as a continuous-wave pump. When the pulse duration is shorter, while keeping the other parameters constant, we notice a deviation from this straight line to higher values of β_{sm} for the same values of β_{eff}. This difference between β_{eff} and β_{sm} increases for shorter pulses. The origin of the dissimilarity between β_{eff} and β_{sm} is due to the fact that the pump is not a continuous wave, but a pulse with a finite duration.

In Fig. 7.5 β_{eff} versus β_{sm} is plotted for different values of the pump pulse duration t_p and the spontaneous emission lifetime τ of the dye. If the pump pulse duration is longer or equal to the spontaneous emission lifetime, the values for β_{eff} and β_{sm} are the same. When the pump pulse duration is shorter than the spontaneous emission lifetime, a similar deviation as shown in Fig. 7.4 is the result. This deviation is related to the ratio of the pump pulse duration and the spontaneous emission lifetime.

Besides the pump pulse duration and the spontaneous emission lifetime, there is a third time scale in the our system: the cavity decay time τ_c. In Fig. 7.6 we plot β_{sm} for different cavity decay times. All the points are calculated for a pump pulse duration of 3 ps. If the pump pulse duration approaches the value of the cavity decay time τ_c, Eq. (7.17) is no longer a good fit to the output versus input power graph. This failure of the fit means that β_{eff} is no longer a parameter that
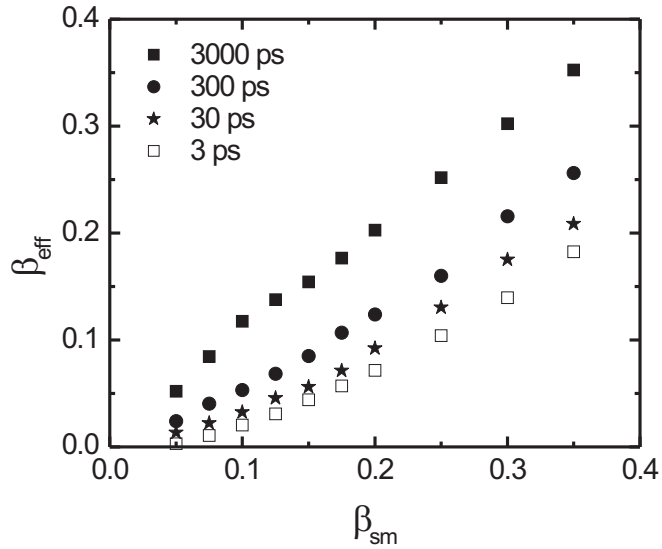
Figure 7.4: Theoretical values of β_{eff} (from the fit of the relation between the output and input power of a laser [Eq. (7.17)] to numerically computed output-input power graphs) versus the input parameter β_{sm} for different pump pulse durations. We choose the input parameters relevant for our experiments: $\tau = 3200$ ps and $\tau_c = 0.1$ ps. In the legend the pump pulse durations are listed.

Figure 7.5: *Theoretical values of β_{eff}, from the fit of Eq. (7.17) to numerically computed output-input power graphs, versus the input parameter β_{sm}. The input parameter τ_c is set to 0.1 ps, relevant to our experiment. The input parameter τ is varied. The pulse duration t_p and τ are listed in the legend.*

can be used to describe the experiment and thus that for our experiment we cannot associate a β factor with the continuous wave approach.

Spontaneous emission factor in the random laser

We learned from the previous two paragraphs that the rate equations and the threshold curve (7.17) can be used for a multi-mode laser, and that these formulas can be used under certain conditions for a pumped laser. We combine these two conclusions and use the rate equations (7.13) and the threshold curve (7.17) for a pulsed multi-mode laser system. We simply change τ_c by $\tau_{\mathrm{c,mm}}$ in the fit formula, and the fitted β_{eff} no longer leads to β_{sm}, but to β_{mm}, and thus p_l. This allows us to extract p_l from the threshold curve of a random laser. In short:

$$
\begin{aligned}
t_p &\geq \tau \gg \tau_c && \text{CW limit: } \beta_{\mathrm{eff}} = \beta_{\mathrm{mm}}, \\
\tau &> t_p > \tau_c && \text{conversion needed: } \beta_{\mathrm{eff}} < \beta_{\mathrm{mm}}, \\
\tau &> \tau_c > t_p && \text{simplified model fails}
\end{aligned}
$$
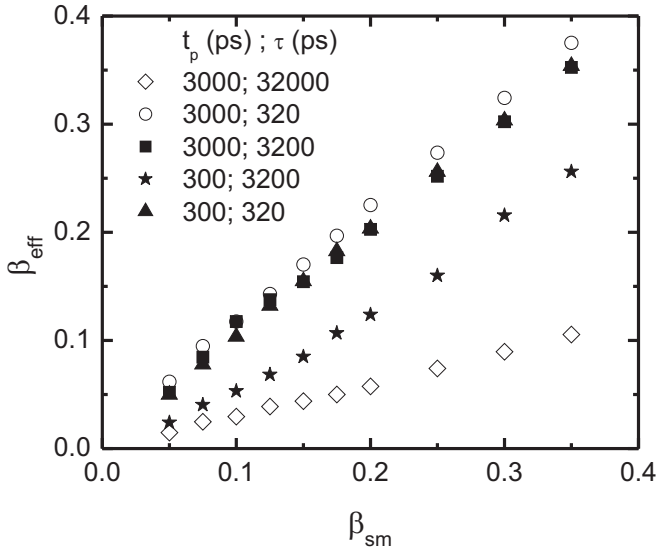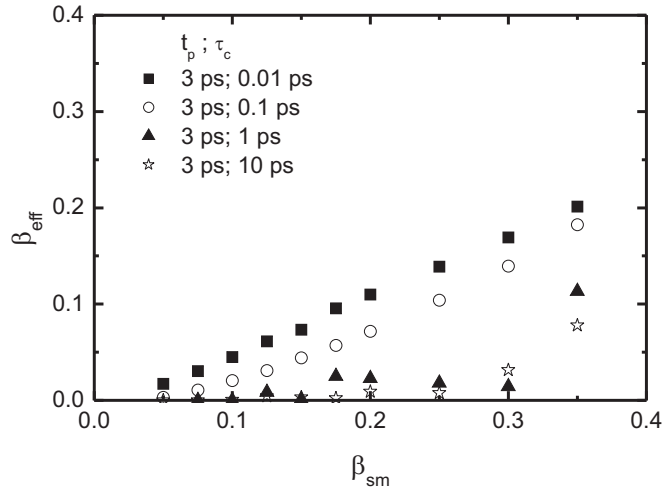
Figure 7.6: Theoretical values of β_{eff}, from the fit of Eq. (7.17) to numerically calculated output-input power graphs, versus the input parameter β_{sm}. The input parameter τ is set to 3200 ps, relevant to our experiment. The input parameter τ_c is varied. The pulse duration t_p and the cavity decay time τ_c are listed in the legend.

7.3.2 Number of modes

The second important parameter needed to calculate the intrinsic fluctuations is N. The total number of modes in the system within the relevant frequency bandwidth $\Delta\omega$ can be calculated using the formula [92]

$$N = \rho(\omega, V)\frac{\Delta\omega}{\omega} \tag{7.18}$$

$$= \frac{8\pi n^3 V}{\lambda_c^3}\frac{\Delta\lambda}{\lambda_c}. \tag{7.19}$$

with $\rho(\omega, V)$ the number of resonant modes falling within a unit (radian) frequency interval in the cavity volume V, $\Delta\lambda$ the full width at half maximum of the emission spectrum, and λ_c the central wavelength of the emission spectrum. All parameters can be deduced from our experiment, except for the volume of the cavity V.

Volume of the cavity

Different approximations and numerical calculations can be used to calculate the volume of the cavity.[99, 109] The main idea is that the gain volume depends on the ratio of the transport mean free path and the absorption length in the sample. In our case, the absorption length is much larger than the transport mean free path,

and we can assume a gain volume in the form of a hemisphere

$$V = \frac{2}{3}\pi r^3,$$ (7.20)

with r the radius of the gain volume, which can be deduced from our experiments. As mentioned in section 7.3.1, increasing the number of incident photons per time scale can lead to a larger gain volume, if the gain is near saturation.

The intrinsic fluctuations depend on the number of modes, and the probability of lasing. By experimentally varying the parameters, the intrinsic intensity fluctuations of the random laser can be controlled.

7.4 Results

We will now calculate with our model the fluctuations of a random laser system pumped with nanosecond or picosecond pulses. We will compare these fluctuations with our experimental observations.

7.4.1 Probability of lasing

The probability of lasing, defined as the probability of lasing in a pseudomode, is computed by a fit of Eq. (7.17) to experimentally determined output versus input power graphs. We have measured the peak of the spectral radiance of the random laser as a function of the pump fluence, as shown in Fig. 7.7. We see a normal laser threshold behavior: a linear increase for low pump fluence and a steeper linear increase for pump fluences above the laser threshold. The solid line is a fit to the data with Eq. 7.17. The input parameter $\tau_{c,mm}$ is approximated by the mean phase-delay time, $\tau_c = 0.1$ ps. We have seen in section 7.3.1 that the determined value of β_{eff} does not depend on τ_c as long as the pump pulse duration t_p is longer than the cavity decay time. In the case of nanosecond pump pulses we have seen that $p_l = \beta_{eff}$. The probability of lasing is

$$p_{l,ns} = 0.07 \pm 0.03,$$ (7.21)

where the error margin corresponds to one standard deviation.

For the picosecond pumped random laser we have also measured the peak of the spectral radiance of the random laser as a function of the pump fluence, see Fig. 7.8. Once more the typical laser curve is the result. In case of picosecond pump pulses, β_{eff} is no longer identical to p_l, as was discussed in section 7.3.1. The fitting parameter β_{eff} has to be converted to β_{mm} (p_l). In our picosecond experiment the pulse duration is 15 ± 0.5 ps and a relevant conversion graph for β_{mm} and β_{eff} is presented in Fig. 7.9. With this graph we convert our values of β_{eff} of 0.03 ± 0.006 to

$$p_{l,ps} = 0.09 \pm 0.015,$$ (7.22)
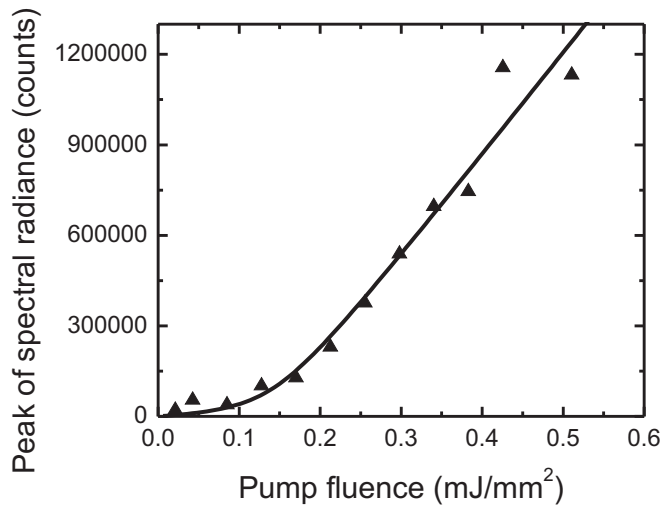
Figure 7.7: Peak of the measured spectral radiance of the random laser versus the pump fluence for a random laser pumped with nanosecond pulses. A normal laser threshold behavior is observed. The solid line is a fit of Eq. (7.17) to our data, with a spontaneous emission lifetime of 3200 ps and a cavity decay time of 0.1 ps. From the fit we obtain $\beta_{\mathrm{eff}} = 0.07$, which in our model equals the probability of lasing p_l.

where the error margin corresponds to one standard deviation.

7.4.2 Calculation of the number of modes

The calculation of the number of modes for our random laser regime is given by Eq. (7.19). In our case we have $n = 1.4837$, $\lambda_c = 595$ nm. The width of the emission spectrum above threshold is 4.3 nm.

Number of modes with nanosecond pump pulses

In the case of nanosecond pump pulses, the volume of the gain medium is given by the volume of a hemisphere. The spatial form of the luminescence coming from the surface of the random laser sample pumped with nanosecond pump pulses was recorded with a charge coupled device camera, while we filter the pump light. We measure a circular spot with a mean radius of 5 ± 0.5 µm, Fig. 7.10. The cross section of the circular spot in the x direction is indicated by the white line and plotted in the inset of the figure. The radius of the luminescent surface is an approximation for the radius of the gain volume and is measured for both the x and
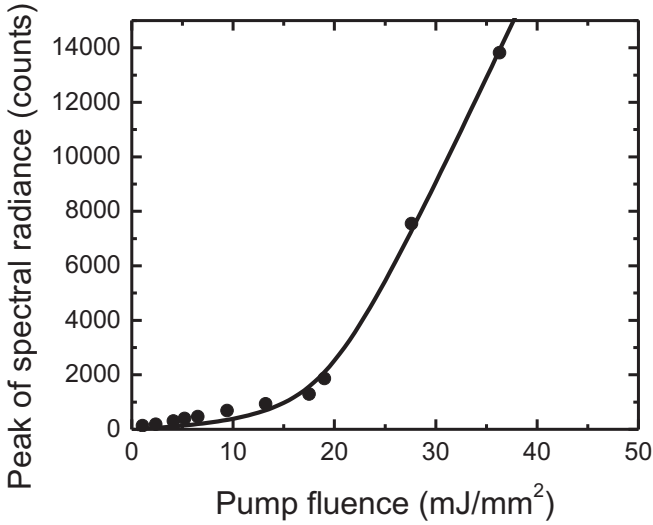
Figure 7.8: Peak of the measured spectral radiance versus pump fluence for a random laser pumped with picosecond pulses. A normal laser threshold behavior is observed. The solid line is a fit of Eq. (7.17) to our data. The spontaneous emission lifetime is 3200 ps, the mean cavity decay time 0.1 ps. From the fit we obtain β_{eff} = 0.03.
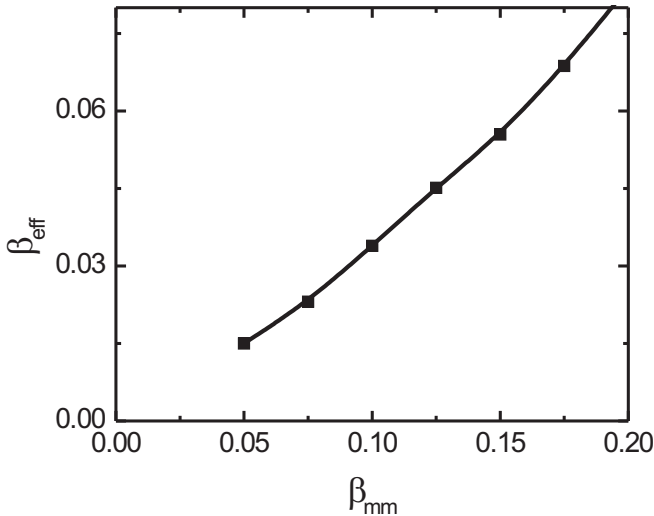
Figure 7.9: Calculated β_{eff} versus the input parameter of the rate equations β_{mm} is shown. The graph is produced for a pump pulse duration of 15 ps, a cavity decay time of 0.1 ps, and a spontaneous emission lifetime of 3200 ps. The solid lines connect the data points. We convert our β_{eff} of 0.03 to a p_l of 0.09.
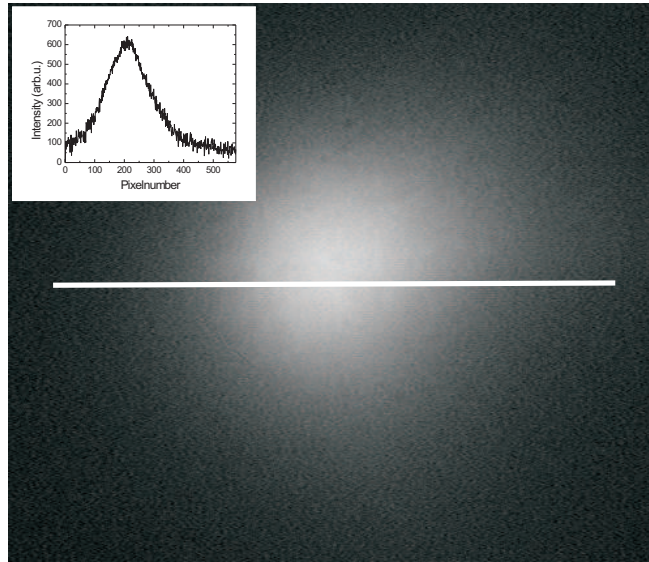
Figure 7.10: Image taken with a high NA microscope objective and a CCD camera (578×578 pixels) of the surface of a random laser. The sample is pumped and the luminescence is recorded, while blocking the pump light. From the image the radius of the gain volume is determined for both the x and y direction. Only the x direction is shown in the figure. The cross section is displayed in the inset. We find a radius of 5 µm.

y direction. The number of modes in our nanosecond pumped random laser is

$$N_{ns} = 746 \pm 256. \tag{7.23}$$

Number of modes with picosecond pump pulses

We did not record the spatial form of the luminescence in case of picosecond pump pulses. However we can speculate about the gain volume in the picosecond pumped system if we have gain saturation. For our random laser, the probability of lasing for the picosecond and for the nanosecond pumped case are within each other error margins, an indication of gain saturation which we shall prove now.

We calculate the lower bound of the gain length with Eq. (7.11). The density of molecules in the random laser is 5.4×10^{23} molecules m^{-3}, and the stimulated emission cross section is 4×10^{-20} m^2, both with a 10% error, leading to a lower bound limit of

$$\ell_{g,b} \geq 75 \text{ µm.} \tag{7.24}$$

For the nanosecond pumped random laser we found a p_l of 0.07 ± 0.03, see Fig. 7.7. The gain length at which p_l equals 0.04 is

$$\ell_{g,b,c} = 60 \text{ µm}. \tag{7.25}$$

The value of $\ell_{g,b,c}$ is lower than the bound limit we calculated. Although this difference does not indicate a serious discrepancy (the error margins on p_l are only one standard deviation), the assumption that the phase-delay time distribution equals the cavity decay time distribution should be investigated. Both gain lengths above are almost equal, proving that we are near the saturation regime. The threshold pump fluence is a factor 100 higher in the case of the picosecond pump pulse, and the pulse duration of the picosecond pump pulse is a factor 100 shorter. Since both pump lasers pump the sample to gain saturation, the gain volume of the picosecond pump pulse is larger than the gain volume of the nanosecond pump pulse. The advantage of using two different pump lasers on one sample is the change in the number of laser modes.

The gain volume for the picosecond case in saturation is at minimum a cylinder with a radius equal to the luminescence spot of the nanosecond pumped random laser and a length equal to L_d. The length L_d is the length that light travels from a point source inside a diffusive medium

$$L_d = \sqrt{Dt}, \tag{7.26}$$

with t the pulse duration of the point source. In our system L_d is 22 ± 3 µm. This leads to a total number of modes in our picosecond pumped random laser of

$$N_{ps} \geq 2407 \pm 885. \tag{7.27}$$

7.4.3 Intrinsic intensity fluctuations of a random laser

The intensity fluctuations derived from our model are given by Eq. (7.5)

$$f_{ns} = (14 \pm 5)\%, \tag{7.28}$$

where the error margin corresponds to one standard deviation. This number for the fluctuations is in good agreement with our experimental observations of $(18 \pm 3)\%$.

The intrinsic fluctuations calculated for a picosecond pump pulse for our own system is

$$f_{ps} \leq (6.8 \pm 1.2)\%, \tag{7.29}$$

where the error margin corresponds to one standard deviation. We could not verify this result experimentally. Anglos and coauthors have performed measurements on a random laser pumped with picosecond pulses.[5] From their paper we can calculate the fluctuations of their system with our model. From the fit to the published

output versus input power graph, and with a conversion from β_{eff} to p_l, we find for their system $p_l = 0.05$. For the gain volume we assumed a cylindrical form, as their excitation spot is much larger than their mean free path. We obtain $f_{ps} = 0.01\%$. From their published measured spectra we can find an estimation for the measured fluctuations. The measured fluctuations are $(3.7 \pm 1.7)\%$, where the error margin corresponds to one standard deviation. These intensity fluctuations include the pump fluctuations. These pump fluctuations can be in the order of 3% for a typical picosecond laser source. Since the expected intrinsic fluctuations are much smaller than the pump fluctuations, the intrinsic fluctuations cannot be measured and our model is not inconsistent with their data.

7.5 Summary

We have developed a model based on quasimodes that predicts the fluctuations of the output power of a random laser pumped with either nanosecond or picosecond pulses. For the system pumped with nanosecond pulses we computed fluctuations of $(14 \pm 5)\%$. This is in good agreement with our experimental fluctuations of $(18 \pm 3)\%$. For a system pumped with picosecond pulses we calculated $f_{ps} = 0.01\%$ for the system measured by Anglos and coauthors [5]. From their measurements we determined fluctuations of $(3.7 \pm 1.7)\%$, which includes fluctuations of the pump laser. Since the intrinsic fluctuations are very small, with most current setups they cannot be measured.

The difference in intrinsic fluctuations between picosecond and nanosecond pumped random lasers is well described by our model and the predictions are identical to our observations for a nanosecond pumped random laser and published observations for a picosecond pumped random laser. Our model can be used to tailor experimental conditions in such a way as to control the intrinsic fluctuations of a random laser system.

<div style="text-align: right">

8

</div>

Relaxation oscillations in random lasers

Relaxation oscillations of lasers are a well-understood phenomenon. Every laser of which the cavity decay time is much faster than the recovery time of the excited state population exhibits these oscillations. Already in 1968 Letokhov predicted the occurrence of relaxation oscillations in random lasers.[58] Different numerical calculations on random lasers also show this oscillatory behavior.[16, 110, 114] Only recently Soukoulis and coauthors have presented measurements of relaxation oscillations in single modes of a picosecond pumped random laser system.[94] To our knowledge, no measurements have been performed on relaxation oscillations in random lasers in the interesting regime of long pulses.

In this chapter we will show the results of our research on the time evolution of a nanosecond pumped random laser system.[106] We compare our experimental observations with a simple model, based on the four-level rate equations for a single-mode cw laser. We start in section 8.1 with the physics behind relaxation oscillations, followed by the model in section 8.2. The experimental apparatus is described in section 8.3, and the experimental results are presented in section 8.4. Finally, we compare the experimental results with the model in see section 8.5.

8.1 Physical origin of relaxation oscillations

Relaxation oscillations occur in many laser systems. In the book by Siegman [92], the term relaxation oscillations is used to describe the quasi-sinusoidal, exponentially damped, small-amplitude oscillations around the steady-state amplitude. The oscillations occur when a continuously operating laser is slightly disturbed. For

<div style="text-align: center">

67

</div>

discrete, sharp, large-amplitude pulses that occur typically at the turn-on phase of many lasers, the term generally used is spiking. In case of random lasers, we will speak only of relaxation oscillations, and not of spiking, when referring to features in the time evolution of the random lasers. In the field of random lasers, the term spiking is already used to describe sharp features in the frequency domain.[27]

Relaxation oscillations are observed in the output power of a laser, and occur when the spontaneous emission time of the population is (much) longer than the laser cavity decay time. We can calculate the output power of a cw laser using the four-level rate equations of a single-mode laser [92]

$$\frac{dN_1(t)}{dt} = P_L(t) - \frac{\beta_{\mathrm{sm}}q(t)N_1(t)}{\tau} - \frac{N_1(t)}{\tau},\tag{8.1a}$$

$$\frac{dq(t)}{dt} = -\frac{q(t)}{\tau_c} + \frac{\beta_{\mathrm{sm}}N_1(t)}{\tau}\left(q(t)+1\right),\tag{8.1b}$$

with N_1 the number of molecules in the excited state, q the cavity photon number, β_{sm} the spontaneous emission factor, P_L the pump rate (in photons per second), τ the spontaneous emission life time of the gain medium (dye), and τ_c the cavity decay time. The cavity photon number is proportional to the output power of a laser.

Relaxation oscillations in the output power of a cw laser system stem from the difference in duration between the cavity decay time and the spontaneous emission time of the excited molecules. To illustrate this physical origin, we will describe two cases: a laser with a cavity decay time much shorter than the spontaneous emission time, and a laser with the cavity decay time equal to the spontaneous emission time. In the first case, we expect relaxation oscillations to occur, while in the second case, no relaxation oscillations should occur.

8.1.1   Cavity decay time shorter than spontaneous emission time

We start with the first extreme case: a cavity decay time much shorter than the spontaneous emission time. In Fig. 8.1 the computed time evolution of the population of the excited state N_1, and of the cavity photon number q is shown for a single-mode cw laser using Eq. (8.1). Note the threshold value of N_1, which is at population inversion, and the steady-state value of q, q_{ss}. We clearly see the oscillation in both q and N for increasing t. At small t, the cavity photon number is approximately 0 (to be more precise: the cavity photon number is at noise level, due to spontaneous-emission events), and the population N_1 is built up by the pump. When N_1 reaches its threshold, at time t_1 in the figure, the system reaches the threshold, and the cavity photon number starts to build up. The excited population increases further until the cavity photon number reaches its equilibrium value, at time t_2. At this point in time the rate of (stimulated) emission of the molecules in the laser is equal to the excitation rate of these molecules by the pump laser. A further increase of q
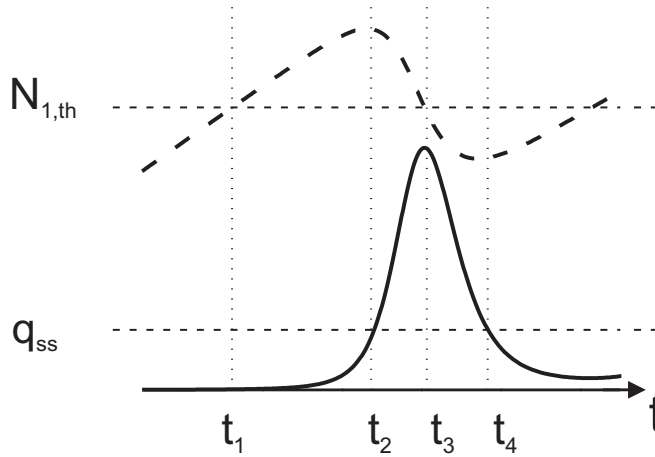
Figure 8.1: *Computed time evolution of the population N_1 (dashed line) and the cavity photon number q (solid line) in a laser. The pump is continuous wave, but turned on abruptly. Population inversion occurs at the threshold of the population, N_{th}. The steady state value of the cavity photon number is q_{ss}. The cavity decay time is chosen much shorter (a factor 1600) than the spontaneous emission time.*

leads to a decrease of N_1. As long as population inversion is present in the system, q will continue to build up. Only when N_1 is below its threshold, at t_3 in the figure, the population inversion is no longer present in the system, and q starts to decrease as well. This decrease of q is rapid: the first term in Eq. (8.1b), $-q/\tau_c$ is larger than the other terms in this equation, since the cavity decay time τ_c is much shorter than the spontaneous emission time τ. Once the cavity photon number is below its steady state value, t_4, the number of stimulated emission events is smaller than the number of excitations due to the pump. The population N_1 can increase again and the above described process starts again. At the end of an oscillation, the value of q will be higher than at the beginning of that oscillation. The oscillations will eventually damp out around the steady-state value q_{ss}, and N_{th}.

8.1.2 Cavity decay time equal to the spontaneous emission time

The second case, where we put the cavity decay time equal to the spontaneous emission life time, is depicted in Fig. 8.2. The time evolution is very different in comparison to the above case: no oscillations occur in this second situation. Once again, we see for small t that the population N_1 is built up by the pump and q is almost zero (at noise level). When the threshold of the population is reached, t_1, the cavity photon number q starts to build up from noise. Although q does not reach its equilibrium value at t_2, the population starts to decrease. This decrease is due to
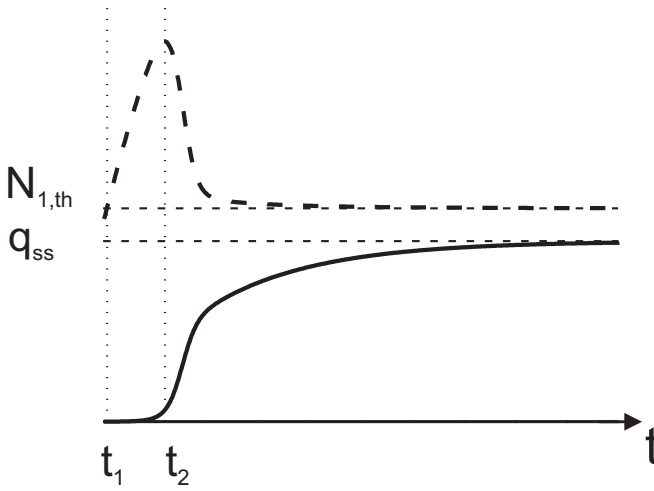
Figure 8.2: *Computed time evolution of population N_1 (dashed line) and q (solid line), the cavity photon number. The pump is continuous wave,but is turned on abruptly. Population inversion occurs at the threshold of the population, N_{th}. The steady state value of the cavity photon number is q_{ss}. The cavity decay time is chosen equal to the spontaneous emission time.*

the stimulated emission that will take place in the system. When we take a closer look at the time evolution of the increase of q, we see a rapid increase, followed by a slower increase. The change in the rate of the increase is due to the change in the number of excited molecules N_1 in the system: Far above threshold N_1 is large, and the cavity photon number can build up rapidly. When the number of excited molecules decreases, the increase of q is slowing down. In Fig. 8.1 this behavior can also be seen.

In this example, where τ is equal to τ_c, N_1 does not decrease rapidly below its threshold value, followed by a rapid decrease of q; The first term in Eq. (8.1b) no longer dominates for large q, and in the rate equations (8.1) the second and third term in both equations are equal, but opposite in sign. The number of photons in the cavity increases, as long as N_1 remains above threshold. There are no relaxation oscillations, and N_1 approaches the threshold value $N_{1,\mathrm{th}}$, and q the steady state value q_{ss} in an overdamped way.

8.2 A simple model

Relaxation oscillations are described by the four-level rate equations (8.1). From these rate equations we can derive an equation for the frequency of the relaxation

oscillations. Siegman has derived this formula for the two cases described previously, neglecting the spontaneous emission.[92] Woerdman and coauthors have generalized the expression and included the spontaneous emission:[115]

$$\omega_{\mathrm{res}} = \sqrt{\left(\frac{M-1}{\tau_c\tau}\right) - \frac{1}{4}\left[\frac{M}{\tau} - \frac{\beta}{\tau_c(M-1)}\right]^2}, \tag{8.2}$$

where ω_{res} is the relaxation oscillations frequency, and M the scaled pump fluence, defined as the ratio of the incoming fluence P and the threshold fluence P_{th}. We apply this model to the multi-mode pulsed random laser by simply changing β to β_{mm} and τ_c to $\tau_{\mathrm{c,mm}}$, i.e. we assume a mean cavity decay time for our multi-mode random laser. More details on this approach have been given in section 7.3.1.

8.3 Experimental apparatus

The time evolution of a titania random laser was measured. The sample consists of a suspension of TiO_2 powder in a 1 mmol/l solution of sulforhodamine B in methanol, and has a transport mean free path of 0.5 µm. A detailed description of titania random laser samples is given in section 6.1.1. For the measurements we used a time-resolved setup, described in section 6.2.2.

8.4 Measured relaxation oscillations

The normalized time trace of the pump pulse and the normalized time trace of the emitted light from the random laser far above threshold are shown in Fig. 8.3. Overall, the duration of the pump laser pulse is longer than the duration of the pulse of light the random laser emits. We see in the pulse emitted by the random laser first a fast decay, followed by a slower exponential decay. The fast decay is due to the stimulated emission in the random laser. In the second part of the decay the population inversion is no longer present, and the spontaneous emission causes a slower decay of intensity. These observations are in agreement with another random laser experiment.[94]

We measured the time evolution for different input fluences. In Fig. 8.4 the normalized intensity is plotted versus time for four different pump fluences. The time traces are shifted vertically with respect to each other for clarity. The time trace at a pump fluence of 0.06 mJ/mm^2 is below threshold, while the time traces with higher pump fluences are above threshold. We observe that relaxation oscillations occur above threshold and become more pronounced when the pump fluence increases.

The frequency of the relaxation oscillations are computed from the time traces. We determine the times at which the intensity is at a local maximum. The difference of two consecutive local maxima Δt is the period, and the frequency of the
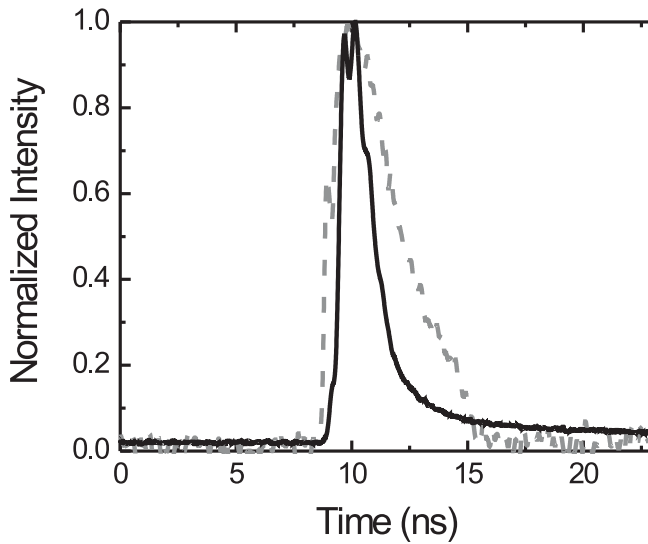
Figure 8.3: *Measured time traces of the pump pulse (gray) and emission output above threshold (black, input fluence = 0.47 mJ/mm²) of a titania random laser. The pump pulse duration is much larger than the duration of the emitted light of the random laser above threshold. Relaxation oscillations in the emitted light are clearly visible near the peak intensity. The decay time of the emitted light is first dominated by stimulated emission. In the second part of the decay-curve, the spontaneous emission is dominating.*
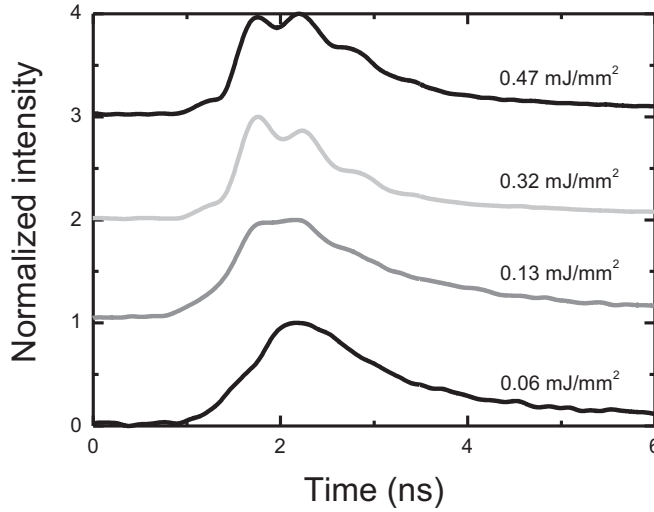
Figure 8.4: Measured time traces of the emission intensities of a titania random laser for four different pump fluences. The traces are vertically shifted with respect to each other for clarity. Relaxation oscillations become more pronounced at higher pump fluences.

relaxation oscillation ν_{res} is given by

$$\nu_{\text{res}} = \frac{1}{\Delta t}. \tag{8.3}$$

8.5 Comparison of the measurements with the model

We have inferred the relaxation oscillation frequency for different pump fluences from our measurements, using Eq. (8.3). In Fig. 8.5 the measured relaxation oscillations frequencies are plotted versus the normalized pump fluence M. The relaxation-oscillation frequency first decreases when the scaled pump fluence increases from 1 to 2. A further increase of the scaled pump fluence does not change the frequency of the relaxation oscillation. The result of Eq. (8.2) is depicted for different cavity decay times. This cavity decay time is the only parameter that could not be directly determined by our experiment. The trend of the model for a fixed cavity decay time is that, in contrast to our measurements, the relaxation-oscillations frequency increases for increasing pump fluence. Only for large (> 3) normalized pump fluence the fit of the model for a cavity decay time of 5 ps fits reasonably.

In section 7.3.1, we have used the distribution of the phase-delay time to deter-
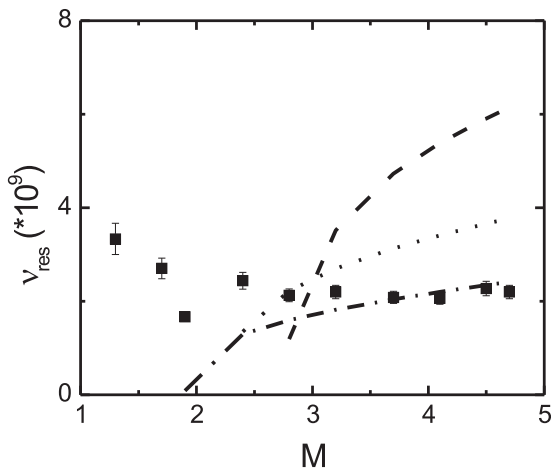
Figure 8.5: Measured relaxation oscillations frequency as a function of the normalized pump fluence (squares). The simple model [Eq. (8.2)] is plotted for different cavity decay times: 0.7 (dashed line), 2 ps (dotted line), and 5 ps (dash-dotted line). The fit of the model for a cavity decay time of 5 ps fits reasonably for high pump fluences, but corresponds to a surprisingly large value of τ.

mine the mean cavity decay time $\overline{\tau_c}$

$$\overline{\tau_c} = \frac{1}{8}\frac{L^2}{D},$$ (8.4)

with L the length of the gain volume and the diffusion constant $D = c_0\ell/(3n')$, where c_0 is the speed of light in vacuum, ℓ the transport mean free path and n' is the real part of the effective refractive index of the medium. This formula for $\overline{\tau_c}$ gives for our titania random laser a $\overline{\tau_c}$ in the order of 10^{-13} s, in contrast to 10^{-12} s that we found by fitting the simple model to our data. The difference between the two cavity decay times is a factor 10. This deviation could originate from the difference between the mean cavity decay time $\overline{\tau_c}$ of all modes and the mean cavity decay time of the lasing modes: The lasing modes inside a random laser are modes with an extreme long cavity decay time.

8.6 Summary

We have seen relaxation oscillations in our random laser, while looking at the time evolution of the total emitted light for different realizations of the sample. Multiple modes contributed to these time traces, and we averaged the time traces over several realizations of disorder of our random laser sample. The resulting time trace still showed relaxation oscillations: a weighted average of the oscillations of all the underlying modes.

The measured relaxation oscillations were compared with a simple model, based on a single-mode continuous-wave laser system. The cavity decay time determined with the fit from the simple model is a factor 10 higher than the mean cavity decay time of our sample. However, the cavity decay time of a random laser mode can be much larger than this mean value.

9

Quantitative analysis of several random lasers

In this chapter we propose a set of experimental data and parameters to be reported in publications on random laser experiments.[105] This set of data allows for a comparison between different experiments, between different theories, and between experiments and theory. The set of data we suggest can be divided in sample properties (section 9.2), experimental details (section 9.2.1), and experimental data (section 9.2.2). After we describe this set of data we will report in section 9.3 on an analysis of published experimental results and new experiments of our own. In section 9.4 we apply our analysis to models.

9.1 Introduction

Models that have been proposed to explain spikes in the emitted spectrum include a local cavity model with interference in a random laser [26], also referred to as the local mode model, and the lucky-photon model without interference taken into account [68], also referred to as the open mode model. As of yet, no consensus exists which physical mechanisms underly spike formation in random lasers, and it is therefore not clear which parameters influence this formation most.[107] A comparison between different experimental studies is very difficult, as the experiments have many parameters not all of which are described completely in literature. To

make meta-studies possible in the future, we list several parameters that should be reported in all (future) publications.

9.2 Optical and material properties of the sample

At least the following optical and material properties of the sample are needed for a comparison:

- transport mean free path ℓ (including the measurement method), as it provides key information about the strength of scattering
- absorption length of the pump light ℓ_a, as it provides information about how far the pump light can travel inside the random laser
- characterization of the scatterers (material, density, and thickness of the sample), for information about, e.g., damage threshold and heat conductivity
- gain material (material, and minimum gain length)
- presence (absence) of window or substrate surrounding the sample

9.2.1 Experimental details

At least the following experimental details are required:

- focus area A of the pump beam on the sample, as it provides information of the size and shape (together with ℓ and ℓ_a) of the amplified volume
- wavelength of the pump laser λ_p
- duration of the pump pulse t_p, as studies have shown that pulse duration is an important parameter[5, 104]
- repetition rate of the pump laser
- pump fluence I for every published spectrum
- integration time for every published spectrum

9.2.2 Experimental data

Before we list the required experimental data, we briefly elaborate on two key criteria: the occurrence of spikes and gain narrowing. The occurrence of spikes in an emission spectrum of a random laser is a central issue. To determine if an emission spectrum contains spikes we take the pump fluence at a peak height (A in Fig. 9.1) and at the highest shoulder of this peak (B in Fig. 9.1). If the difference is more than 5% of the highest shoulder value, we count a spike. Smaller features cannot be resolved reliably in many experiments. The width of the spike is derived from a Lorentzian fit to the data. We analyze each emission spectrum, count the number of spikes, and determine the height and width of each spike. From these heights and widths we calculate their mean value and standard deviation.
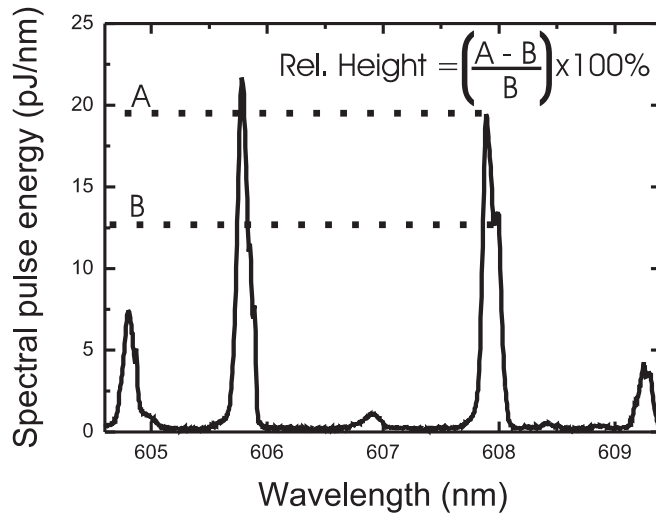
Figure 9.1: A measured emission spectrum of a gallium phosphide random laser. Our method to determine whether or not a sharp feature is a spike is displayed. We take the spectral pulse energy A at a peak height and the spectral pulse energy B at the highest shoulder of this peak. The formula for the relative height is displayed in the figure. If the relative height is more than 5%, the feature is counted as a spike.

Gain narrowing can be quantified by the narrowing factor NF, defined as the spectral width of the emitted light far above threshold divided by the spectral width far below threshold.

In conclusion, for a thorough quantitative analysis at least the following experimental data of the random laser are needed:

- number of spikes
- if the spectral position of spikes is fixed (yes/no)
- average width w and standard deviation of width distribution (preferably in units of energy) of spikes
- average relative height h and standard deviation of height distribution of spikes
- emission spectrum around the central emission wavelength λ_e.
- narrowing factor NF
- pump fluence at threshold, I_{th}

9.3 Analysis of experimental data

With this quantitative framework in mind, we have done a specific literature search to compare a number of different published experimental results. Out of the more

than 150 publications on random lasers, we found only 8 that were complete enough for this analysis, resulting in 13 spectra (number 1-13). The properties of each sample and the corresponding experimental details were taken and, where possible, translated to the properties described above. We analyzed experimental results by scanning the published emission spectra of the several random lasers. In addition, we analyzed our own experimental data on a gallium phosphide random laser[107], the analyzed single-shot spectrum (number 14) is shown in Fig. 9.1.

The sample properties and experimental details of our compilation are listed in table 9.1. The experimental data is presented in table 9.2 for experiments where spikes occurred in the emission spectrum. When we compare the different experimental data in table 9.2, we notice that the average Q factor of the laser modes (defined as λ_e/w in units of energy) is very much alike. Only our own measurement on a porous gallium phosphide random laser (no. 14) has an average Q-factor that is a factor 3 larger. When we compare the heights, we observe that all the height distributions are similar, except for number 9, 10 and 14. The spectra 9 and 10 are from a very special random laser: a photonic crystal with disorder. We conclude that, surprisingly, all experimental results are similar within the uncertainty, except for our own. The reason for this difference could be the very low mean free path ℓ of our sample.

9.4   Analysis of the open-mode model

Now we will proceed to analyze the models together with the experimental data the apply to. We only found one paper by Mujumdar *et al.* [68], that showed both the outcome of experiment and a model (the open-mode model). We determined the characteristics of the spikes in both the experimental and theoretical published spectra. The result is listed in table 9.3. Our comparison between their model and their experiments shows that the width distribution of their experimental spikes extracted by us is predicted correctly by their model. The width is not discussed explicitly in their paper. However, the height distribution extracted by our analysis of their model differs substantially from their experimental result.

9.5   Conclusions

In conclusion we have prescribed in this chapter the sets of data needed for a thorough quantitative analysis for both random-laser experiments and models. With these sets a comparison is possible between experiments, and between experiments and models. Surprisingly, all experimental results are similar within the experimental uncertainty except for our own porous gallium phosphide random laser.

no. [ref.]	ℓ [μm]	ℓ_a [μm]	scatt.	scatt. density [m^{-3}]	gain *	ℓ_g [μm]	A [mm^2]	λ_p [nm]	t_p [ps]	I [MW/mm^2]
1 [56]	200	172.5	TiO$_2$	2.8 $\times$ 10^{10}	R640P	n.p.	2.5	532	7000	0.15
2 [68]	87.8	18.0	ZnO	n.p.	R6G	n.p.	0.0035	532	25	n.p.
3 [68]	538	18.0	ZnO	n.p.	R6G	n.p.	0.0035	532	25	n.p.
4 [5]	9.5	n.a.	ZnO	6.55$\times$ 10^{19}	ZnO	n.p.	5	248	5	13.4
5 [26]	8.5	86.3	ZnO	2.5 $\times$ 10^{11}	R640P	n.p.	n.p.^{b}	532	25	36000
6 [26]	3.0	86.3	ZnO	1 $\times$ 10^{12}	R640P	n.p.	n.p.^{b}	532	25	20714
7 [26]	4.9	86.3	ZnO	6 $\times$ 10^{11}	R640P	n.p.	n.p.^{b}	532	25	24286
8 [117]	2	n.p.	ZnO	3.66$\times$ 10^{18}	ZnO	n.p.	0.00005	355	20	11
9 [36]	$\geq$ 500	89.8	SiO$_2$	5.23$\times$ 10^{19}	R6G	n.p.	var.	532	var.	0.1
10 [36]	$\geq$ 500	89.8	SiO$_2$	5.23$\times$ 10^{19}	R6G	n.p.	var.	532	var.	0.15
11 [74]	12	89.8	TiO$_2$	8.6 $\times$ 10^9	R6G	n.p.	var.	532	100	n.p.
12 [74]	12	89.8	TiO$_2$	8.6 $\times$ 10^9	R6G	n.p.	var.	532	100	n.p.
13 [69]	n.p.	15	Al$_2$O$_3$	n.p.	R6G	n.p.	n.p.	532	10000	n.p.
14 [107]	0.6	22	GaP	$\sharp$	R640P	12	0.000003	567	3000	0.016

n.p. : not presented, var.: different values were listed, introducing ambiguity about what value is relevant

* R640P = Rhodamine 640 perchlorate, and R6G = Rhodamine 6G. All the dyes are dissolved in methanol, except for numbers 9 and 10, here ethylene glycol is used. $\sharp$ Porosity GaP 45% air ^{b} Based on the used lens and pump wavelength we estimate $A = 5.6 \times 10^{-6}$ mm^2

Table 9.1: The sample properties and experimental details of several random lasers from literature. Listed are the transport mean free path ℓ, absorption length ℓ_a, the scatter material and the density of the scatterers, the gain material and the gain length ℓ_g, the size of the focus of the pump light on the sample A, the pump wavelength λ_p, the pulse duration of the pump pulse t_p and the pump fluence of the spectrum under consideration I.

no.	[ref]	spikes	NF	I_{th}	w	$\sigma(w)$	h	$\sigma(h)^{\sharp}$	λ_e	Q
				[MW/mm^2]	[cm^{-1}]	[cm^{-1}]	[%]	[%]	[nm]	
2	[68]	13	n.p.	n.p.	13.7	8.3	27	24	585	1250
3	[68]	11	n.p.	n.p.	9.6	3.5	28	28	585	1780
6	[26]	12	3	7143	12.2	7.2	30	16	608	1350
7	[26]	8	3.4	11429	18.4	10.7	18	6	608	894
8	[117]	10	3.4	9	50.7	20.2	37	21	375	526
9	[36]	3	4.4	0.01	17.8	17.8	122	114	565	994
10	[36]	13	4.4	0.01	10.1	1.6	107	159	565	1750
11	[74]	12	10	n.p.	15.2	10.4	46	29	562	1170
12	[74]	13	10	n.p.	10.2	3.7	35	30	562	1740
14	[107]	9	13.3	0.008	3.0	1.4	102	170	607	5490

n.p. : not presented.

Table 9.2: The experimental results for different published experimental emission spectra of random lasers that feature spikes, and our own emission spectrum. Listed are the number of spikes, the narrowing factor of the spectrum NF, the threshold of the pump fluence I_{th}, the mean value of the width w and the standard deviation of the distribution of spikes, the mean value of the relative height h and the standard deviation of the height distribution of spikes, the central wavelength of the emission spectrum under consideration λ_e, and the Q factor.

	ℓ	spikes	w	$\sigma(w)$	h	$\sigma(h)$
	[λ_e]		[cm^{-1}]	[cm^{-1}]	[%]	[%]
Exp.*	150.1	13	13.7	$\pm$ 8.3	27.3 $\pm$	23.9
Mod.$^{\natural}$	150.1	11	13.9	$\pm$ 5.4	176	$\pm$ 380
Exp.*	920	11	9.62	$\pm$ 3.49	27.6 $\pm$	28.3
Mod.$^{\natural}$	920	6	11.0	$\pm$ 6.9	199	$\pm$ 317

* Exp. = Experiment, $^{\natural}$ Mod. = Model.

Table 9.3: Characterization of the spikes from the experiment and open-mode model by Mujumdar et al. [68] . The width of the spikes predicted by the model is within one standard deviation of the experimental width. The prediction of the height distribution differs substantially from their experimental result.

Spatial extent of random laser modes

In the past few years a debate on the origin of the narrow spectral features (spikes) that occur in the emission spectrum of some random lasers has started [4, 6, 25, 32, 64, 68, 72, 89, 96]. On one hand Cao et al. [25], as well as Sebbah and Vanneste [89] and Apalkov et al. [6], attribute the spikes to local cavities (local modes, LM) for light, which are formed by multiple scattering. A recent numerical study also supports this LM model.[118] On the other hand Mujumdar et al. [68], as well as Pinheiro and Sampaio [72], attribute the spikes to single spontaneous emission events that, by chance, follow very long light paths (open modes, OM) in the sample and hence pick up a very large gain. The LM and the OM model we cite represent divergent answers to the question what the spatial extent is of the modes responsible for the spikes.

The spatial extent of the modes is a crucial factor for the fundamental behavior of a random laser. If the spatial extent of the modes is small, and the modes do not spatially overlap, the laser effectively consists of a collection of single-mode lasers. In contrast, spatially overlapping modes inside the random laser lead to distinctly multi-mode behavior, such as mode competition. Mode competition can also be observed in short-cavity dye lasers [46] and in many solid-state lasers.

In this chapter, we present the first systematic study of the spatial extent of the modes of a random laser, and show the crossover from essentially single-mode to multi-mode behavior in a new type of random laser: single crystal porous gallium phosphide [87], filled with liquid dye solution.[107] Among other conclusions, our results indicate that the LM model describes the physics of our random laser better than the OM model, but the LM model needs more sophistication.

10.1   Experimental apparatus

For the measurements described in this chapter, two gallium phosphide random laser samples were used. A complete description of the fabrication of these samples is given in section 6.1.2. All measurements, except the measurement of the mode competition described in section 10.3 are performed with one typical sample. The transport mean free path ℓ of this sample filled with pure methanol is measured with an enhanced-backscatter cone experiment [102, 116] and is 0.5 ± 0.2 µm at $\lambda = 633$ nm ($k\ell = 5.7 \pm 1.8$, with k the vacuum wave number, $n_{\text{eff}} = 2.2 \pm 0.3$ with a porosity of 43.6% air). The transport mean free path ℓ of the sample used for the measurement of the mode competition (section 10.3) filled with pure methanol is also measured with an enhanced-backscatter cone experiment [102, 116] and is 0.6 ± 0.3µm at $\lambda = 633$ nm ($k\ell = 6.4 \pm 2.8$, with k the vacuum wave number, $n_{\text{eff}} = 2.0 \pm 0.3$, with a porosity of 52.7% air).

The gallium phosphide sample has three characteristics which set it apart from other random laser. Firstly, due to the solid backbone of the crystal the realization of disorder is rigidly fixed. Secondly, the available gain in the system is high, as rhodamine 640 perchlorate in methanol is an efficient laser dye. Finally, the contrast of the refractive indices in the sample is the highest ever reported for random lasers: n = 1.33 for methanol and 3.4 for gallium phosphide, resulting in an index contrast of 2.56.

All measurements with the setup described in section 6.2.3. The pump energy on the sample was at maximum 0.32 µJ/pulse. The emission light of the random laser is collected through the same objective and detected by a spectrometer (resolution, 1 cm^{-1}) and an electron-multiplier charge-coupled device camera (C9100-02, Hamamatsu) The slit of the spectrometer was opened to 55 ± 15 µm. Due to this opening, a change in the incident angle of the light caused the spectral position to shift. The spectra shown in this chapter were corrected for this displacement where necessary.

All measurements presented in this chapter are measured at an input energy of twice the threshold input energy. This threshold is defined as the collapse of full width at half maximum (FWHM) of the emitted light, see for more details section 5.1.1. The FWHM of the spectrum far above threshold is 13 times narrower than the FWHM of the emitted light below threshold.

We performed a detailed calculation, presented in appendix E, that showed that the collected emitted laser-light of the sample is generated inside the pores of the gallium phosphide, and not e.g. by the dye between the window and the sample.
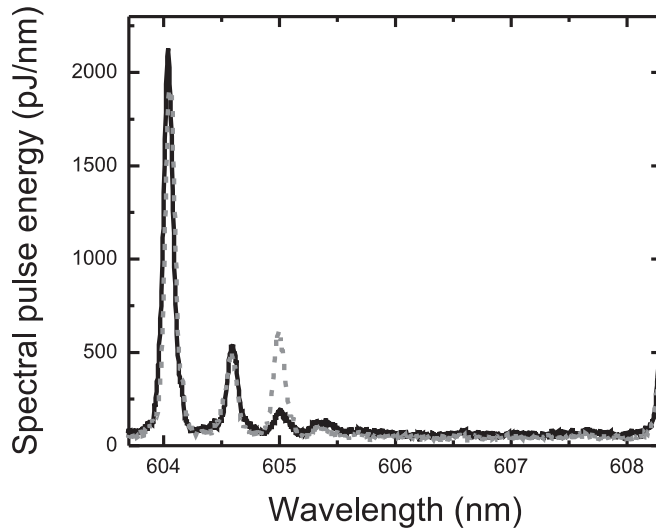
Figure 10.1: Two emission spectra of the random laser collected at the same spot on the sample. One spectrum (black solid line) before, and one (gray dashed line) after shifting the sample by 37 µm and back. Apparently, the frequencies of the modes are fully determined by the realization of the disorder.

10.2 Fixed spectral position of modes

To discriminate between current models, and possibly stimulate new theoretical approaches, we want to investigate whether mode frequencies are completely determined by the realization of disorder inside the random laser. In contrast to the frequencies of the modes, we expect that in all cases the peak intensities will depend on the pump energy; as we have pulse-to-pulse fluctuations of our pump source, we expect a different overall scale factor for our peak intensities for every shot. We collected several spectra above threshold at a single position on the sample. In between measurements, the sample was translated 37 µm and back. Two of the resulting spectra are shown in Fig. 10.1. Hysteresis of the stepper motor causes the sample not to return exactly to the same position (systematic error 0.04 µm). The gray spectrum is shifted accordingly by 0.07 nm. The spectral positions of the modes reproduce, proving that the frequencies of the modes are completely determined by the realization of disorder, and not selected by spontaneous-emission events.

10.3   Mode competition

In addition to the expected overall scale factor the peak intensities above threshold differed individually from shot-to-shot, as is shown in Fig. 10.1. To investigate the origin of this height-distribution variation, we looked at the emission spectrum of the random laser at a single position for different pump energies. We took 50 single shot measurements, and used the measured pulse-to-pulse variation of the pump source to obtain a range of pump energies. Above threshold we observed a linear relation between the total energy of the emitted light and the pump energy. A typical emission spectrum is shown in Fig. 10.2. We determined the energies in the observed 4 narrow peaks in the emission spectrum (integration of spectrum over 0.576 nm). In Fig. 10.3 we plotted these energies versus the total pulse energy of the emitted light. When the total emitted pulse energy increases above a threshold of 50 pJ, we observed that a single mode starts to lase (star symbol). In this regime, the random laser can be described as a single-mode laser. We found a decrease of the width of this single mode for increasing pulse energy in the mode, in correspondence with the well-known Schawlow-Townes behavior [85]. At higher emitted pulse energies (125 to 150 pJ) two more modes of the random laser start to lase, whereas the energy in the first mode does not increase anymore. This leveling-off is a clear sign that the modes are competing for the available energy, and thus are overlapping in space. This spatial mode competition causing the height-distribution variation is not related to the frequencies of the modes.

10.4   The spatial extent of a mode

To directly observe the spatial extent of the modes *inside* the random laser, we measured emission spectra at different positions of the random laser sample. In contrast to this direct method, the spatial extent of the modes *on the surface* of a random medium can be determined using speckle correlation techniques [25]. In our experiment the sample was horizontally translated with steps of 506 ± 4 nm, and for every position of the sample 50 single-shot-emission spectra were collected. We displaced the sample 20 µm in total, which is 10 times the diameter of the pump spot. In Fig. 10.4 zoom-in of collected spectra at 5 consecutive positions are shown. Spectra of Fig. 10.4 are shifted with respect to the top one by 0.154 nm, 0.211 nm, 0.274 nm, 0.288 nm, respectively. Figure 10.4 is a visualization of a typical evolution of a peak in the emission spectrum as the position of the sample is changed. The peak energy is related to the gain inside the mode. First only a small part of the spatial extent of the mode is in the gain region, and a low peak is visible. Further displacement of the sample leads to a larger overlap of the mode and the gain region, to more gain in the mode, and thus to a higher peak intensity. When the mode leaves the gain region again, the peak intensity decreases as well.
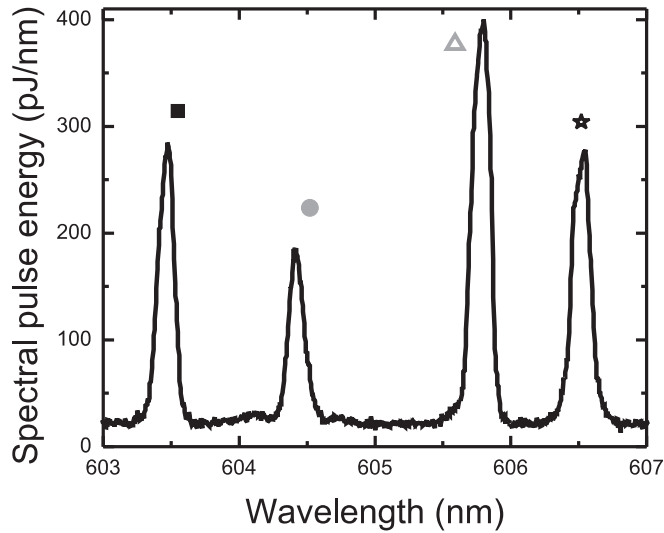
Figure 10.2: One of the 50 single-shot-emission spectrum of our random laser system collected at one position of the sample. The symbols near the peaks correspond to the pulse energy of those peaks in Fig. 10.3.
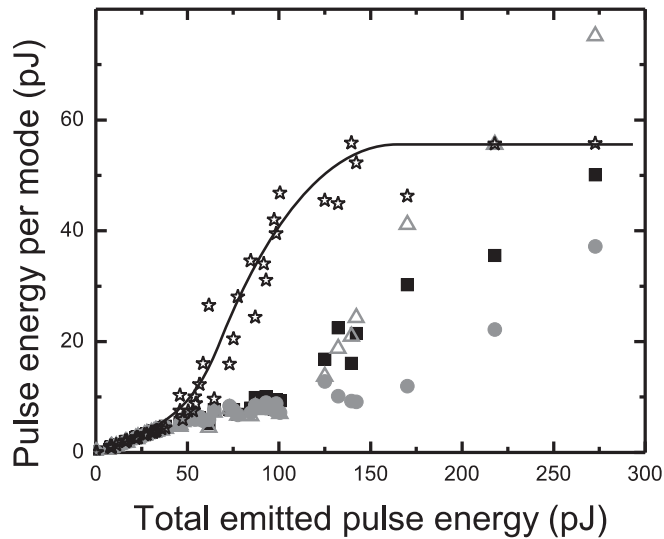
Figure 10.3: Pulse energy in 4 modes [see for single-shot emission spectrum Fig. 10.2] versus the total emitted pulse energy of the collected light for 50 single-shot spectra. The measured errors are smaller than the symbol size. The solid line is a guide to the eye for the star symbols. Clearly, one mode starts to lase (star symbol), before the other modes begin to lase at higher pump energies.
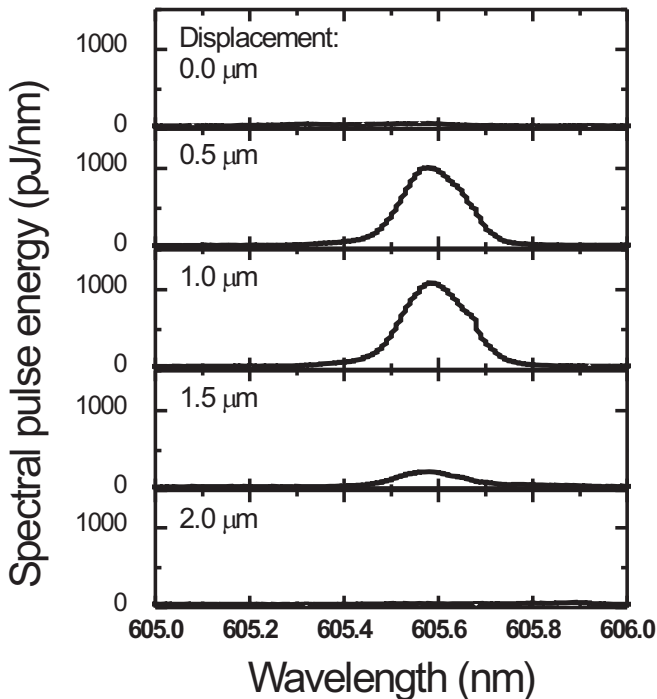
Figure 10.4: Enlargement of a part of the emission spectra where a peak is visible. Between consecutive spectra, the sample is translated by 506 nm.

The displacement between the position of the sample where the peak appears and the position of the sample where the peak disappears is a measure for the spatial extent of a mode. In the specific case of Fig. 10.4 the spatial extent is 2.5 ± 0.5 µm.

For all the modes measured during the translation of the sample, we have determined the spatial extent. In Fig. 10.5 the distribution of the spatial extent of the modes is plotted, together with a marker of the diameter of the focus of the pump source on the sample. Almost 80% of the modes have a spatial extent smaller than the diameter of the spot size of the focus (2 µm). The other 20% of the modes are larger than the diameter of the spot size of the focus. For the LM (OM) model, we would expect all modes to have a spatial extent much smaller (larger) than the focus diameter of the pump spot. Apparently, our measured distribution consists of both open and local modes, and disagrees with the expectation of the two models. The selection mechanism for a mode to become a lasing mode is its dwell time [104]. Given the observed limited spatial extent of lasing modes our experiments suggest that modes with long dwell times have a small spatial extent. Although maybe not that surprising, this connection has never been put forward before.
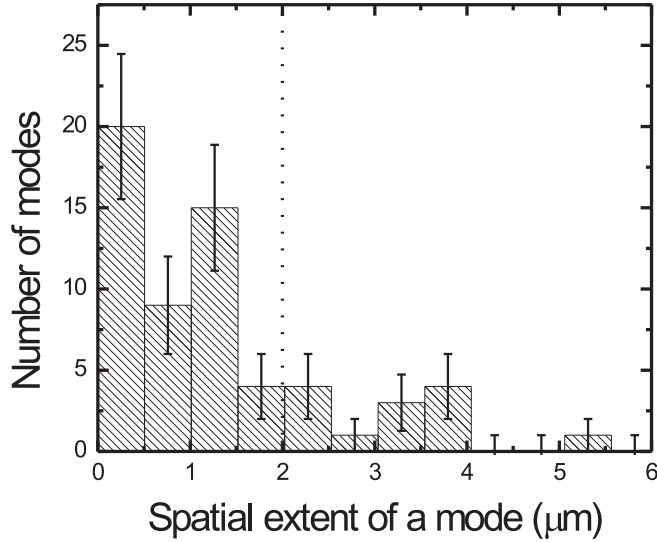
Figure 10.5: *Measured distribution of the spatial size of the modes determined with a displacement measurement. The dotted line is a marker for the diameter of the focus of the pump source on the sample.*

10.5 Statistics of spectral spacings of modes

We will now focus on the statistics of spectral spacings of the modes. For 11 spectra taken at widely spaced positions, we determined the spectral spacing between two adjacent peaks. These 11 spectra are statistically independent but equivalent. The only difference is the position on the sample where the data was collected. Therefore we combine the spectral spacings of these 11 spectra in one distribution. In Fig. 10.6 we plot this distribution of the spectral mode spacing. Surprisingly, our observations show that the statistics are determined by level repulsion, i.e. the spectral repulsion of the modes, in complete analogy to level repulsion in quantum mechanics [13, 71]. A first experimental indication of spectral level repulsion was shown by Cao *et al.* [24].

To describe spectral repulsion quantitatively we compare our observed statistics of the spectral mode spacings to the results of random-matrix theory. Although the random matrix theory does not necessarily apply to our situation, it does describe avoided crossings. The distribution of the mode spacings according to the Gaussian orthogonal ensemble (GOE) of random-matrix theory is given by Wigner's surmise [44]

$$P(x) = Cxe^{-\pi x^2/(4\Delta^2)}, \tag{10.1}$$

89
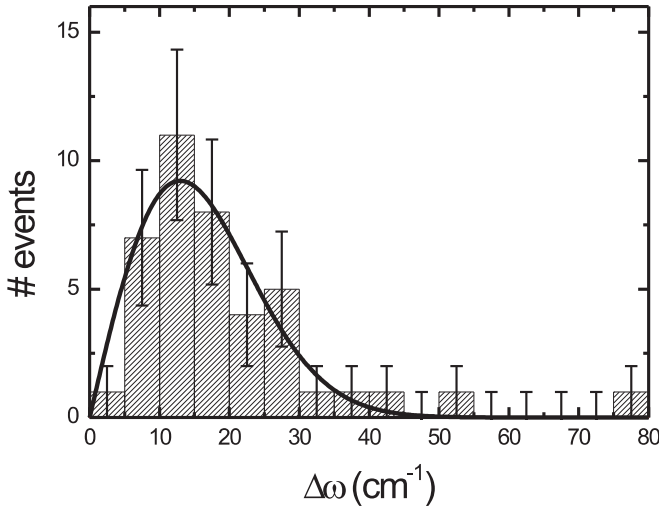
Figure 10.6: Measured distribution of the spectral mode spacing for 11 emission spectra. The solid line is a fit of Wigner's surmise (10.1). The fit parameter is the mean mode spacing Δ, we find $\Delta = 16.2$ cm^{-1}.

where P is the distribution of the mode spacing x of the modes, Δ the mean mode spacing, and C a scaling factor. In a system with uncorrelated scattering, where level repulsion is not present, Poissonian statistics of the mode spacing is expected [44]. In Fig. 10.6 we plot the fit of Eq. (10.1) (black line), with a mean GOE mode spacing Δ of 16.2 ± 0.9 cm^{-1}. Apparently, the selection mechanism for random lasing (only modes with long enough dwell times give rise to lasing [104]) causes the level statistics to change from Poissonian statistics to level repulsion.

10.6 Summary

We have performed a systematic study of random lasing in porous gallium phosphide. The frequencies of the modes in our sample are determined by the realization of disorder. We have observed a variation in the height distribution of the lasing modes in our multi-mode random laser system. This variation is attributed to spatial mode overlap and gain competition. The distribution of the spectral mode spacings shows clear level repulsion and can be described with the Gaussian orthogonal ensemble. We hope that our observations of small spatial extent of the lasing modes and level repulsion in the frequency domain stimulate more theoretical work.

Appendices

Avoiding violation of Kramers-Kronig relations

The mathematical treatment of gain is quite subtle, as it is strongly related to the question of causality which is expressed by agreement with Kramers-Kronig relations. To our surprise we have found that in a number of papers the gain is introduced in such a way that it violates Kramers-Kronig relations. Apparently this is a subtle and easy to make mistake. To make our point clear we will show below with very relevant examples what the problem is, and how to circumvent it.

General response theory

We start with a brief summation of the general response theory as can be found in books.[34, 65] In the general linear response theory the polarization of a medium in the scalar approximation is given by Eq. (9) on page 60 of Ref. [65] or Eq. (2.42) of Ref. [34], which for our particular case leads to

$$P(t) = \int_{-\infty}^{t} \alpha(t - \tau)E(\tau)d\tau, \tag{A.1}$$

with $E(t)$ the incident electric field and $\alpha(t)$ the polarizability which has the following properties, see also Eq. (14), on page 61 of Ref. [65] and Eq. (3.21) of Ref. [34]

$$\alpha(t) = -\alpha(-t), \tag{A.2}$$

$$\alpha(t) = -\alpha^*(t). \tag{A.3}$$

The criterium for a stable system (with no gain) is given by Refs. [65] and [43]

$$\text{Dissipation:} \qquad -i\omega \int \frac{d\alpha(t)}{dt} e^{-i\omega t} dt \geq 0. \qquad \text{(A.4)}$$

If we want to describe gain rather than dissipation, we obtain

$$\text{Gain:} \qquad -i\omega \int \frac{d\alpha(t)}{dt} e^{-i\omega t} dt < 0. \qquad \text{(A.5)}$$

We define the (Fourier) Laplace transform of $P(t)$ for a complex frequency z by Eq. (2.46a) of Ref. [34]

$$P[z] \equiv 2i \int_0^\infty e^{izt} P(t) dt, \quad \text{with } Im(z) > 0, \qquad \text{(A.6)}$$

and $P[z]$ can only be defined if the integral exists and converges, which puts constraints on $P(t)$; $P[z]$ can also be defined for $Im(z) < 0$, see also Eq. (2.46b) of Ref. [34]. We can see from Eq. (A.1) that

$$P[z] = \alpha[z]E[z]. \qquad \text{(A.7)}$$

For physical relevant systems, $z \to \omega \pm i\epsilon$, where $\epsilon \downarrow 0$, and we will analyze the case for $z = \omega + i\epsilon$.

$$\lim_{\epsilon \downarrow 0} \alpha[\omega + i\epsilon] \equiv \alpha'(\omega) + i\alpha''(\omega). \qquad \text{(A.8)}$$

Note the difference between the square brackets (Fourier Laplace transform) and the normal round brackets (Fourier transform). In the following we will leave out the $\lim_{\epsilon \to 0}$ notation, but this notation is always implicitly present.

The dissipation criterium in the time domain can be translated to the frequency domain (Ref. [65] and Eq. (2.69) of Ref. [34])

$$\text{Dissipation:} \qquad \omega\alpha''(\omega) \geq 0, \qquad \text{(A.9)}$$
$$\text{Gain:} \qquad \omega\alpha''(\omega) < 0. \qquad \text{(A.10)}$$

We know that both $\alpha''(\omega)$ and $\alpha'(\omega)$ depend on $\alpha(t)$ in the following way

$$\alpha''(\omega) = \int \alpha(t) e^{i\omega t} dt = 2i \int_0^\infty \sin(\omega t)\alpha(t) dt, \qquad \text{(A.11)}$$

$$\alpha'(\omega) = 2i \int_0^\infty \cos(\omega t)\alpha(t) dt. \qquad \text{(A.12)}$$

From these two equations we can deduce the Kramer-Kronig relations, keeping in mind that $\alpha(t)$ is an odd function and purely imaginary:

$$\alpha'(\omega) = \frac{1}{\pi} P \int_{-\infty}^\infty \frac{\alpha''(x)}{x - \omega} dx, \qquad \text{(A.13a)}$$

$$\alpha''(\omega) = \frac{1}{\pi} P \int_{-\infty}^\infty \frac{\alpha'(x)}{x - \omega} dx. \qquad \text{(A.13b)}$$

In the following sections we will give three examples for a harmonically bound charge oscillator. The first example is the damped case. The second example is a harmonic oscillator with gain, introduced as we have seen in literature. The third example that will be discussed is a pumped three-level system. In this system, gain is introduced in such a way, that Kramers-Kronig relations (A.13) remain satisfied.

Example 1: damped bound charged harmonic oscillator

The equation of motion of a charged bound oscillator with a harmonic driving electric field $E(t) = E_0 e^{-i\omega t}$ is given by Eq. (6), on page 82 of Ref. [65] and Eq. (3.3) of Ref. [54]

$$\frac{d^2 Q(t)}{dt^2} + \gamma \frac{dQ}{dt} + \omega_0^2 Q(t) = \frac{q}{m} E(t), \tag{A.14}$$

with the solution in the long time limit

$$Q(t) = \frac{q/m}{\omega_0^2 - \omega^2 - i2\omega\gamma} E_0 e^{-i\omega t}, \tag{A.15}$$

with ω_0 the resonance frequency and γ the (radiation) damping. We use the induced dipole moment p to find the polarization α, as can be seen in Eq. (3.5) of Ref. [54]

$$p(t) = qQ(t) \equiv \alpha_1[\omega + i\epsilon] E_0 e^{-i\omega t}, \tag{A.16}$$

where the subscript 1 is used to differentiate between our three examples. We find for the complex polarizability

$$\alpha_1[\omega + i\epsilon] = \alpha_0 \frac{\omega_0^2}{\omega_0^2 - \omega^2 - i2\omega\gamma}, \quad \text{with } \gamma > 0, \tag{A.17}$$

where $\alpha_0 = \frac{q^2}{\omega_0^2 m}$. We can deduce $\alpha(t)$ and simplify the equation by assuming $\omega_0 \gg \gamma$ (Eq. (8) on page 41 of Ref. [65])

$$\alpha_1(t) = -\frac{i}{2}\alpha_0 \omega_0 \sin(\omega_0 t) e^{-\gamma t}. \tag{A.18}$$

The response functions in the frequency domain of this example, i.e. $\alpha_1'(\omega)$ and $\alpha_1''(\omega)$, obey Kramers-Kronig relations (A.13) and thus causality. The complex polarizability $\alpha_1[z]$ in Eq. (A.17) is analytic in the upper half complex plane (note $\gamma > 0$).

Example 2: harmonic oscillator with gain, violating causality

We refer to the polarizability in this example as $\alpha_2(t)$. A widely spread method to introduce gain is changing only the sign of the damping term γ in Eq. (A.17). Here

we will demonstrate that this method of introducing gain has drastic consequences and violates Kramers-Kronig relations. The polarizability is given by

$$\alpha_2[\omega + i\epsilon] = \alpha_0 \frac{\omega_0^2}{\omega_0^2 - \omega^2 + i2\omega\gamma_g} \quad \text{with } \gamma_g > 0. \tag{A.19}$$

Inspection shows that $\alpha_2''(\omega$ and $\alpha_2'(\omega)$ are not related by Kramers-Kronig relations (A.13); there is a sign difference. If we look in detail to $\alpha(t)$, and change the sign of γ in Eq. (A.18) we obtain

$$\alpha_2(t) = -\frac{i}{2}\alpha_0\omega_0 \sin(\omega_0 t)e^{\gamma_g t}. \tag{A.20}$$

As can be seen immediately, equation (A.20) is not the inverse Laplace transform of equation (A.19) as the integral does not converge. Even stronger, Eq. (A.19) does not have an inverse (Fourier) Laplace transform. Therefore, the frequency-dependent response function (A.19) has no response function associated with it and an interpretation of this function as a stationary frequency domain function is for this reason absolutely unphysical.

A visualization of what happens is shown in Fig. A.1. The position of the poles is shown for a damped bound charged harmonic oscillator (squares), and a harmonic oscillator with gain, violating causality (circles). Poles that are in the lower half of the complex plane are consistent with Kramers-Kronig relations (A.13), thus with causality. However, allowing γ to go from negative (damping) to positive (gain), equals the transition from the lower half complex plane to the upper half complex plane.

Example 3: harmonic oscillator with gain, in agreement with causality

We refer to the polarizability in this example as $\alpha_3(t)$. We have to come up with an $\alpha_3(t)$ obeying Eq. (A.5):

$$-i\omega \int \frac{d\alpha_3(t)}{dt}e^{-i\omega t}dt < 0. \tag{A.21}$$

A sign change of γ, as was demonstrated in example 2, leads to unphysical results and will not obey the criterion (A.21). A very simple example of introducing gain consistently is for instance by changing the sign of $\alpha(t)$

$$\alpha_3(t) = -\alpha_1(t), \tag{A.22}$$
$$\alpha_3[\omega + i\epsilon] = -\alpha_1[\omega + i\epsilon]. \tag{A.23}$$

By doing so, we will always fulfill Kramers-Kronig relations (A.13), as can be deduced from Eq. (A.11) and (A.12). Effectively, Eq. (A.22) states that in Eq. (A.17) the sign of the whole denominator is changed, and not only the sign of γ.
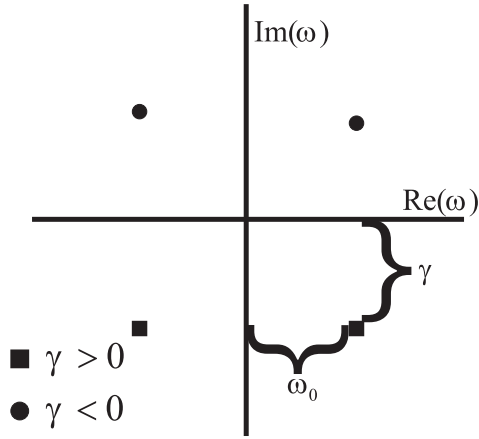
Figure A.1: Complex frequency plane, the position of the poles is indicated for damping (squares) and gain (circles).

Of course a microscopic justification of pumping schemes should be developed to verify Eq. (A.22) or any other $\alpha_3(t)$, an example can be found in Ref. [84]. But every microscopic polarizability $\alpha(t)$ that follows the dissipation criterion (A.5) would be a consistent way to describe gain in the system.

General conclusions

Generally speaking, if $\alpha[z]$ is analytic in the upper half complex plane (so its poles can only be in the lower half complex plane) an inverse (Fourier) Laplace transform $\alpha(t)$ exists and the frequency-dependent response functions $\alpha'(\omega)$ and $\alpha''(\omega)$ are related by Kramers-Kronig relations.

However, if the poles of $\alpha[z]$ are located in the upper half complex plane, a time-dependent response function exists, but this time-dependent response function is not the inverse Laplace of the frequency-dependent response functions. Therefore the Kramers-Kronig relations are not fulfilled. This corresponds to an a-causal situation, if the results are interpreted as time-independent.

$\mathcal{B}$

Solution of diffusion equation for slab geometry with internal source

In this appendix we will calculate the solution of the diffusion equation for a slab geometry with a source in the center of the slab. This solution is necessary to compute the (Taylor expansion of) electric field correlation function. From the electric field correlation function the mean cavity decay time can be calculated.

We consider the diffusion of scalar waves through a slab of random material. The slab fills the space $0 \leq z \leq L$ and is infinite in the other directions. In this geometry it is convenient to use Fourier transformed coordinates $\mathbf{q}_\perp \equiv (q_x, q_y)$ for the traverse directions. In the Fourier space the translational symmetry between x and y in a slab geometry reduces the two variables x and y to only one: $\mathbf{q}_\perp$. The slab is illuminated from the inside of the slab, as is the case in a random laser, by a pulse at time $t = 0$. Since the light quickly loses its directionality due to scattering, it is possible to model the incoming light by a diffuse source at position z_0 inside the material. The ensemble averaged energy density of diffuse light I is described by the diffusion equation:

$$\left[\partial_t - D\nabla^2 + \frac{1}{\tau_{\text{abs}}}\right] I(\mathbf{r}, t) = \delta(z - z_0)\delta(t)S(x, y), \tag{B.1}$$

with on the left hand side $\partial_t \equiv \partial/\partial t$, D the diffusion constant, and τ_{abs} the absorption time. We assume that the phase velocity is equal to the energy velocity. The right hand side of Eq. (B.1) is the source term, where the delta function $\delta(t)$ gives the time at which the pulse is released, the delta function $\delta(z - z_0)$ gives the

position of the source, and S describes the transverse distribution of the source and has the dimension of energy. The total energy in the source pulse is given by $S(\mathbf{q}_\perp = 0)$. [112]

We solve the diffusion equation analytically in the frequency domain. This solution can conveniently be used to find the field correlation function, the total transmission and the average diffuse traversal time (decay time).

Take the Fourier transform of the diffusion equation (B.1) with respect to x, y, and t. We start with the left hand side of this diffusion equation (B.1):

$$
\begin{aligned}
lhs &= \int\int\int dxdydt \left\{ \partial_t - D[\partial_x^2 + \partial_y^2 + \partial_z^2 - \alpha^2] \right\} I(x,y,z,t)e^{-iq_x x}e^{-iq_y y}e^{-i\Omega t}, \\
&= \int\int dydt \left\{ \partial_t - D[(iq_x)^2 + \partial_y^2 + \partial_z^2 - \alpha^2] \right\} I(q_x,y,z,t)e^{-iq_y y}e^{-i\Omega t}, \\
&= \int dt \left\{ \partial_t - D[(iq_x)^2 + (iq_y)^2 + \partial_z^2 - \alpha^2] \right\} I(q_x,q_y,z,t)e^{-i\Omega t}, \\
&= \left\{ i\Omega - D[(iq_x)^2 + (iq_y)^2 + \partial_z^2 - \alpha^2] \right\} I(q_x,q_y,z,\Omega), \quad\quad\quad\text{(B.2)}
\end{aligned}
$$

with $\partial_x \equiv \frac{\partial}{\partial x}$. On the right side of Eq. (B.1) we do the same:

$$
\begin{aligned}
rhs &= \int\int\int dxdydt \left\{ \delta(z-z_0)\delta(t)\mathbf{S}(x,y) \right\} e^{-iq_x x}e^{-iq_y y}e^{-i\Omega t}, \\
&= \mathbf{S}(\mathbf{q}_\perp)\delta(z-z_0). \quad\quad\quad\text{(B.3)}
\end{aligned}
$$

Combining these two and substituting

$$
\eta \equiv \sqrt{\frac{i\Omega}{D} + \mathbf{q}_\perp^2 + \alpha^2}, \quad\quad\quad\text{(B.4)}
$$

we finally find

$$
\left[\eta^2 + \partial_z^2\right] I(\eta, \mathbf{q}_\perp, z) = \frac{\mathbf{S}(\mathbf{q}_\perp)}{D}\delta(z-z_0). \quad\quad\quad\text{(B.5)}
$$

We first look for the homogenous solution of Eq. (B.5) by setting the right part to zero and take a solution of the form $I_H(\eta, \mathbf{q}_\perp, z) = e^{-i\lambda z}$. When we insert this solution into Eq. (B.5) and divide the result by $e^{-i\lambda z}$, we obtain the characteristic equation and the roots of the homogeneous solution:

$$
\left[\eta^2 + \lambda^2\right] = 0, \quad\quad\quad\text{(B.6a)}
$$

$$
\lambda = \pm i\eta. \quad\quad\quad\text{(B.6b)}
$$

The complete homogeneous solution is thus given by

$$
I_H(\eta, \mathbf{q}_\perp, z) = A(\eta)e^{\eta z} + B(\eta)e^{-\eta z}. \quad\quad\quad\text{(B.7)}
$$

We can find the particular solution by taking the Fourier transform with respect to z of Eq. (B.5)

$$\int dz[\eta^2 + \partial_z^2]I_P(\eta, \mathbf{q}_\perp, z)e^{-iq_z z} = \int dz\frac{\mathbf{S}(\mathbf{q}_\perp)}{D}\delta(z - z_0)e^{-iq_z z}, \tag{B.8}$$

$$[\eta^2 + q_z^2]\, I_P(\eta, \mathbf{q}_\perp, q_z) = \frac{\mathbf{S}(\mathbf{q}_\perp)}{D}e^{-iq_z z_0}, \tag{B.9}$$

and take the back transform

$$I_P(\eta, \mathbf{q}_\perp, z) = \frac{1}{2\pi}\int dq_z I_P(\eta, \mathbf{q}_\perp, q_z)e^{iq_z z}, \tag{B.10a}$$

$$= \frac{1}{2\pi}\int dq_z \frac{\mathbf{S}(\mathbf{q}_\perp)}{D(\eta^2 + q_z^2)}e^{-iq_z z_0}e^{iq_z z}. \tag{B.10b}$$

We can solve the integral on the right hand side using contour integration and the residue theorem. This theorem states that if $f(z)$ is analytic within and on the boundary C of a region ξ except at a finite number of poles $a, b, c, \ldots$ within ξ, having residues a_{-1}, b_{-1}, c_{-1}, respectively, then

$$\oint_C f(z)dz = 2\pi i(a_{-1} + b_{-1} + c_{-1} + \ldots), \tag{B.11}$$

i.e. the integral of $f(z)$ is $2\pi i$ times the sum of the residues of $f(z)$ at the poles enclosed by C.[95]

Integral (B.11) can be split in two:

$$\oint_C f(z)dz = \int_{-\infty}^{\infty} f(z)dz... + \int_C f(z)dz...$$

The second term of the right hand side can be calculated using the lemma

If $\lim_{z\to\infty} f(z)(z - a) = A$, then $\lim_{p\to\infty}\int_{C_p} f(z)dz = iA\alpha$.

Hereby is C_p the closed curve with radius p.

In our case

$$f(q_z) = \frac{1}{(\eta^2 + q_z^2)}e^{-iq_z z_0}e^{iq_z z}, \tag{B.12}$$

$$\lim_{q_z\to\pm\infty} f(q_z)(q_z \pm i\eta) = \lim_{q_z\to\pm\infty}\frac{1}{(\eta^2 + q_z^2)}e^{-iq_z z_0}e^{iq_z z}(q_z \pm i\eta), \tag{B.13}$$

$$= \lim_{q_z\to\pm\infty}\frac{1}{(\eta^2 + q_z^2)}e^{-iq_z z_0}e^{iq_z z}(q_z \pm i\eta), \tag{B.14}$$

$$= \lim_{q_z\to\pm\infty}\frac{1}{(q_z \mp i\eta)}e^{-iq_z z_0}e^{iq_z z}, \tag{B.15}$$

$$= 0, \tag{B.16}$$

$$\int_C f(z)dz = 0. \tag{B.17}$$

We get for the residue equal to $i\eta$

$$
\begin{aligned}
\text{Residue} &= \lim_{q_z \to i\eta} \left\{ (q_z - i\eta) \frac{e^{iq_z(z-z_0)}}{\eta^2 + q_z^2} \right\}, \\
&= \lim_{q_z \to i\eta} \left\{ (q_z - i\eta) \frac{e^{iq_z(z-z_0)}}{(q_z + i\eta)(q_z - i\eta)} \right\}, \\
&= \lim_{q_z \to i\eta} \left\{ \frac{e^{iq_z(z-z_0)}}{(q_z + i\eta)} \right\}, \\
&= \frac{e^{-\eta(z-z_0)}}{2i\eta}.
\end{aligned}
\tag{B.18}
$$

The same derivation can be done for the residue $-i\eta$:

$$
\begin{aligned}
\text{Residue} &= \lim_{q_z \to -i\eta} \left\{ (q_z + i\eta) \frac{e^{iq_z(z-z_0)}}{\eta^2 + q_z^2} \right\}, \\
&= \lim_{q_z \to -i\eta} \left\{ (q_z + i\eta) \frac{e^{iq_z(z-z_0)}}{(q_z + i\eta)(q_z - i\eta)} \right\}, \\
&= \lim_{q_z \to -i\eta} \left\{ \frac{e^{iq_z(z-z_0)}}{(q_z - i\eta)} \right\}, \\
&= \frac{e^{\eta(z-z_0)}}{-2i\eta}.
\end{aligned}
\tag{B.19}
$$

The outcome for the contour-integral in both cases should be identical. As the integral over C vanishes, the integral is totally determined by the residue.

In case of $i\eta$ (thus $q_z > 0$) we have

$$
I_P(\eta, \mathbf{q}_\perp, z) = \frac{1}{2\pi} \int dq_z \frac{\mathbf{S}(\mathbf{q}_\perp)}{D(\eta^2 + q_z^2)} e^{-iq_z z_0} e^{iq_z z}, \tag{B.20}
$$

$$
= \frac{\mathbf{S}(\mathbf{q}_\perp)}{2\pi} \left[2\pi i \frac{e^{-\eta(z-z_0)}}{2i\eta} \right], \tag{B.21}
$$

$$
= \frac{\mathbf{S}(\mathbf{q}_\perp)}{2} \frac{e^{-\eta(z-z_0)}}{\eta}, \tag{B.22}
$$

In case of $-i\eta$ (thus $q_z < 0$) we have

$$
I_P(\eta, \mathbf{q}_\perp, z) = \frac{1}{2\pi} \int dq_z \frac{\mathbf{S}(\mathbf{q}_\perp)}{D(\eta^2 + q_z^2)} e^{-iq_z z_0} e^{iq_z z}, \tag{B.23}
$$

$$
= \frac{\mathbf{S}(\mathbf{q}_\perp)}{2\pi} \left[-2\pi i \frac{e^{\eta(z-z_0)}}{-2i\eta} \right], \tag{B.24}
$$

$$
= \frac{\mathbf{S}(\mathbf{q}_\perp)}{2} \frac{e^{\eta(z-z_0)}}{\eta}, \tag{B.25}
$$

The particular solution for all z is given by

$$
I_P(\eta, \mathbf{q}_\perp, z) = \frac{\mathbf{S}(\mathbf{q}_\perp)}{2} \frac{e^{-\eta|z-z_0|}}{\eta} \tag{B.26}
$$

The total solution $I(\eta, \mathbf{q}, z)$ can be written down, by combining the homogeneous (B.7) and particular solution (B.26)

$$I(\eta, \mathbf{q}_\perp, z) = \frac{\mathbf{S}(\mathbf{q}_\perp)}{D\eta} \left[e^{-\eta|z-z_0|} + A(\eta)e^{\eta z} + B(\eta)e^{\eta(L-z)} \right]. \tag{B.27}$$

In the last term, we replaced $-z$ with $L-z$, this can be done as it just results in a change of the not yet determined pre-factor $B(\eta)$. The homogeneous solution is explicitly symmetric around the middle of the slab. The prefactors $A(\eta)$ and $B(\eta)$ can be determined by using boundary conditions. In our case, we choose the following boundary conditions

$$I(\eta, \mathbf{q}_\perp, 0) = 0, \tag{B.28a}$$

$$I(\eta, \mathbf{q}_\perp, L) = 0. \tag{B.28b}$$

These boundary conditions lead to

$$A(\eta) = \frac{e^{\eta z} - e^{-\eta z}}{1 - e^{2\eta L}}, \tag{B.29}$$

$$B(\eta) = \frac{e^{\eta(L-z_0)} - e^{-\eta(L-z_0)}}{1 - e^{2\eta L}}. \tag{B.30}$$

When we insert the solution of $A(\eta)$ and $B(\eta)$ into Eq. B.27, we obtain a general solution of the diffusion equation B.1:

$$I(\eta, \mathbf{q}_\perp, z) = \frac{\mathbf{S}(\mathbf{q}_\perp)}{D\eta} [e^{-\eta|z-z_0|} + \frac{e^{2\eta z} - 1}{1 - e^{2\eta L}} + \frac{e^{\eta(L-z_0)} - e^{-\eta(L-z_0)}}{1 - e^{2\eta L}} e^{\eta(L-z)}]. \tag{B.31}$$

As an example, we set $z_0 = L/2$ in Eq. (B.31), and we obtain the solution of the diffusion equation (B.1) with a source positioned in the middle of the slab:

$$I(\eta, \mathbf{q}_\perp, z) = \frac{\mathbf{S}(\mathbf{q}_\perp)}{D\eta} \left[e^{-\eta|z-L/2|} - \left(\frac{e^{\eta(z-L/2)} + e^{\eta(L/2-z)}}{1 + e^{\eta L}} \right) \right],$$

$$= \frac{\mathbf{S}(\mathbf{q}_\perp)}{D\eta} \left[e^{-\eta|z-L/2|} - \left(e^{-\eta L/2} \frac{\cosh(\eta(z-L/2))}{\cosh(\eta L/2)} \right) \right]. \tag{B.32}$$

For illustration purposes, a plot of the intensity distribution inside the sample is shown in Fig. B.1, in the limit $\eta \to 0$. For $I_0 \equiv \lim_{\eta \to 0} I(\eta, \mathbf{q}_\perp, z)$, we obtain for $z > L/2$

$$I_0(z) = \lim_{\eta \to 0} \left[\frac{S(\mathbf{q}_\perp)}{D\eta} \left(e^{-\eta(z-L/2)} - \left(e^{-\eta L/2} \frac{\cosh(\eta(z-L/2))}{\cosh(\eta L/2)} \right) \right) \right],$$

$$= \lim_{\eta \to 0} \left[\frac{S(\mathbf{q}_\perp)}{D} \left(\frac{\cosh(\eta L/2)e^{-\eta(z-L/2)} - e^{-\eta L/2}\cosh(\eta(z-L/2))}{\eta \cosh(\eta L/2)} \right) \right],$$
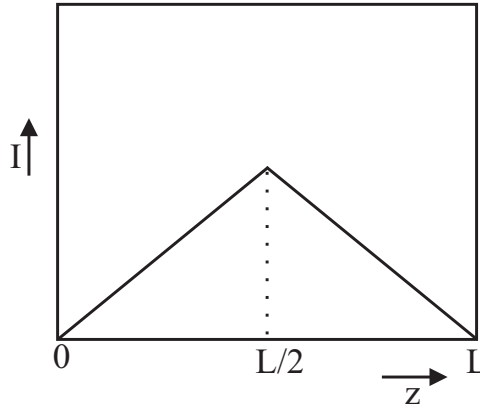
Figure B.1: The calculated light intensity of a source in a slab geometry. The source is positioned at $z = L/2$.

The numerator becomes with the rule of l'Hôpital

$$= \lim_{\eta \to 0} \Big[-(z - L/2)\cosh(\eta L/2)e^{-\eta(z-L/2)} + L/2\sinh(\eta L/2)e^{-\eta(z-L/2)}$$
$$+ L/2\cosh(\eta(z - L/2))e^{-L/2\eta} - (z - L/2)\sinh(-\eta(z - L/2))e^{-L/2\eta} \Big],$$
$$= L - z. \tag{B.33}$$

The denominator becomes:

$$= \lim_{\eta \to 0}[\cosh(\eta L/2) + \eta\sinh(\eta L/2)L/2],$$
$$= 1. \tag{B.34}$$

For $z < L/2$ we obtain for the numerator:

$$= \lim_{\eta \to 0} \Big[(z - L/2)\cosh(\eta L/2)e^{-\eta(z-L/2)} + L/2\sinh(\eta L/2)e^{-\eta(z-L/2)}$$
$$+ L/2\cosh(\eta(z - L/2))e^{-L/2\eta} - (z - L/2)\sinh(-\eta(z - L/2))e^{-L/2\eta} \Big],$$
$$= z. \tag{B.35}$$

The denominator does not change for the different value for z. The total solution for $I_0(z)$ is

$$I_0(z) = \begin{cases} L - z & \text{for} \quad z > L/2 \\ z & \quad z < L/2 \end{cases} \tag{B.36}$$

The intensity as function of the position in the slab is plotted in Fig. B.1. The maximum of the intensity is at the source, and it decays linearly. This is typical for diffusion processes.

$\mathcal{C}$

Calculation of the electric field correlation function

With the solution of the diffusion equation found in appendix B we can now calculate the electric field correlation function, needed to compute the mean cavity decay time.

The normalized electric field correlation function is given by [61]

$$C_E(\Omega, z) \equiv \frac{\langle E^*(\omega, z)E(\omega + \Omega, z)\rangle}{\sqrt{\langle |E(\omega, z)|^2\rangle\langle |E(\omega + \Omega, z)|^2\rangle}}. \tag{C.1}$$

We can rewrite this electric field correlation function in terms of $I(\Omega, z)$. We start with the numerator:

$$\langle E^*(\omega, z)E(\omega + \Omega, z)\rangle = A\langle \int d\omega E^*(\omega, z)E(\omega + \Omega, z)\rangle, \tag{C.2a}$$

$$= A\langle E^*(\Omega, z) \otimes E(\Omega, z)\rangle, \tag{C.2b}$$

$$= A\langle \int dt e^{-i\Omega t}E^*(t, z)E(t, z)\rangle, \tag{C.2c}$$

$$= A\int dt e^{-i\Omega t}I(t, z), \tag{C.2d}$$

$$= AI(\Omega, z). \tag{C.2e}$$

In the first step, the assumption is made that the electric field correlation function is constant in the bandwidth used here. The factor A comes in, a constant that falls

out with the normalization procedure. For the derivation of the denominator we use

$$\langle |E(\omega)|^2 \rangle \approx \langle |E(\omega + \Omega)|^2 \rangle. \tag{C.3}$$

Approximation (C.3) holds in our model, as $\omega \gg \Omega$ and $\langle |E|^2 \rangle$ is nearly constant in our frequency range. The denominator of rhs of Eq. (C.1) becomes

$$\sqrt{\langle |E(\omega, z)|^2 \rangle \langle |E(\omega + \Omega, z)|^2 \rangle} = \langle |E(\omega, z)|^2 \rangle, \tag{C.4}$$

$$= \langle E(\omega, z) E^*(\omega, z) \rangle, \tag{C.5}$$

$$= AI(\Omega = 0, z). \tag{C.6}$$

Inserting Eq. (C.2e) and (C.6) in Eq. (C.1)

$$C_E(\Omega, z) = \frac{I(\Omega, z)}{I(\Omega = 0, z)}. \tag{C.7}$$

To calculate the decay time in our sample, we need the solution at the border of our random laser sample. We choose $z = L$. The fraction of the rhs of Eq. (C.7) is undefined for $z = L$, as in the limit of $z \to L$ both the numerator and the denominator vanish. Using the rule of l'Hôpital, we obtain

$$C_E(\Omega, z) = \frac{\partial_z I(\Omega, z)}{\partial_z I(\Omega = 0, z)}, \tag{C.8}$$

$$= \frac{L}{z_0} e^{(L-z_0)\sqrt{i\Omega/D}} \frac{e^{2z_0\sqrt{i\Omega/D}} - 1}{e^{2L\sqrt{i\Omega/D}} - 1}, \tag{C.9}$$

The case of no absorption is treated ($\alpha = 0$).

We calculate the Taylor expansion of the electric field correlation function:[39]

$$\lim_{\Omega \to 0} C_E(\Omega) = 1 - ia\Omega + b\Omega^2 + \mathcal{O}(\Omega^3), \tag{C.10}$$

$$= 1 - i\frac{1}{6}\frac{L^2 - z_0^2}{D}\Omega - \frac{7L^4 - 10L^2 z_0^2 + 3z_0^4}{360D^2}\Omega^2 + \mathcal{O}(\Omega^3). \tag{C.11}$$

We find for a and b

$$a = \frac{1}{6}\frac{L^2 - z_0^2}{D}, \tag{C.12a}$$

$$b = -\frac{7L^4 - 10L^2 z_0^2 + 3z_0^4}{360D^2}, \tag{C.12b}$$

where a is the mean cavity decay time $\overline{\tau_c}$. This equality can be derived as follows, using the Taylor expansion of the electric field correlation function around $\Omega = 0$:

$$C_E(\Omega, z) = \frac{\langle E^*(\omega, z)E(\omega + \Omega, z)\rangle}{\langle E(\omega, z)E^*(\omega, z)\rangle}, \tag{C.13}$$

$$= \frac{\langle E^*(\omega, z)E(\omega, z)\rangle + \langle \Omega \frac{\partial}{\partial \Omega}\left[E^*(\omega, z)E(\omega + \Omega, z)\right]\rangle}{\langle E(\omega, z)E^*(\omega, z)\rangle}, \tag{C.14}$$

$$= 1 + \frac{\langle \Omega E^*(\omega, z)\frac{\partial}{\partial \Omega}E(\omega + \Omega, z)\rangle}{\langle E(\omega, z)E^*(\omega, z)\rangle}, \tag{C.15}$$

We set $E(\omega) = A(\omega)e^{-i\phi(\omega)}$, \hfill (C.16)

$$= 1 + \frac{\langle \Omega A(\omega)e^{i\phi(\omega)}\frac{\partial}{\partial \omega}\left[A(\omega)e^{-i\phi(\omega)}\right]\rangle}{\langle A^2(\omega)\rangle}, \tag{C.17}$$

$$= 1 + \frac{\langle \Omega A(\omega)\left[\frac{\partial A(\omega)}{\partial \omega} - iA(\omega)\frac{\partial \phi(\omega)}{\partial \omega}\right]\rangle}{\langle A^2(\omega)\rangle}, \tag{C.18}$$

We are interested in a, thus in the imaginary part only:

$$\mathrm{Im}(C_E(\Omega, z)) = -\frac{\langle A^2(\omega)\Omega\frac{\partial \phi(\omega)}{\partial \omega}\rangle}{\langle A^2(\omega)\rangle}. \tag{C.19}$$

When we compare this result with Eq. (C.10), we obtain

$$a = \langle \frac{\partial \phi(\omega)}{\partial \omega}\rangle, \tag{C.20}$$

$$= \overline{\tau_c} \tag{C.21}$$

For the case that a source is positioned in the middle of the slab, $z_0 = L/2$, we obtain

$$a = \frac{1}{8}\frac{L^2}{D}, \tag{C.22}$$

$$b = \frac{-5}{384}\frac{L^4}{D^2}. \tag{C.23}$$

Calculation of the distribution of phase-delay times

In this appendix we will calculate the distribution of phase-delay times. We use this distribution for the distribution of the decay times of modes inside a random laser, since at the moment there is no analytic formula for the distribution of these decay times.

The probability distribution of a single channel phase-delay time has been calculated by Genack and coauthors and by Van Tiggelen and coauthors. [39, 88] This distribution is normalized to the mean phase-delay time. We are interested in the distribution that is normalized to 1. We simply change the scale by

$$\tau_d = \psi\overline{\tau_d}, \tag{D.1}$$

with τ_d the decay time and $\psi \equiv \tau_d/\overline{\tau_d}$ the normalized decay time [1], and and $\overline{\tau_d}$ the ensemble averaged decay time. The probability distribution of the normalized decay time is given by [39]

$$P(\psi) = \frac{1}{2}\frac{Q}{[Q+(\psi-1)^2]^{3/2}}, \tag{D.2}$$

Q is a factor that is given by coefficients a and b from Eq. (C.12), as was derived in [39].

$$Q \equiv -2b/a^2 - 1 \tag{D.3}$$

$$= \frac{2}{5}\frac{L^2+z_0^2}{L^2-z_0^2}. \tag{D.4}$$
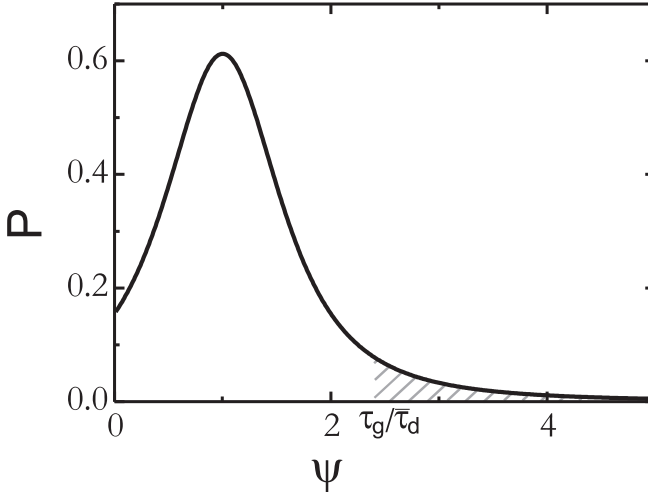
Figure D.1: The probability distribution of the decay time is plotted. In the figure the ensemble averaged decay time $\overline{\tau_d}$ is shown. Furthermore, the gain time τ_g of the system is pointed out. The hatched area shows all the modes with a decay time longer than the gain time: the lasing modes.

For a source positioned in the middle of the slab, $z_0 = L/2$, we find

$$Q = \frac{2}{3}, \tag{D.5}$$

$$P(\psi) = \frac{1}{3[2/3 + (\psi - 1)^2]^{3/2}}. \tag{D.6}$$

The distribution of the phase-delay times for a slab geometry, with the source positioned in the middle of the slab, is shown in Fig. D.1. The probability of the distribution will go to zero for both infinity and minus infinity. Negative phase-delay times do exist. However, any physical decay time will be positive. As there is to our knowledge at the moment no analytic expression of the distribution of the decay times, we will use the phase-delay time distribution for a source positioned in the middle of the slab instead and assume that the influence of the negative times is negligible.

E

Origin of observed spikes in porous gallium phosphide

Our gallium phosphide random laser sample was placed on top of a sapphire window, as is described in section 6.2.3. Due to our etching procedure, there was a small gap between the porous gallium phosphide and the sapphire window. An important question is, whether the sharp features we observed in our measurements were produced by modes inside our random laser, or by modes outside our random laser. Sharp features in the emitted light of a random cavity do occur.[31] In Fig. E.1 a schematic representation of our sample in its holder is depicted. Two cavities can be pointed out: one between the sapphire-air interface and the boarder of the porous gallium phosphide (A), and one between the sapphire-dye solution interface and the boarder of the porous gallium phosphide (B). With Fresnel's equations, the losses of the cavities can be calculated.[35]

In cavity A, at an angle of incidence of 0 degrees, the loss due to the reflection at the sapphire-air interface is 92%, and the loss due to the reflection at the dye solution-gallium phosphide interface is 80%. These losses cannot be compensated by the received gain of the light in the small path through the dye solution in the gap between the sapphire window and the porous gallium phosphide, as we will show below. If the angle of incidence is much larger than 0 degrees, the losses will be smaller. However, the spatial extent of a mode increases enormous if the angle of incidence is increased, while we conclude from our measurements, presented in section 10.4, that more than 80% of the modes is smaller than the size of the spot of our pump focus.
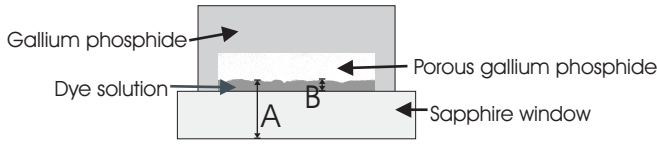
Figure E.1: Schematic enlargement of our random laser system in its holder. The pump light enters the sample via the sapphire window. We collect the emitted light also via the sapphire window. A small (∼ 5 µm) space between the sample and the window is filled with Rhodamine 101 dissolved in methanol. Two cavities are presented in the figure: one between the sapphire-air interface and the boarder of the porous gallium phosphide (A), the other one between the sapphire-dye solution interface and the boarder of the porous gallium phosphide (B).

In cavity B, at an angle of incidence of 0 degrees, the loss due to the reflection at the dye solution-gallium phosphide interface is 80%, and the loss due to the reflection at the methanol-sapphire interface is 98%. These losses might be compensated, if the path length through the gain medium (methanol) results in an amplification of the light with a factor 250, thus if the path length is 5.5 times the gain length. The minimal gain length in our system is approximately 12 µm. The path length should be in the order of 66 µm, which is clearly not the case. The same numbers hold for cavity A.

Another reason why the cavity A or B could not lead to the observed sharp features in our emitted light, is that we needed to tune the pump wavelength of our random laser to obtain enough gain in our system. The dye solution in the gap between the sapphire window and the porous gallium phosphide was in all cases saturated. Tuning the pump wavelength would not result in a different behavior.

A third reason is that as soon as we saw a change in the surface of the porous gallium phosphide, due to damage of the sample, the sharp features disappeared. The change on the surface of the porous gallium phosphide is a melting of the gallium phosphide. The surface will remain rough, and modes of a random cavity would still appear in our collected spectra. We conclude from the above arguments, that the emitted light that we collect originates from within the pores of our random laser sample.

Samenvatting

Tegenwoordig is de laser niet meer weg te denken uit onze maatschappij. De laser wordt dagelijks gebruikt, denk bijvoorbeeld maar eens aan cd- en dvd-spelers, of aan ziekenhuizen waar lasers worden gebruikt voor zeer nauwkeurige chirurgische handelingen. De doorlopende ontwikkelingen in de nanotechnologie (bijvoorbeeld het steeds verder verkleinen van geïntegreerde optische componenten) hebben geleid tot een zoektocht naar heel kleine lasers, nanolasers. In dit proefschrift zullen we experimenten van twee verschillende kleine lasers beschrijven, die een hoofdingrediënt delen: de terugkoppeling is gebaseerd op verstrooiing van licht. Vanwege deze manier van terugkoppeling worden deze kleine lasers door ons ook wel scattering lasers genoemd.

De werking van een laser berust op terugkoppeling en versterking van licht. In een 'gewone' laser wordt het licht teruggekoppeld door twee spiegels: licht beweegt tussen de spiegels heen en weer. Een versterkend medium wordt tussen de spiegels gezet. In dit versterkend medium, dat meestal bestaat uit gassen of kristallen, wordt licht versterkt door omzetting van energie uit een andere (externe) bron. Deze externe bron geeft energie aan het versterkend medium en wordt ook wel de pomp genoemd. Je kunt zo'n versterkend medium vergelijken met een heel speciale "glow-in-the-dark" sticker: als je een dergelijke sticker eerst in het licht houdt ("pompt") en vervolgens in het donker zal de sticker nog een hele tijd licht geven (uitzenden). Het versterkend medium in een laser heeft ook een opslag mecha-

113

nisme voor licht, maar op veel kortere tijdschalen: in plaats dat het minuten/uren duurt voordat licht uitgezonden wordt, zal licht binnen een miljoenste van een seconde al worden uitgezonden. Daarnaast zal het versterkend medium niet alleen energie opslaan en uitzenden, het zal ook het bestaande licht versterken: een soort "glow-in-the-light" sticker dus. De combinatie van de versterking en het terugkoppelen kan leiden tot een laser. In dit proefschrift beschrijf ik experimenten van scattering lasers: lasers waar het licht niet door spiegels wordt teruggekoppeld, maar door veelvuldige verstrooiing van licht.

Het eerste deel van dit proefschrift gaat over scattering lasers die maar uit één deeltje bestaan. Een enkel deeltje, bijvoorbeeld een waterdruppel of een plastic bolletje, kan licht van richting laten veranderen. In principe kan elk deeltje licht verstrooien, maar voor bolvormige deeltjes is precies bekend hoe dat gebeurt. Aan het begin van de twintigste eeuw werkten wetenschappers als Mie en Lorentz aan een beschrijvende theorie, die nu bekend staat als de Mie-theorie. Deze theorie beschrijft hoe licht dat op een bol valt, zijn weg vervolgt. Een uitbreiding van de Mie-theorie beschrijft hoe het licht van interne lichtbronnen zich voortplant binnen en buiten het bolletje. Deze theorie kunnen we gebruiken voor het beschrijven van de bolvormige nanolaser.

Voor de experimenten aan de bolvormige nanolaser is gebruik gemaakt van plastic bolletjes met een diameter van 0.01 millimeter, zo'n tien keer de golflengte van zichtbaar licht. De interne lichtbronnen zijn kleurstof moleculen. Dat zijn een soort moleculen die lichtdeeltjes (fotonen) uitzenden onder invloed van een externe energiebron. Als de kleurstof moleculen dicht genoeg op elkaar zitten, kunnen ze elkaar stimuleren om meer fotonen uit te zenden: het bolletje is een laser. De experimentele waarnemingen zijn vergeleken met de uitbreiding van de Mie-theorie, en er is gebleken dat er een discrepantie tussen de gangbare theorie en onze observaties zit. Deze discrepantie kan worden opgelost door de theorie aan te passen, bijvoorbeeld door rekening te houden met de dynamica van de externe energiebron, en met het gedrag van de dye moleculen in de bol. Door deze aanpassingen wordt de lichtversterking in de theorie tijdsafhankelijk en zal de theorie het gedrag van de lichtbronnen exact kunnen beschrijven.

In het tweede deel van dit proefschrift wordt een ander soort scattering laser beschreven: een "random laser". Deze scattering laser bestaat uit heel veel deeltjes, in tegenstelling tot de hierboven beschreven bolvormige nanolaser. Deze deeltjes zijn wanorderlijk gepositioneerd, vandaar de naam random laser. In een medium dat veel kleine deeltjes bevat met een diameter in de buurt van de golflengte van het licht, is het mogelijk om licht te "pesten". Het licht kan namelijk niet meer normaal door het medium gaan, zoals het geval is bij glas, maar zal veelvuldig verstrooid worden. Veelvuldige verstrooiing van licht, zoals dat gebeurt in mist, melk en verf, speelt in vrijwel alle takken van wetenschap en techniek een rol. In lasers probeert men verstrooiing meestal te voorkomen, omdat verstrooid licht niet door

de spiegels wordt opgesloten en dus verloren gaat. Maar meervoudige verstrooiing van licht kan juist een goede manier zijn om licht op te sluiten: de voorplanting van licht in een verstrooiend materiaal gaat langs willekeurige dronkemanswandelingen, waardoor het licht lang in hetzelfde gebied blijft. Wanneer er in dit gebied interne lichtbronnen aanwezig zijn, dan kan er versterking optreden, zoals hierboven al beschreven werd. Op deze manier maakt men een wanorderlijke laser, een random laser.

Er zijn veel verschillende soorten random lasers. In dit proefschrift hebben we gemeten aan twee verschillende random lasers die bestaan uit een groot aantal verstrooiende deeltjes, die geplaatst zijn in een versterkend medium. In het geval van de titania random laser zijn de verstrooiende deeltjes los poeder. De andere random laser waar we aan gemeten hebben bestaat uit een soort spons van gallium fosfide, die in het versterkend medium is geplaatst. Een belangrijk verschil tussen de twee random lasers is dat de positie van de verstrooiers in het geval van de titania random laser aan verandering onderhevig is, terwijl in de spons random laser deze positie vast is.

Licht zal door het sterk verstrooiende medium van de random laser een dronkemanswandeling maken, afhankelijk van de positie van de verstrooiers. Er zijn heel veel verschillende mogelijkheden voor het licht om zo een wandeling te maken, en elke wandeling zal een bepaalde tijd duren. De tijd die het licht nodig heeft om een bepaalde wandeling af te leggen wordt de verblijftijd genoemd. Een andere tijd die belangrijk is in een random laser is de versterkingstijd. Dit is de tijd dat het licht in het medium moet blijven om voldoende versterkt en teruggekoppeld te worden om van het verstrooiend medium een laser te maken. Deze versterkingstijd hangt af van de sterkte van de externe pomp en de hoeveelheid interne lichtbronnen die aanwezig zijn in het medium. Het gebiedje waarin een wandeling plaatsvindt zal in het vervolg een mode genoemd worden. In een random laser zijn er erg veel modes. Modes waarvan de verblijftijd langer is dan de versterkingstijd zullen gaan laseren.

In de titania random laser, met wisselende posities van de verstrooiers, zal elke nieuwe meting een andere verzameling van dronkemanswandelingen bevatten. Het is dan ook gebleken uit ons onderzoek dat het vermogen van het licht dat de laser uitzendt enorm fluctueert, ook al is de externe lichtbron (een gepulste laser) constant. De oorsprong van deze intrinsieke fluctuaties hebben we met behulp van een model beschreven: de verandering van de positie van de verstrooiers veroorzaakt de fluctuaties.

Er zijn wereldwijd veel experimenten aan random lasers gedaan, en onverwacht is in 1998 gevonden dat sommige van deze lasers spectraal zuiver licht produceren. De precieze oorsprong van dit licht is omstreden: komt het uit kleine gebiedjes of juist uit het gehele volume van de laser? Om deze vraag te beantwoorden hebben we een bijzondere wanorderlijke laser gemaakt, uitgaande van een galliumfosfide

spons, het sterkst verstrooiende niet-absorberende materiaal voor zichtbaar licht. Het licht van deze laser is spectraal vijfmaal zo zuiver als het licht van andere wanorderlijke lasers. Door de laser nauwkeurig te verplaatsen en met een microscoop te bestuderen is aangetoond dat het licht uit zeer kleine gebiedjes komt, een aanwijzing dat sterke verstrooiing in staat is licht op onverwacht kleine schaal op te sluiten.

Het combineren van versterking en verstrooiing leidt tot waardevolle nieuwe inzichten in beide fenomenen. Mogelijke toepassingen vinden wanorderlijke lasers, die eenvoudig te maken maar niet ná te maken zijn, in de waarmerking en codering van documenten, betaalmiddelen en informatie.

Summary

Part 1 In this thesis we describe experiments and theory of two types of scattering lasers, i.e. lasers in which the feedback is provided via multiple scattering of light. The first part of this thesis, chapter 1, consists of a broad introduction to scattering lasers in general.

Part 2 The second part of this thesis, chapter 2 to 4, describes experiments and theory of the first type of scattering lasers: the Mie laser. The Mie laser consists of a Mie sphere (in our case a polystyrene sphere with a diameter of 10 micrometer) doped with dye. Chapter 2 gives an specific introduction to Mie lasers, followed in chapter 3 by a detailed description of the experiment and the sample.

  Chapter 4, entitled "Laser threshold of Mie resonances", describes an experimental and theoretical study of the laser properties of a Mie laser. Many scientists incorporate gain in the Mie theory via a positive imaginary part of the refractive index. We show that time-independent scattering coefficients calculated from the extrapolated Mie theory to the gain regime have physical meaning only if the gain is below a critical value. This critical value is identified by us as the laser threshold. Based on this newly developed insight, we performed experiments on dielectric spheres with gain trapped with optical tweezers.

Part 3 The third part of this thesis describes the second type of scattering lasers: random lasers. In our experiments random lasers consist of a gain medium in which

random scatterers are positioned. In this third part we first give a more detailed description of random lasers (chapter 5), and the experiments themselves (chapter 6). We have done experiments on two types of random lasers. The first random laser consists of a suspension of titanium dioxide (titania) powder in a solution of sulforhodamine B in methanol. In this titania random laser the position of the scatterers is not fixed in time. In contrast, the second random laser we used in our experiments consists of porous gallium phosphide positioned in a solution of methanol and rhodamine 640. This second type of random laser combines three characteristics which set it apart from other random lasers: firstly, due to the solid backbone of the crystal the realization of disorder is rigidly fixed. Secondly, the available gain in the system is high, as rhodamine 640 in methanol is an efficient laser dye. Finally, the contrast of the refractive indices in the sample is the highest ever reported for random lasers: n = 1.33 for methanol and 3.4 for gallium phosphide.

In chapter 7, entitled "Intrinsic intensity fluctuations in random lasers", we study a recently discovered phenomenon: shot-to-shot fluctuations in the emitted light of the random laser, while the system is pumped by a pulsed pump source with constant energy output. These fluctuations occurred only with a random laser system pumped with nanosecond pulses, and not for the same system pumped with picosecond pulses. We will present our elaborated experimental and theoretical study of the statistics of shot-to-shot fluctuations and introduce a model that clarifies their existence. We performed measurements on a titania random laser pumped with both picosecond and nanosecond pulses. Our model includes an effective β factor, with which we can model our multi-mode random laser using the rate-equations of a single mode cw laser.

Chapter 8, entitled "Relaxation oscillations in random lasers", deals with a well-known laser phenomenon: relaxation oscillations. We will show the results of our research on the time evolution of a nanosecond pumped titania random laser system. We compare our experimental observations with a simple model, based on the four-level rate equations for a single-mode cw laser.

A prescript for future publications on random lasers is given in chapter 9, entitled "Quantitative analysis of several random lasers". This set of data allows for a comparison between different experiments, between different theories, and between experiments and theory. The set of data we suggest can be divided in sample properties, experimental details, and experimental data. We will report on an analysis of published experimental results and new experiments of our own. Finally, this analysis is also applied to models.

The final chapter of this thesis, chapter 10 entitled "Spatial extent of random laser modes", is a contribution to the debate on the origin of narrow spectral features ("spikes") that occur in the emission spectrum of some random lasers. This debate has started a few years ago. Two models are discussed: the local mode

model, in which the spikes are attributed to local cavities for light, formed by multiple scattering, and the open mode model, in which the spikes are attributed to single spontaneous emission events that, by chance, follow very long light paths in the sample and hence pick up a very large gain. These two models represent divergent answers to the question what the spatial extent is of the modes responsible for the spikes. The spatial extent of the modes is a crucial factor for the fundamental behavior of a random laser. If the spatial extent of the modes is small, and the modes do not spatially overlap, the laser effectively consists of a collection of single-mode lasers. In contrast, spatially overlapping modes inside the random laser lead to distinctly multi-mode behavior, such as mode competition. We present the first systematic study of the spatial extent of the modes of a random laser, and show the crossover from essentially single-mode to multi-mode behavior in a porous gallium-phosphide random laser.

References

[1] *A different notation is used, here we use $\tau \equiv \hat{\phi}'$ [39]* — p.109.

[2] *Sachtleben Chemie GmbH, Hombitan RCL 66 Titandioxid, 89+% TiO$_2$-rutile, surface coated with alumina/silica, mean diameter of 180 nm.* — p.40.

[3] N. G. Alexoupoulos and N. K. Uzunoglu, *Electromagnetic scattering from active objects: invisible scatterers*, Appl. Opt. **17**, 235 (1978) — p.15, 23, and 24.

[4] L. Angelani, C. Conti, G. Ruocco, and F. Zamponi, *Glassy Behavior of Light*, Phys. Rev. Lett. **96**, 065702 (2006) — p.33 and 83.

[5] D. Anglos, A. Stassinopoulos, R. N. Das, G. Zacharakis, M. Psyllaki, R. Jakubiak, R. A. Vaia, E. P. Giannelis, and S. H. Anastasiadis, *Random laser action in organic-inorganic nanocomposites*, J. Opt. Soc. Am. B **21**, 208 (2004) — p.33, 49, 64, 65, 78, and 81.

[6] V. M. Apalkov, M. E. Raikh, and B. Shapiro, *Random resonators and prelocalized modes in disordered dielectric films*, Phys. Rev. Lett. **89**, 016802 (2002) — p.33, 35, and 83.

[7] A. Ashkin, *Acceleration and trapping of particles by radiation pressure*, Phys. Rev. Lett. **24**, 156 (1970) — p.21.

[8] A. Ashkin and J. M. Dziedzic, *Observation of Resonances in the Radiation Pressure on Dielectric Spheres*, Phys. Rev. Lett. **38**, 1351 (1977) — p.6, 11, and 21.

[9] R. M. Balachandran, N. M. Lawandy, and J. A. Moon, *Theory of laser action in scattering gain media*, Opt. Lett. **22**, 319 (1997) — p.35.

[10] M. L. M. Balistreri, D. J. W. Klunder, F. C. Blom, A. Driessen, J. P. Korterik, L. Kuipers, and N. F. v. Hulst, *Experimental analysis of the whispering-gallery modes in a cylindrical optical microcavity*, J. Opt. Soc. Am. B **18**, 465 (2001) — p.12.

[11] W. Bäumler, A. X. Schmalzl, G. Gößl, and A. Penzkofer, *Fluorescence decay studies applying a cw femtosecond dye laser pumped ungated inverse time-correlated single photon counting system*, Meas. Sci. Technol. **3**, 384 (1992) — p.40.

[12] G. Beckering, S. J. Zilker, and D. Haarer, *Spectral measurements of the emission from highly scattering gain media*, Opt. Lett. **22**, 1427 (1997) — p.33.

[13] C. W. J. Beenakker, *Random-matrix theory of quantum transport*, Rev. Mod. Phys. **69**, 731 (1997) — p.89.

[14] C. W. J. Beenakker, J. C. J. Paaschens, and P. W. Brouwer, *Probability of Reflection by a Random Laser*, Phys. Rev. Lett. **76**, 1368 (1996) — p.24.

[15] R. E. Benner, P. W. Barber, J. F. Owen, and R. K. Chang, *Observation of Structure Resonances in the Fluorescence Spectra from Microspheres*, Phys. Rev. Lett. **44**, 475 (1980) — p.12.

[16] G. A. Berger, M. Kempe, and A. Z. Genack, *Dynamics of stimulated emission from random media*, Phys. Rev. E **56**, 6118 (1997) — p.67.

[17] C. F. Bohren and D. R. Huffman, *Absorption and Scattering of Light by Small Particles* (John Wiley and Sons, Inc., New York, 1983) — p.11, 12, 14, and 24.

[18] A. Bott and W. Zdunkowski, *Electromagnetic energy within dielectric spheres*, J. Opt. Soc. Am. A **4**, 1361 (1987) — p.28.

[19] B. Bret, *Multiple light scattering in porous gallium phosphide*, Ph.D. thesis, University of Twente (2005) — p.40.

[20] M. Cai, O. Painter, K. J. Vahala, and P. C. Sercel, *Fiber-coupled microsphere laser*, Opt. Lett. **25**, 1430 (2000) — p.12 and 23.

[21] A. J. Campillo, J. D. Eversole, and H. B. Lin, *Cavity Quantum Electrodynamic Enhancement of Stimulated Emission in Microdroplets*, Phys. Rev. Lett. **67**, 437 (1991) — p.23 and 28.

[22] H. Cao, *Lasing in random media*, Waves in Random Media **13**, R1 (2003) — p.33.

[23] H. Cao, *Review on latest developments in random lasers with coherent feedback*, J. Phys. A: Math. Gen. **38**, 10497 (2005) — p.33.

[24] H. Cao, X. Jiang, Y. Ling, J. Y. Xu, and C. M. Soukoulis, *Mode repulsion and mode coupling in random lasers*, Phys. Rev. B **67**, 161101 (2003) — p.89.

[25] H. Cao, Y. Ling, J. Y. Xu, and A. L. Burin, *Probing localized states with spectrally resolved speckle techniques*, Phys. Rev. E **66**, 025601(R) (2002) — p.33, 83, and 86.

[26] H. Cao, J. Y. Xu, S. H. Chang, and S. T. Ho, *Transition from amplified spon-*

taneous emission to laser action in strongly scattering media, Phys. Rev. E **61**, 1985 (2000) — p.34, 35, 37, 77, 81, and 82.

[27] H. Cao, Y. G. Zhao, H. C. Ong, S. T. Ho, J. Y. Dai, J. Y. Wu, and R. P. H. Chang, *Ultraviolet lasing in resonators formed by scattering in semiconductor polycrystalline films*, Appl. Phys. Lett. **73**, 3656 (1998) — p.31, 33, 49, and 68.

[28] H. Chew, *Transition rates of atoms near spherical surfaces*, J. Chem. Phys. **87**, 1355 (1987) — p.11 and 14.

[29] H. Chew, *Radiation and lifetimes of atoms inside dielectric particles*, Phys. Rev. A **38**, 3410 (1988) — p.11 and 14.

[30] V. V. Datsyuk, *Gain effects on microsphere resonant emission structures*, J. Opt. Soc. Am. B **19**, 142 (2002) — p.15, 23, and 24.

[31] P. C. de Oliveira, J. A. McGreevy, and N. M. Lawandy, *Speckle-mirror laser*, Opt. Lett. **22**, 700 (1997) — p.111.

[32] L. I. Deych, *Effects of Spatial Nonuniformity on Laser Dynamics*, Phys. Rev. Lett. **95**, 043902 (2005) — p.33 and 83.

[33] B. H. Erné, D. Vanmaekelbergh, and J. J. Kelly, *Morphology and strongly enhanced photoresponse of GaP electrodes made porous by anodic etching*, J. Electrochem. Soc. **143**, 305 (1996) — p.40.

[34] D. Forster, *Hydronamic Fluctuations, Broken Symmetry, and Correlation Functions*, No. 47 in Frontiers in Physics (W.A. Benjamin, Inc., New York, 1975) — p.93 and 94.

[35] G. R. Fowles, *Introduction to modern optics* (Dover publications, Inc., New York, 1975), 2nd ed. — p.111.

[36] S. V. Frolov, Z. V. Vardeny, A. A. Zakhidov, and R. H. Baughmann, *Laser-like emission in opal photonic crystals*, Opt. Commun. **162**, 241 (1999) — p.33, 49, 81, and 82.

[37] C. G. B. Garrett, W. Kaiser, and W. L. Bond, *Stimulated Emission into Optical Whispering Modes of Spheres*, Phys. Rev. **124**, 1807 (1961) — p.12.

[38] P. A. Gass and J. R. Sambles, *Angle-frequency relationship for a practical acousto-optic deflector*, Opt. Lett. **18**, 1376 (1993) — p.21.

[39] A. Z. Genack, P. Sebbah, M. Stoytchev, and B. A. van Tiggelen, *Statistics of Wave Dynamics in Random Media*, Phys. Rev. Lett. **82**, 715 (1999) — p.106, 109, and 121.

[40] F. Gittes and C. F. Schmidt, *Thermal noise limitations on micromechanical experiments*, Eur. Biophys. J. **27**, 75 (1998) — p.22.

[41] J. Gómez Rivas, D. H. Dau, A. Imhof, R. Sprik, B. P. J. Bret, P. M. Johnson, T. W. Hijmans, and A. Lagendijk, *Experimental determination of the refractive index in strongly scattering media*, Opt. Commun. **220**, 17 (2003) — p.40.

[42] J. Gómez Rivas, A. Lagendijk, R. W. Tjerkstra, D. Vanmaekelbergh, and J. J. Kelly, *Tunable photonic strength in porous GaP*, Appl. Phys. Lett. **80**, 4498

(2002) — p.40 and 41.

[43] I. S. Gradshteyn and I. M. Ryzhik, *Table of Integrals, Series, and Products* (Academic Press, San Diego, 1994), fifth ed., Page 1184, SN27 — p.94.

[44] T. Guhr, A. Müller-Groeling, and H. A. Weidenmüller, *Random matrix theories in quantum physics: Common concepts*, Physics Reports **299**, 189 (1998) — p.89 and 90.

[45] J. Heinrichs, *Light amplification and absorption in a random medium*, Phys. Rev. B **56**, 8674 (1997) — p.24.

[46] S. E. Hodges, M. Munroe, W. Gadomski, J. Cooper, and M. G. Raymer, *Turn-on transient dynamics in a multimode, compound-cavity laser*, J. Opt. Soc. Am. B **14**, 180 (1997) — p.83.

[47] S. Holler, N. L. Goddard, and S. Arnold, *Spontaneous emission spectra from microdroplets*, J. Chem. Phys. **108**, 6545 (1998) — p.12.

[48] B. A. Hunter, M. A. Box, and B. Maier, *Resonance structure in weakly absorbing spheres*, J. Opt. Soc. Am. A **5**, 1281 (1988) — p.15, 23, and 24.

[49] Z. Jiu-Gao, Z. He-Yan, D. Die-Chi, D. Ge-Guo, and L. Fu-Ming, *Optimization of scatterer concentration in high-gain scattering media*, Chin. Phys. Lett. **18**, 519 (2001) — p.33.

[50] M. Kerker, *Electromagnetic scattering from active objects*, Appl. Opt. **17**, 3337 (1978) — p.15, 23, and 24.

[51] M. Kerker, *Resonances in electromagnetic scattering by objects with negative absorption*, Appl. Opt. **18**, 1180 (1979) — p.15, 23, and 24.

[52] M. Kerker (ed.), *Selected papers on light scattering, Parts 1 and 2* (SPIE - the International Society for Optical Engineering, Bellingham, WA, 1988) — p.23.

[53] M. Kuwata-Gonokami, K. Takeda, H. Yasuda, and K. Ema, *Laser Emission from Dye-Doped Polystyrene Microsphere*, Jap. J. Appl. Phys. **31**, L99 (1992) — p.12 and 23.

[54] A. Lagendijk and B. A. Van Tiggelen, *Resonant multiple scattering of light*, Physics Reports **270**, 143 (1996) — p.95.

[55] H. M. Lai, C. C. Lam, P. T. Leung, and K. Young, *Effect of perturbations on the widths of narrow morphology-dependent resonances in Mie scattering*, J. Opt. Soc. Am. B **8**, 1962 (1991) — p.14.

[56] N. M. Lawandy, R. M. Balachandran, A. S. L. Gomes, and E. Sauvain, *Laser action in strongly scattering media*, Nature (London) **368**, 436 (1994) — p.7, 31, and 81.

[57] J. Lekavich, *Basics of Acousto-Optic Devices*, Lasers & Applications 59–64 (1986) — p.21.

[58] V. S. Letokhov, *Generation of light by a scattering medium with negative resonance absorption*, Sov. Phys. JETP **26**, 835 (1968) — p.7 and 67.

[59] H. B. Lin, J. D. Eversole, and A. J. Campillo, *Spectral properties of lasing*

microdroplets, J. Opt. Soc. Am. B **9**, 43 (1992) — p.12 and 23.

[60] Y. Ling, H. Cao, A. L. Burin, M. A. Ratner, X. Liu, and R. P. H. Chang, *Investigation of random lasers with resonant feedback*, Phys. Rev. A **64**, 063808 (2001) — p.52.

[61] R. Loudon, *The Quantum Theory of Light* (Oxford Science Publications, New York, 2000), 3rd ed. — p.105.

[62] X. Ma, J. Q. Lu, R. S. Brock, K. M. Jacobs, P. Yang, and X. H. Hu, *Determination of complex refractive index of polystyrene microspheres from 370 to 1610 nm*, Phys. Med. Biol. **48**, 4165 (2003) — p.26.

[63] T. H. Maiman, *Stimulated Optical Radiation in Ruby*, Nature (London) **187**, 493 (1960) — p.3.

[64] V. M. Markushev, M. V. Ryzhkov, C. M. Briskina, and H. Cao, *UV Radiation of Powdered ZnO Pumped by Nanosecond Pulses*, Laser Physics **15**, 1611 (2005) — p.33 and 83.

[65] P. C. Martin, *Measurements and Correlation Functions* (Gordon & Breach Science Pub, New York, 1968) — p.93, 94, and 95.

[66] G. Mie, *Beitrage zur Optik trüber Medien, speziell kolloidaler Metallösungen*, Ann. Physik **25**, 337 (1908) — p.11.

[67] V. Milner and A. Z. Genack, *Photon localization laser: low-threshold lasing in a random amplifying layered medium via wave localization*, Phys. Rev. Lett. **94**, 073901 (2005) — p.33 and 49.

[68] S. Mujumdar, M. Ricci, R. Torre, and D. S. Wiersma, *Amplified Extended Modes in Random Lasers*, Phys. Rev. Lett. **93**, 053903 (2004) — p.33, 34, 35, 36, 37, 49, 77, 80, 81, 82, and 83.

[69] M. A. Noginov, H. J. Caufield, N. E. Noginova, and P. Venkateswarlu, *Line narrowing in the dye solution with scattering centers*, Opt. Commun. **118**, 430 (1995) — p.33 and 81.

[70] H. M. Nussenzveig, *High-Frequency Scattering by a Transparent Sphere. I. Direct Reflection and Transmission*, J. Math. Phys. **10**, 82 (1969) — p.24.

[71] M. Patra, *On Quantum optics in random media*, Ph.D. thesis, University of Leiden (2000) — p.89.

[72] F. A. Pinheiro and L. C. Sampaio, *Lasing threshold of diffusive random lasers in three dimensions*, Phys. Rev. A **73**, 013826 (2006) — p.33, 34, 35, and 83.

[73] R. C. Polson, M. E. Raikh, and Z. V. Vardeny, *Universal Properties of Random Lasers*, IEEE J. Sel. Top. Quantum Electron. **9**, 120 (2003) — p.49.

[74] R. C. Polson and Z. V. Vardeny, *Organic random lasers in the weak-scattering regime*, Phys. Rev. B **71**, 045205 (2005) — p.33, 81, and 82.

[75] A. Pralle, M. Prummer, E.-L. Florin, E. H. K. Stelzer, and J. K. H. Hörber, *Three-dimensional High-Resolution Particle Tracking for Optical Tweezers by Forward Scattering Light*, Micr. Res. Tech. **44**, 378 (1999) — p.22.

[76] B. R. Prasad, H. Ramachandran, A. K. Sood, C. K. Subramanian, and N. Kumar, *Lasing in active, sub-mean-free path-sized systems with dense, random, weak scatterers*, Appl. Opt. **36**, 7718 (1997) — p.33.

[77] S. X. Qian, J. B. Snow, H. M. Tzeng, and R. K. Chang, *Lasing Droplets: Highlighting the Liquid-Air Interface by Laser Emission*, Science **231**, 486 (1986) — p.12.

[78] H. Ramachandran, *Mirrorless lasers*, Pramana J. Phys. **58**, 313 (2002) — p.31.

[79] J. Ripoll, C. M. Soukoulis, and E. N. Economou, *Optimal tuning of lasing modes through collective particle resonance*, J. Opt. Soc. Am. A **21**, 141 (2004) — p.15, 23, and 24.

[80] A. Rohrbach and E. H. K. Stelzer, *Three-dimensional position detection of optically trapped dielectrix particles*, J. Appl. Phys. **91**, 5474 (2001) — p.22.

[81] A. Rose, Z. Zhu, C. F. Madigan, T. M. Swager, and V. Bulovic, *Sensitivity gains in chemosensing by lasing action in organic polymers*, Nature (London) **434**, 876 (2005) — p.31.

[82] V. Sandoghdar, F. Treussart, J. Hare, V. Lefévre-Seguin, J. M. Raimond, and S. Haroche, *Very low threshold whispering-gallery-mode microsphere laser*, Phys. Rev. A **54**, R1777 (1996) — p.12 and 23.

[83] T. Savels, *Scattering lasers*, Ph.D. thesis, University of Amsterdam (2007) — p.4, 6, 8, and 32.

[84] T. Savels, A. P. Mosk, and A. Lagendijk, *Light scattering from three-level systems: The T matrix of a point dipole with gain*, Phys. Rev. A **71**, 043814 (2005) — p.97.

[85] A. L. Schawlow and C. H. Townes, *Infrared and Optical Masers*, Phys. Rev. **112**, 1940 (1958) — p.86.

[86] F. J. P. Schuurmans, *Light in complex dielectrics*, Ph.D. thesis, University of Amsterdam (1999) — p.41.

[87] F. J. P. Schuurmans, D. Vanmaekelbergh, J. van de Lagemaat, and A. Lagendijk, *Strongly Photonic Macroporous Gallium Phosphide Networks*, Science **284**, 141 (1999) — p.83.

[88] P. Sebbah, O. Legrand, B. A. van Tiggelen, and A. Z. Genack, *Statistics of the cumulative phase of microwave radiation in random media*, Phys. Rev. E **56**, 3619 (1997) — p.109.

[89] P. Sebbah and C. Vanneste, *Random laser in the localized regime*, Phys. Rev. B **66**, 144202 (2002) — p.33, 35, and 83.

[90] W. L. Sha, C. H. Liu, and R. R. Alfano, *Spectral and temporal measurements of laser action of Rhodamine 640 dye in strongly scattering media*, Opt. Lett. **19**, 1922 (1994) — p.33.

[91] D. Sharma, H. Ramachandran, and N. Kumar, *Lévy statistics of emission from a novel random amplifying medium: an optical realization of the Arrhenius*

cascade, Opt. Lett. **31**, 1806 (2006) — p.33.

[92] A. E. Siegman, *Lasers* (Stanford University, University Science Books, Mill Valley, CA, Oxford, 1986) — p.3, 5, 27, 33, 54, 55, 59, 67, 68, and 71.

[93] J. Skaar, *Fresnel equations and the refractive index of active media*, Phys. Rev. E **73**, 026605 (2006) — p.24.

[94] C. M. Soukoulis, X. Jiang, J. Y. Xu, and H. Cao, *Dynamic response and relaxation oscillations in random lasers*, Phys. Rev. B **65**, 041103 (2002) — p.33, 67, and 71.

[95] M. R. Spiegel, *Advanced Mathematics for engineers and scientists* (McGraw-Hill, New York, 1971) — p.101.

[96] A. D. Stone and H. E. Tureci, *Multi-mode lasing theory for complex or random lasers*, In *Photonic Metamaterials: From Random to Periodic on CD-ROM* (The Optical Society of America, Washington, DC, 2006), vol. WC2   — p.33 and 83.

[97] K. Svoboda and S. M. Block, *Biological applications of Optical Forces*, Ann. Rev. Biophys. Biomol. Struct. **23**, 247 (1994) — p.22.

[98] R. W. Tjerkstra, J. Gómez Rivas, D. Vanmaekelbergh, and J. J. Kelly, *Porous GaP Multilayers Formed by Electrochemical Etching*, Electrochemical and Solid-State Letters **5**, G32 (2002) — p.40 and 41.

[99] K. Totsuka, G. van Soest, T. Ito, A. Lagendijk, and M. Tomita, *Amplification and diffusion of spontaneous emission in strongly scattering medium*, J. Appl. Phys. **87**, 7623 (2000) — p.59.

[100] H. M. Tzeng, K. F. Wall, M. B. Long, and R. K. Chang, *Laser emission from individual droplets at wavelengths corresponding to morphology-dependent resonances*, Opt. Lett. **9**, 499 (1984) — p.12.

[101] K. J. Vahala, *Optical microcavities*, Nature (London) **424**, 839 (2003) — p.11, 12, and 23.

[102] M. P. van Albada and A. Lagendijk, *Observation of weak localization of light in a random medium*, Phys. Rev. Lett. **55**, 2692 (1985) — p.40, 41, and 84.

[103] H. C. van de Hulst, *Light scattering by Small Particles* (Dover Publications, Inc., New York, 1981) — p.11, 12, and 13.

[104] K. L. van der Molen, A. P. Mosk, and A. Lagendijk, *Intrinsic fluctuations in random lasers*, Phys. Rev. A **74**, 053808 (2006) — p.49, 78, 88, and 90.

[105] K. L. van der Molen, A. P. Mosk, and A. Lagendijk, *Quantitative analysis of several random lasers*, arXiv cond–mat/0612352 (2006) — p.77.

[106] K. L. van der Molen, A. P. Mosk, and A. Lagendijk, *Relaxation oscillations in long-pulsed random lasers*, arXiv physics/0703045 (2007) — p.67.

[107] K. L. van der Molen, R. W. Tjerkstra, A. P. Mosk, and A. Lagendijk, *Spatial Extent of Random Laser Modes*, accepted by Phys. Rev. Lett., arXiv cond–mat/0612328 (2006) — p.77, 80, 81, 82, and 83.

[108] K. L. van der Molen, P. Zijlstra, A. Lagendijk, and A. P. Mosk, *Laser threshold*

of Mie resonances, Opt. Lett. **31**, 1432 (2006) — p.23.

[109] G. van Soest, *Experiments on random lasers*, Ph.D. thesis, University of Amsterdam, www.randomlasers.com (2001) — p.59.

[110] G. van Soest, F. J. Poelwijk, R. Sprik, and A. Lagendijk, *Dynamics of a Random Laser above Threshold*, Phys. Rev. Lett. **86**, 1522 (2001) — p.67.

[111] B. A. van Tiggelen, P. Sebbah, M. Stoytchev, and A. Z. Genack, *Delay-time statistics for diffuse waves*, Phys. Rev. E **59**, 7166 (1999) — p.54.

[112] I. M. Vellekoop, P. Lodahl, and A. Lagendijk, *Determination of the diffusion constant using phase-sensitive measurements*, Phys. Rev. E **71**, 056604 (2005) — p.100.

[113] D. Wiersma and A. Lagendijk, *Laser action in very white paint*, Physics World 33–37 (1997) — p.34.

[114] D. S. Wiersma and A. Lagendijk, *Light diffusion with gain and random lasers*, Phys. Rev. E **54**, 4256 (1996) — p.67.

[115] J. P. Woerdman, M. P. van Exter, and N. J. van Druten, *Quantum noise of small lasers*, Adv. At., Mol., Opt. Phys. **47**, 205 (2001) — p.54, 56, and 71.

[116] P. E. Wolf and G. Maret, *Weak localization and Coherent Backscattering of Photons in Disordered Media*, Phys. Rev. Lett. **55**, 2696 (1985) — p.40, 41, and 84.

[117] X. H. Wu, A. Yamilov, H. Noh, H. Cao, E. W. Seelig, and R. P. H. Chang, *Random lasing in closely packed resonant scatterers*, J. Opt. Soc. Am. B **21**, 159 (2004) — p.81 and 82.

[118] A. Yamilov, X. Wu, H. Cao, and A. Burin, *Absorption-induced confinement of lasing modes in diffusive random media*, Opt. Lett. **30**, 2430 (2005) — p.33 and 83.

[119] S. F. Yu, C. Yuen, S. P. Lau, W. I. Park, and G. C. Yi, *Random laser action in ZnO nanorod arrays embedded in ZnO epilayers*, Appl. Phys. Lett. **84**, 3241 (2004) — p.31 and 33.